VEGF, IL-8, or c-Met-specific short hairpin RNA-expressing oncolytic adenovirus elicits potent inhibition of angiogenesis and tumor growth

Ji Young Yoo

Department of Medical Science

The Graduate School, Yonsei University

VEGF, IL-8, or c-Met-specific short hairpin RNA-expressing oncolytic adenovirus elicits potent inhibition of angiogenesis and tumor growth

Directed by Professor Chae-Ok Yun

The doctoral Dissertation submitted to the Department of Medical science,
the Graduate School of Yonsei University in partial fulfillment of the requirements for the degree of
Doctor of Medical Science

Ji Young Yoo

December 2007

This certifies that the doctoral dissertation of Ji Young Yoo is approved

_____

Thesis Supervisor : Chae-Ok Yun

_____

Joo-Hang Kim

_____

Hoguen Kim

_____

Hyun Cheol Chung

_____

Jaemyeon Lee

The Graduate School

Yonsei University

December 2007

ACKNOWLEDGEMENTS

식물 단백질을 전공한 제가 바이러스를 이용한 암 유전자 치료에 대한 막연한 동경심으로 두려움과 설렘으로 시작한 박사과정이 엊그제 같은데, 벌써 4년이라는 시간이 지나 부족하지만 작은 결실을 얻게 되었습니다. 때로는 많이 힘들기도 지치기도 했지만, 논문을 완성하고 보니 고마운 분들이 너무나 많은 저는 무척이나 행운아였던 것 같습니다. 그 분들께 이 지면을 빌어 짧게나마 감사의 뜻을 전하고자 합니다.

먼저 연구에 대한 기본적인 자세와 열정, 실험에 대한 진정한 재미와 의미를 알게 해주시고, 다양한 연구를 할 수 있는 많은 기회들을 주시고, 무엇보다도 열심히 하시는 모습으로 모범이 되어주신 윤채옥 교수님, 항상 환한 웃음으로 격려해 주시고, 실험적 결과에 대해 임상적 관점에서 예리하게 짚어 주시는 따뜻한 김주항 교수님께 깊은 감사를 드립니다. 제가 가진 그릇이 10이고, 아무리 노력해도 20밖에 될 수 없었을 제가, 두 분의 제자가 되어 50이 되었다고 생각합니다. 더 많은 노력으로 나머지 50을 채워나가 당당한 제자로써 교수님의 가르침에 보답하겠습니다. 그리고 바쁘신 와중에도 부족한 이 논문의 완성을 위해 꼼꼼하게 심사해 주신 김호근 교수님, 정현철 교수님, 이재면 교수님께 깊이 감사 드립니다. 석사를 마치고, 취직을 하겠다 했을 때, 공부하라 야단쳐 주시고, 서울 오시면 술 사주시며 한결같이 격려해 주시고 응원해 주시는, 보답해야 할 게 너무 많은 존경하고 사랑하는 이상렬 교수님께 너무나 감사 드립니다.

다정다감하신 손주혁 선생님, 열정적이신 조병철 선생님, 언니처럼 다정한 최혜진 선생님, 바쁘단 핑계로 연락도 자주 못 드리지만 항상 먼저 챙겨주시고 맘 써주시는 김현희 선생님, 친구 같은 영숙언니, 똑소리 나는 은희언니, 동물실험의 대가 황경화 선생님, 자기의 꿈을 위해 성실하게 노력하는 윤아에게도 감사의 마음을 전합니다. 진정한 방장의 모습을 몸소 보여주신 최고의 선배 재성선배님, 진정한 커피 한잔의 여유 진선언니, 만능 맥가이버 김인욱 선생님, 나의 든든한 정신적 지주 민정언니, 열정적이고 적극적인 경주, 꼼꼼한 평환이, 첨엔 삐걱거렸으나 지금은 누구보다 편안한 친구 지훈씨, 애교많은 아름이, 곰돌이 엄마 정선이, 착하고 성실한 일규, 나의 주말 파트너 송남이, 매력 만점 첫 제자 민주, 성실하고 반듯한 오

준이, 팔방미인 성미, 실험 배우느라 열심인 새내기 7차원 지성이와 남동생 혜원이에게 고맙다는 말을 전합니다. 가족들 보다 더 많은 시간을 함께했던 실험실 선후배 님들께 깊은 감사를 드립니다.

석사시절 처음 파이펫 잡는 것부터 때로는 따끔한 충고로, 때로는 따뜻한 격려로, 진정한 실험의 재미를 알게 해준 멋진 교수님이 되신 균오선배, 선배 만나 일복이 많아졌다 투정부리면서도, 선배가 하던 실험 자세와 후배들에게 잔소리 하는 것까지 닮아버린 저를 보며, 너무나 많은 것을 배운 것 같아 항상 감사한 마음입니다. 세심하게 잘 챙겨주는 중로선배, 큰오빠 용훈선배, 작은오빠 승식선배, 든든한 수권선배, 새신랑 연옥선배, 나의 든든한 석사동기 정찬선배, 멋진 호희언니, 미스센터 진호선배…단백질 방 선후배님들께 깊은 감사를 드립니다.

바쁘단 핑계로 연락도 않는 나를 항상 걱정하고 챙겨주는 소중한 나의 친구들, 기원이, 종숙이, 명희, 의경이, 명숙이, 멀리 있어도 그 존재만으로도 큰 힘이 되는 사랑하는 친구들 현미, 정미, 희영, 미애, 같은 꿈을 갖고 같은 길을 준비하는 든든한 친구 이박사 정순이, 떨어져 있어도 매일같이 전화로 나의 얘기 잘 들어주고 때로는 따뜻하게 안아주고, 때로는 냉정하게 잔소리해주는 소중한 친구 주영이, 만난지 5년이지만 가까이 있어 오래된 친구들보다 더 많은 시간을 함께하는 나의 든든하고 고마운 소중한 벗 연호에게 고마운 맘을 전합니다.

마지막으로 나에게는 어리게만 보이는 철부지 막내였지만 이제는 한 가족의 가장이 된 막내 지태와 올케, 그리고 두 아이의 엄마가 되어 이제는 언니 같은 동생 지현이와 제부, 공부하느라 자주 만나지도 놀아주지도 못하는 고모, 이모를 잘 따라주는 조카들, 그리고 여러 가지 힘든 일들이 많았지만, 많이 부족한 큰딸 걱정할까 말하지 않고, 모든 일들을 이겨내고, 믿고 공부에만 전념할 수 있도록 사랑과 용기를 주시는 부모님께 말로는 표현하기 힘든 감사하는 마음과 이 작은 결실을 바칩니다.

이러한 감사의 마음 잊지 않고 언제나 열심히 할 것을 다짐하며, 여러분 모두들 행복하시길 바랍니다.

TABLE OF CONTENTS

LIST OF FIGURES

LIST OF TABLES

ABSTRACT

VEGF, IL-8, or c-Met-specific short hairpin RNA-expressing oncolytic adenovirus elicits potent inhibition of angiogenesis and tumor growth

Ji Young Yoo

Department of Medical science

The Graduate School, Yonsei University

(Directed by Professor Chae-Ok Yun)

RNAi, due to its target specificity may be highly effective as a novel therapeutic modality but direct delivery of synthetic siRNA still remains a major obstacle for this approach. To induce long term expression and specific gene silencing, novel delivery vector system is also required. To overcome this shortcoming, I constructed an oncolytic adenovirus (Ad)-based shRNA expression system (Ad-ΔB7-shVEGF) against vascular endothelial growth factor (VEGF), a key mediator in angiogenesis. To demonstrate VEGF-specific nature of this newly engineered Ad-based shRNA, replication-

incompetent Ad expressing VEGF-specific shRNA (Ad-ΔE1-shVEGF) was also generated. Ad-ΔE1-shVEGF was highly effective in reducing VEGF expression, and elicited anti-angiogenenic effect *in vitro* as well as *in vivo*. Similarly, Ad-ΔB7-shVEGF exhibited potent anti-angiogenic effects in the matrigel plug assay *in vivo*. Moreover, Ad-ΔB7-shVEGF also demonstrated enhanced antitumor effect and survival advantage compared to its cognate control oncolytic Ad, Ad-ΔB7. Tumor histological analysis revealed that Ad-ΔB7-shVEGF induced significant reduction in tumor vasculature, verifying the anti-angiogenic mechanism. Furthermore, the duration and magnitude of the gene silencing effect following infection with Ad-ΔB7-shVEGF was longer and more effective than the replication-incompetent Ad, Ad-ΔE1-shVEGF. Taken together, these results suggest that the combined effects of oncolytic viral therapy and cancer cell-specific expression of VEGF-targeted shRNA elicits greater anti-tumor effect than an oncolytic Ad alone.

To select effective promoters for expression of shRNAs, I used IL-8, a potent pro-angiogenic factor. I also manufactured replication-incompetent Ads (Ad-ΔE1-CMVshIL8 and Ad-ΔE1-U6shIL8) under the control of the CMV and U6 promoters, respectively. Ad-ΔE1-U6shIL8 was highly effective in reducing IL-8 expression, and was much more effective in driving IL-8

specific shRNA than the CMV promoter-driven vector. The reduced IL-8 expression then translated into decreased angiogenesis *in vitro* as measured by migration, tube formation, and rat aortic ring sprouting assays. In addition to its effect on endothelial cells, Ad-ΔE1-U6shIL8 also effectively suppressed the migration and invasion of cancer cells. I also have generated an efficient oncolytic adenovirus (Ad)-based shRNA expression system (Ad-ΔB7-U6shIL8) against IL-8, a potent pro-angiogenic factor. *In vivo*, intra-tumoral injection of Ad-ΔB7-U6shIL8 significantly inhibited the growth of Hep3B and A549 human tumor xenografts. Histopathological analysis of Ad-ΔB7-U6shIL8-treated tumors revealed an increase in apoptotic cells and a reduction in mcro-vessel density. Finally, Ad-ΔB7-U6shIL8 was also shown to inhibit the growth of disseminated MDA-MB-231 breast cancer metastases. Taken together, these findings demonstrate the utility and anti-tumor effectiveness of oncolytic Ad expressing shRNA against IL-8.

To develop effective shRNA inhibition system, I compared single or dual shRNA expression system. c-Met, receptor tyrosine kinase for hepatocyte growth factor (HGF) is overexpressed and/or mutated a variety of human tumors. Since HGF-Met signaling contributes to tumor survival, growth, angiogenesis, and metastasis, various approaches have been explored to inhibit the function of HGF or Met. In this study, I generated recombinant

adenovirus expressing c-Met-specific shRNA and compared single and dual shRNA expression system, too. All constructed c-Met specific shRNA-expressing Ads inhibited c-Met expression. Among these, dual shMet-expressing Ad, Ad-ΔE1-shMet4+5, was more effective than single shRNA-expressing-Ads in driving c-Met specific shRNA. Cells infected with shMet-expressing Ads were showed dramatic growth inhibition and characteristic changes in morphology. That is, phenotypes such as enlarged and flattened cell morphology, increased granularity and the appearance of many vacuolated cells were typical senescence-like phenotype and mRNA level of the genes commonly associated with cellular senescence like SM22, TGase II, and PAI-I was increased. Also, it was observed that the reduced c-Met expression could inhibit cancer cell proliferation by arresting cells at G2/M phase using cell cycle analysis. Reduced c-Met expression down-regulated VEGF expression and reduced angiogenesis *in vitro* as measured by migration, tube formation, and rat aortic ring sprouting assays. In addition to inhibition of endothelial cell functioning, Ad-ΔE1- shMet4+5 effectively suppressed the migration and invasion of cancer cells. Moreover, intra-tumoral injection of Ad-ΔE1-shMet4+5 inhibited tumor growth significantly more than single shMet-specific shRNA expresiing Ad, Ad-ΔE1-shMet4 or Ad-ΔE1-shMet5. Histopathological analysis of tumors treated with Ad-ΔE1-shMet4+5 revealed

an inhibition of cancer cell proliferation and reduction in vessel density. Furthermore, treatment of Ad-ΔE1-shMet4+5 inhibited the growth of disseminated MDA-MB-231 breast cancer metastases. Taken collectively, these findings demonstrate that the inhibition of c-Met function by dual c-Met specific shRNA expressing Ad suppress cancer cell proliferation via senescence mechanism and tumor growth, invasion, metastasis and angiogenesis.

Key words: Cancer gene therapy; vascular endothelial growth factor (VEGF), IL-8, c-Met, Hepatocyte growth factor (HGF); short hairpin RNA (shRNA), oncolytic adenovirus

VEGF, IL-8, or c-Met-specific short hairpin RNA-expressing oncolytic adenovirus elicits potent inhibition of angiogenesis and tumor growth

Ji Young Yoo

Department of Medical science

The Graduate School, Yonsei University

(Directed by Professor Chae-Ok Yun)

I. INTRODUCTION

It has recently been shown that the introduction in a mammalian cell of double-stranded oligoribonucleotides (also called siRNA) triggers the degradation of the endogenous mRNA to which the siRNA hybridizes to. Initial investigations of RNAi in cells relied on transfection with synthetic RNA oligonucleotides [1,2], or plasmids designed to drive expression of siRNAs through the use of RNA polymerase III promoters [3-5]. This knock down technology has been successfully applied to inhibit target gene expression but its utility is limited by its short half-life. To achieve therapeutic *in vivo* gene silencing in mammalian tissues, it would require intracellular transcription

expression rather than transient transfection of dsRNA [6]. One means to achieve this long lasting expression of siRNA is to use a vector-based delivery system such as recombinant viral vectors.

E1/E3-deleted replication-defective adenovirus (Ad) has been widely used for cancer gene therapy because it offers, in contrast to other vectors, much higher transduction efficiency and transgene expression in a broad spectrum of cell types [7]. However, replication-deficient viral vectors have thus far been used with limited success in cancer gene therapy mainly due to limited transduction efficiency and short duration of therapeutic gene expression. It is thus expected that delivery of shRNAs interfering with the expression of genes involved in tumor cell survival using non-replicating vectors will meet similar difficulties. Oncolytic Ads are being developed as selectively replicating antitumoral agents, and currently number of clinical trials with such viruses are ongoing to treat a variety of cancers [8-12]. A clear benefit is the potential amplification of its effect in which the replicating vector would be able to infect and deliver the therapeutic gene to adjacent cancer cells, ultimately enhancing the potential of a viral-based therapy to deal with the complexity of a human tumor [13].

Angiogenesis, the formation of new capillaries from existing blood vessels, plays an important role in the growth, metastasis, and malignancy of

tumors [14]. Number of growth factors have been identified as positive regulators of angiogenesis [15]. Among them, vascular endothelial growth factor (VEGF) seems to be the predominant growth factor found in a wide variety of conditions associated with angiogenesis [15,16]. Therapeutic effect in terms of inhibiting tumor growth and metastasis by inhibiting VEGF activity or disabling the function of its receptors has been shown in the clinic [17-20].

In this report, the main objectives were to construct an efficient oncolytic Ad-based shRNA expression system and to explore oncolytic Ad-mediated RNAi for efficient and long-term gene silencing. I show here that E1A- and E1B-double mutant oncolytic Ad expressing VEGF-specific shRNA, Ad-ΔB7-shVEGF, induces silencing of VEGF gene effectively *in vitro* as well as *in vivo*. I show for the first time that VEGF-specific shRNA expressed from an oncolytic virus can induce potent anti-angiogenesis, resulting in tumor suppression as well as survival benefits. In addition, I demonstrate for the first time that the oncolytic Ad-mediated shRNA expression results in improved efficacy as well as sustained gene silencing effect than the replication-incompetent Ad, Ad-ΔE1-shVEGF.

Interleukin-8 (IL-8), a member of the CXC chemokine family, was initially discovered as a leukocyte chemo-attractant, recent studies have revealed that IL-8 plays an important role as a potent pro-angiogenic factor

[21,22]. IL-8 is produced by various tumors including melanoma, lung, prostate, gastric, ovarian, and bladder cancers [23]. Experimental and clinical studies have shown positive correlations between IL-8 expression and tumor growth and metastasis [24]. Recently, it has been shown that a blockade of IL-8 activity using a neutralizing antibody or an IL-8 antisense oligodeoxynucleotides inhibited both the growth and metastasis of tumors in a variety of animal models [25-27].

Using IL-8, I compared two promoters, CMV and U6, in their efficiency of shRNA expression. I also investigated the potential of an oncolytic Ad-mediated shRNA expression targeted to IL-8 in inhibiting both tumor growth and angiogenesis. Our results show that the U6 promoter is superior to CMV in its ability to express shRNA specific to IL-8, and that the expression of IL-8-specific shRNA can strongly and specifically silence IL-8 mRNA and protein expression in various human cancer cell lines. I show for the first time that IL-8-specific shRNA expressed from an oncolytic adenovirus can induce potent anti-angiogenic effects, resulting in inhibition of tumor growth and metastasis. I further show that E1A-mediated suppression of angiogenesis and induction of apoptosis in tumors likely contributes to additional anti-tumor activity, leading to enhanced therapeutic efficacy. Findings in this report strongly suggest that the use of cancer cell-specific

replicating oncolytic adenovirus in the delivery of IL-8 specific shRNA may hold strong promise for the treatment of cancer.

Receptor tyrosine kinases (RTKs) regulate many key processes in mammalian cell growth and survival, organ morphogenesis, neovascularization, and tissue repair and regeneration, especially. Overactivation and/or defective downregulatiuon of RTKs have been implicated as causative factors in the development and progression of numerous human cancers. There are now over 75 known human receptor tyrosine kinase (RTKs), and many of them are known to be proto-oncogenes involved in oncogenesis [28]. Based on this, RTKs could be an attractive molecular target for efficient therapeutic tool in anticancer therapy, and it has been developed many of tumor RTK-targeted drugs such as trastuzumab, imatinib, bevacizumab, and gefitinib. c-Met, one of RTK proto-oncogenes, is a disulfide-linked α-β heterodimeric receptor tyrosine kinase and is overexpressed and/or dysregulated in a variety of human tumors including melanoma, lung, prostate, gastric, ovarian, and bladder. Various c-Met mutations have been well described in multiple solid tumors. It was reported that most of c-Met mutations was in juxtamembrane and a cytosolic c-

terminal domain with tyrosine kinase activity, so it can induce constitutive activation of the HGF signaling pathway.

Since Met signaling contributes to tumor survival, growth, angiogenesis, and metastasis, it could be a potential target for cancer therapy. Various approaches have been explored to inhibit the HGF or Met-mediated function in experimental systems. One of the approaches is the use of neutralizing monoclonal antibody (Cao et al., 2001) or ribozyme [29-31] to block the HGF activity or HGF/Met expression. According to this study, the inhibition of the HGF/Met function suppressed both tumor growth, and metastasis in a variety of animal tumor models. Also, it was also reported other ways to block the HGF/Met interaction like the inhibition of Met tyrosine kinase activity by small molecule inhibitors [17,32,33], impairment of receptor dimerization either by dominant-negative Met [34,35] or by a dual-function decoy Met receptor that interferes with both HGF binding to Met and Met homodimerization [36], and ligand displacement by a competitive inhibitor of HGF [37].

The activation of c-Met protein is involved in the induction of vascular endothelial growth factor [38,39] through downregulation of the antiangiogenesis factor thrombospodin-1 [40]. Recently, it was shown that a

selective small molecule inhibitor of c-Met, PHA665752, inhibits tumorigenicity and angiogenesis [41] and another small molecule inhibitor of c-Met, PF-2341066, exhibits cytoreductive antitumor efficacy through antiproliferative and antiangiogenic mechanism [42].

Using c-Met, I compared single or dual shRNA expression system, in their efficiency of shRNA expression. To effectively inhibit c-Met expression, I generated three kinds of recombinant adenovirus expressing single shRNA, Ad-ΔE1-shMet4 and Ad-ΔE1-shMet5, and dual shRNA, Ad-ΔE1-shMet4+5 and examined their efficiency for c-Met knockdown. Our results show that Ad-ΔE1-shMet4+5 can strongly and specifically silence c-Met mRNA and protein expression in various human cancer cell lines tested. Also, I observed that reduced c-Met expression induce dramatic inhibition of cell proliferation inhibition by senescence mechanism. Functional analyses showed that the inhibition of c-Met effectively inhibited not only cell proliferation and tube formation of primary cultured human endothelial cells *in vitro* but also rat aorta ring sprouting of endothelial cells *ex vivo*. Furthermore, it significantly suppressed the growth of established U343 human glioma xenograft model in nude mice. In addition, I demonstrate for the first time that the dual c-Met-specific shRNA expression results in

improved efficacy as well as sustained gene silencing effect than the single shRNA expression. These observations strongly suggest that the inhibition of c-Met expression using dual c-Met specific shRNA-expressing Ad, Ad-ΔE1-shMet4+5 may hold strong promise for the cancer treatment.

II. MATERIAL AND METHODS

Cell lines and cell culture

All cell lines with the exception of Hep3B, which was maintained in modified Eagle's medium (MEM; Gibco BRL, Grand Island, NY), were cultured in Dulbecco's modified Eagle's medium (DMEM; Gibco BRL) supplemented with 10% fetal bovine serum (Gibco BRL), L-glutamine (2 mM), penicillin (100 IU/ml), and streptomycin (50 μg/ml). A human embryonic kidney cell line expressing the Ad E1 region (HEK293), brain cancer cell lines (U343 and U87MG), liver cancer cell lines (Hep3B, HepG2, Huh7, and Hep1), and a non-small lung cancer cell line (A549) were purchased from the American Type Culture Collection (ATCC, Manassas, VA). Human umbilical vein endothelial cells (HUVECs), isolated from human umbilical cord veins by collagenase treatment as described previously [43], were maintained and propagated in M199 medium (Invitrogen, Carlsbad, CA) containing 20% fetal bovine serum (FBS), penicillin-streptomycine (100 IU/ml), 3 ng/ml basic fibroblast growth factor (Upstate Biotechnology, Lake Placid, NY), and 5 units/ml heparin. HUVECs were used between passages 2 and 7. All cell lines were maintained at 37°C in a humidified atmosphere at 5% CO_2.

Construction of expression plasmids expressing VEGF-specific shRNA

Two target siRNA sequences for VEGF were selected using a dedicated program provided by Ambion Inc. (Ambion, Austin, TX). Two double-stranded RNA oligonucleotides, corresponding to two regions at nucleotides 124-144 (shVEGF-1) and 379–399 (shVEGF-2) of human VEGF mRNA (GenBank accession number gi: 6631028), were then synthesized using Silencer™ siRNA construction kit (Ambion, Austin, TX) (Fig. 1A). To generate shRNA targeting VEGF, the DNA fragment for the expression of shRNA targeting the positions 124-144 or 379-399 of human VEGF was generated by annealing the sense oligonucleotide 5′-gatccc AAGTTCATGGATGTCTATCAGttcaagagaCTGATAGACATCCATGAACTT ttttttggaaa-3′ and its cognate antisense oligonucleotide 5′-agcttttccaaaaaaAAGTTCATGGATGTCTATCAGtctcttgaaCTGATAGACATC CATGAACTTgg-3′ or the sense oligonucleotide 5′-gatcccAAATGTGAATGCAGACCAAAGttcaagagaCTTTGGTCTGCATTCA CATTTttttttggaaa-3′ and its cognate antisense oligonucloetide 5′-agcttttccaaaaaaAAATGTGAATGCAGACCAAAGtctcttgaaCTTTGGTCTGC ATTCACATTTgg-3′ for shVEGF-1 and shVEGF-2, respectively. The 21-nucleotide VEGF target sequences are indicated in uppercase letters, whereas the 9-nucleotide hairpin and the sequences necessary for the directional

cloning are depicted in lowercase letters. After digestion with *Bam*HI and *Hind*III, the fragments were inserted into a pSilencer-2.1-hygro-U6 vector (Ambion), resulting in pshVEGF-1 and pshVEGF-2. The control vector (psc-shRNA) was constructed by inserting a sequence that expresses a siRNA with limited homology to sequences in the human and mouse genomes.

Synthesis and transfection of siRNAs specific for IL-8 or c-Met

Four synthetic double-stranded oligonucleotides corresponding to four 21-nt sequences from human IL-8 (GenBank accession number gi: 28610153; Table 1) and Five synthetic double-stranded oligonucleotides specific to human c-Met (GenBank accession number gi: 4557746; Table 2), were designed using RNAi software (Ambion: www.ambion.com/techlib/misc/siRNA_finder.html) and synthesized using the Ambion Silencer TM siRNA construction kit (Ambion, Austin, TX). To determine the most effective siRNA, one μg of each of the synthesized siRNAs and two control siRNAs specific to lamin A/C and luciferase were introduced into Hep3B (IL-8) or U343 (c-Met) cells (3×10^5) in 6-well dishes using lipofectamine plus reagent (Invitrogen, Carlsbad, CA). After 48 hr, cells were harvested and total RNA was extracted using the RNeasy mini kit (Qiagen, Valencia, CA) according to the manufacturer's instructions. Semi-quantitative RT-PCR was then performed using β-actin as an internal control

to normalize gene expression.

Generation of VEGF -specific shRNA-expressing shuttle vector

To generate Ads expressing VEGF-specific shVEGF at the E3 region of Ad, shVEGF gene excised from pshVEGF-2 was first subcloned into pSP72-E3 Ad shuttle vector [44] using *EcoR*I-*Hind*III, generating a pSP72-E3/U6-shVEGF. The newly constructed pSP72-E3/U6-shVEGF E3 shuttle vector was then co-transformed with a replication-incompetent Ad total vector expressing lacZ at E1 region, pdl-ΔE1, or replication-competent Ad total vector, pdl-ΔB7, into *Escherichia coli* BJ5183 for homologous recombination, generating pAd-ΔE1-shVEGF and pAd-ΔB7-shVEGF Ad vectors, respectively.

Generation of IL-8 -specific shRNA-expressing shuttle vector

To generate Ads expressing IL-8-specific shRNA, DNA fragment targeting position 194-212 of human IL-8 was first generated by annealing the sense oligonucleotide 5′-gatccGAACTTAGATGTCAGTGCATAttcaagagaAATATGCACTGACATCTAAGTtttttggaaa-3′ and its cognate antisense oligonucleotide 5′-agcttttccaaaaaaGAACTTAGATGTCAGTGCATAtctcttgaaAATATGCACTGACATCTAAGTgg-3′. The 19-nucleotide IL-8 target sequences are indicated in uppercase letters, whereas the 9-nucleotide hairpin and sequences necessary

for directional cloning are depicted in lowercase letters. After annealing with sense and antisense oligonucleotides, the fragments were inserted into a pSilencer-2.1-hygro-U6 vector (Ambion), resulting in pshU6IL-8. The shIL-8 gene expression cassette excised from pshU6IL-8 was then subcloned into the pSP72-E3 Ad shuttle vector [44] using *Eco*RI-*Hind*III, generating pSP72-E3/U6-shIL8. In addition, the annealed IL-8-specific shRNA DNA fragment was subcloned into the pSP72-E3/CMV Ad shuttle vector [44], generating pSP72-E3/CMV-shIL8. The newly constructed pSP72-E3/U6-shIL8 and pSP72-E3/CMV-shIL8 E3 shuttle vectors were linearized with *Xmn*I and co-transformed with pdl-ΔE1, a replication-incompetent Ad total vector expressing lacZ at E1 region, or pdl-ΔB7, a replication-competent Ad total vector, into *Escherichia coli* BJ5183 for homologous recombination, generating the pAd-ΔE1-U6shIL8, pAd-ΔE1-CMVshIL8, pAd-ΔB7-U6shIL8, and pAd-ΔB7-CMVshIL8 Ad vectors.

Generation of c-Met -specific shRNA-expressing shuttle vector

To generate Ads expressing c-Met-specific shRNA, a DNA fragment targeting position 1987-2007 and 3142-3162 of human c-Met was first generated by annealing, the following oligonucleotides were used: c-Met #4: sense oligonucleotide: 5′-gatcccAAACTAGAGTTCTCCTTGGAAttcaagagaTTCCAAGGAGAACTCT

AGTTTttttttggaaa-3′ and its cognate antisense oligonucleotide: 5′-agcttttccaaaaaaAAACTAGAGTTCTCCTTGGAAtctcttgaaTTCCAAGGAGAACTCTAGTTTgg-3′; c-Met #5: sense oligonucleotide: 5′-gatcccAATTAGTTCGCTACGATGCAAttcaagagaTTGCATCGTAGCGAACTAATTtttttggaaa-3′ and its cognate antisense oligonucleotide: 5′-agcttttccaaaaaaAATTAGTTCGCTACGATGCAAtctcttgaaTTGCATCGTAGCGAACTAATTgg-3′. The 19-nucleotide c-Met target sequences are indicated in uppercase letters, whereas the 9-nucleotide hairpin and sequences necessary for directional cloning are depicted in lowercase letters. Each annealed fragments were inserted into a pSilencer-2.1-hygro-U6 vector (Ambion) digested with BamHI and HindIII, resulting in pshMet4 and pshMet5. The shMet4 and shMet5 gene expression cassette excised from pshMet4 and pshMet5 was then subcloned into the pSP72-E3 Ad shuttle vector using EcoRI-HindIII, generating pSP72-E3/shMet4 and pSP72-E3/shMet5. In addition, to generate Ad expressing both shMet4 and shMet5, U6-shMet5 region of pshMet5 was amplified by polymerase chain reaction (PCR) with the following primer set: 5'-GTCAAGCTTGAATTCCCCAGTGGAAAGACG-3' as the sense primer and 5'-GTCGAATTCAAGCTTCCAAAAAAAATTAGTTCG-3' as the antisense primer. The primers were designed to create *Hind*III sites (underlined), and

the pshMet5 containing U6-shMet5, was used as a template. The PCR product containing U6-shMet5 was digested with *Hind*III, and then was subcloned into the pSP72-E3/shMet4, generating pSP72-E3/shMet4+5. The newly constructed pSP72-E3/shMet4, pSP72-E3/shMet5, and pSP72-E3/shMet4+5 E3 shuttle vectors were linearized with XmnI and co-transformed with pdl-ΔE1, a replication-incompetent Ad total vector expressing lacZ, into Escherichia coli BJ5183 for homologous recombination, generating the pAd-ΔE1-shMet4, pAd-ΔE1-shMet5, and pAd-ΔE1-shMet4+5 Ad vectors. To verify homologous recombinants, plasmid DNA purified from overnight *E. coli* cultures was digested with HindIII, and the digestion pattern was analyzed. Correct homologous recombinant Ad plasmid DNA was digested with PacI and transfected into 293 cells to generate Ad-ΔE1-shMet4, Ad-ΔE1-shMet5, and Ad-ΔE1-shMet4+5 Ads. E1-deleted, replication-incompetent Ad (Ad-ΔE1) was also prepared.

Generation of VEGF-, IL-8 -, or c-Met-specific shRNA-expressing Ads

All viruses were propagated in 293 cells, and purification, titration, and quality analysis of all Ads used were performed as previously described. The titer (plaque forming units per ml, PFU/ml) used in this study was determined by limiting dilution assay in 293 cells.

Quantitation of VEGF, IL-8, c-Met, and MMP-2 by ELISA

Concentrations of Human VEGF-A, IL-8, c-Met, and MMP-2 in conditioned medium, cell lysate, or tumor tissue lysates were measured using commercially available ELISA kits according to instructions provided by the vendor (VEGF: R & D Systems, Minneapolis, MN; IL-8: Biosource International Inc., Camarillo, CA; c-Met: Biosource International Inc.). Cells were plated in six-well plates in medium containing 10% FBS. When the cells reached subconfluence, cells were infected with Ads at different MOIs. Conditioned media and cells were harvested 72 hr after transduction for recombinant Ads. To remove endogenously expressed, medium was replaced with serum free DMEM 30 hr before each respective harvest time point. Tumor tissue was removed from mice and snap-frozen in liquid nitrogen. Tissues were homogenized in ice-cold PBS with protein inhibitor cocktail (Sigma, Cat #P8340). Homogenates were centrifuged in a high-speed microcentrifuge for 10 min and analyzed for total protein content using a BCA protein assay reagent kit (Bio-rad, Hercules, CA). Levels of VEGF, IL-8, c-Met, or MMP-2 in supernatant were determined by ELISA according to the manufacturer's instructions. Serial dilutions of purified recombinant human VEGF-A, IL-8, c-Met, and MMP-2 were used to establish standard curves. ELISA results were normalized relative to the total protein concentration in

each sample and were calculated as picograms per milligram of total protein.

Tube formation assay

First, 250 µl of growth factor-reduced Matrigel (Collaborative Biomedical Products, Bedford, MA) was pipetted into a 16-mm diameter tissue culture well and polymerized for 30 min at 37°C. HUVECs incubated in M199 containing 1% FBS for 6 hr were harvested after trypsin treatment and suspended in M199 containing 1% FBS. HUVECs were then plated onto the layer of Matrigel at a density of 2 x 10^5 cell/well, and conditioned media from Ad-infected cells were added. VEGF (Upstate Biotechnology, Lake Placid, NY) at 10 ng/ml and conditioned media from uninfected cells were used as controls. Cells were then allowed to form tubes for 20 hr at 37°C, and photographed (×40, ×100). The area covered by the tube network was determined using an optical imaging technique in which pictures of the tubes were scanned into Adobe Photoshop and quantitated using Image-Pro Plus software (Media Cybermetics Inc., Silver Spring, MD).

Ex vivo aortic ring sprouting assay

Aortas were harvested from Sprague Dawley rats (6 weeks old), as described previously [45]. After removing the surrounding fibro-adipose tissues and rinsing with Hank's balanced salt solution (HBSS) buffer, aortas were cut into 1 mm ring segments. Plates (48-well) were coated with 120 µl of

Matrigel; after gelling, rings were placed in the wells and sealed in place with an overlay of 50 µl of Matrigel. Conditioned media from Ad-infected cells (250 µl) were added to the wells. VEGF (20 ng/ml, Upstate Biotechnology) and conditioned media from uninfected cells were used as controls. On day 6, cells were fixed and stained with Diff-Quick. Each ring was scored from 0 (least positive) to 5 (most positive) depending on the degree of vessel sprouting observed. Cultures were scored in a double-blinded manner by three independent observers.

In vivo Matrigel plug assay

U343 cells (2 X 10^5 cells) were plated in 6-well plates and infected with replication-incompetent Ad (Ad-ΔE1, Ad-ΔE1-shVEGF) or replication-competent Ad (Ad-ΔB7, Ad-ΔB7-shVEGF), along with PBS as a negative control. After 2 hr, treated cells were harvested after trypsin treatment, washed three times with 5 ml of HBSS buffer. Cells were then mixed with 600 µl of cold Matrigel and injected with a 1 ml syringe into subcutaneous space above the flank region of the male athymic nu/nu mice. The injected Matrigel rapidly formed a single, solid gel plug. After 14 days, the animals were sacrificed and the skin of each mouse was pulled back to expose the Matrigel plug, which remained intact. To quantify the blood vessel formation, Matrigel plugs were embedded in O.C.T. compound (Sakura Finetec, Torrance, CA),

and cut into 10-μm sections. The cyrosections were treated with purified a monoclonal rat anti-mouse CD31 (platelet/endothelial cell adhesion molecule 1; BD Biosciences PharMingen), at a dilution of 1:50 as a primary antibody, and then with goat anti-rat IgG-HRP (Santa Cruz Biotechnology, Inc., Santa Cruz, CA) as a secondary antibody. All slides were counterstained with Meyer's hematoxylin. Six mice were used for each group.

Migration assay

The lower surface of 6.5-mm-diameter polycarbonate filters (8-μm pore size, Corning Costar, Cambridge, MA) was coated by immersion in 0.1% gelatin. Conditioned media from PBS or Ad-infected cells was placed in the lower part of Transwell chambers, and HUVECs, Hep3B, A549, or U343 cells were placed on the filter membrane on the top chamber. Cultures were incubated at 37 °C for 4 hr, and cells remaining on the upper surface of the filter were removed with a cotton swab. Filters were stained with H&E, and cells that migrated through to the underside of the filter membrane were counted at 200x magnification. Ten fields were counted for each assay, and experiments were repeated at least three times.

Matrigel invasion assay

In vitro invasion assays were carried out using Transwell chambers with 6.5-mm diameter polycarbonate filters (Corning Costar, Cambridge,

MA) according to the manufacturer's instructions. Conditioned media from Ad-infected cells were placed in the lower chambers and Hep3B, A549, or U343 cells (1 x 10^5 cells/ 100 μl) were seeded onto Matrigel-coated filters in the upper chambers. After 24 hr incubation, cells on the upper surface of the filters were removed with a cotton swab, and filters were fixed with 100% methanol and stained with H&E. Cells that had invaded to the lower side of the filters were viewed under an optical microscope. Invasive activity is expressed as the mean number of cells in ten fields from three independent experiments.

Gelatin Zymography

Gelatin zymography was performed in 10% SDS–polyacrylamide gels containing 0.1% gelatin. Samples with conditioned media used in migration and invasion assay were prepared in nonreducing loading buffer. After electrophoresis, SDS was removed by renaturation buffer (2.5% Triton X-100) to renature gelatinases. Gels were then incubated in developing buffer (50 mM Tris-HCl (pH 7.5), 150 mM NaCl and 10 mM $CaCl_2$) for 16 hr at 37°C, and then were stained with 0.25% Coomassie Blue R 250. All experiments were performed at least in triplicate, and representative experiments are shown.

MTT assay

Cells were seeded in 24-well plates to 30-70% confluency and were infected with Ad-ΔE1-shMet4, Ad-ΔE1-shMet5, and Ad-ΔE1-shMet4+5 at MOIs of 50 to 500. At indicated times post infection, 250 ㎕of 3-(4,5-dimethylthiazol-2-yl)-2,5-diphenyl-tetrazolium bromide (MTT; Sigma Chemical Corp.) in phosphate-buffered saline (PBS) was added to each well. After 4 hr incubation at 37℃, the supernatant was discarded and the precipitate was dissolved with 1 ml of dimethylsulfoxide (DMSO). Plates were then read on a microplate reader at 540 nm. All assays were performed in triplicate. Number of living cells was calculated from non-infected cells cultured and treated with MTT in the same condition, as were the experimental groups.

Reverse transcription (RT)-Polymerase chain reaction (PCR) analysis

U343 cells (3×10^5) in 6-well plates were transduced with Ad-ΔE1-shMet4, Ad-ΔE1-shMet5, and Ad-ΔE1-shMet4+5 at MOIs of 50 MOI. Forty-eight hr later, the cells were harvested and total RNA was extracted by using the RNeasy mini kit (Qiagen, Valencia, CA) according to the manufacturer's instructions. For RT-PCR, 1 μg of total RNA was converted to cDNA by treatment with 200 units of M-MLV reverse transcriptase and 500 ng of oligo(dT) primer in 50 mM Tris-HCl (pH 8.3), 75 mM KCl, 3 mM $MgCl_2$, 10

mM dithiothreitol, and 1 mM dNTPs at 37°C for 1 hr. The reaction was stopped by heating at 70°C for 15 min. Two μl of the cDNA mixture was then used for enzymatic amplification. PCR was performed in 50 mM KCl, 10 mM Tris-HCl (pH 8.3), 1.5 mM $MgCl_2$, 0.2 mM dNTPs, 2.5 units of *Taq* DNA polymerase, and 0.1 μM each of primers. The sequences of oligonucleotide primers used in RT–PCR for verification of senescence and the expected transcript sizes are listed in Table 3. The amplification was performed in a DNA thermal cycler (model PTC-200; MJ Research) under the following condition: denaturation at 94°C for 10 min for the first cycle and for 1 min starting from the second cycle, annealing at 55°C for 1 min, and extension at 72°C for 1 min for 30 repetitive cycles. The reaction was terminated with a final cycle of extension (72°C for 10 min). Semi-quantitative RT-PCR was performed using β-actin as an internal control to normalize gene expression for the PCR templates.

Cell cycle analysis

Cells were infected with Ad-ΔE1 or Ad-ΔE1-Met4+5 Ads at an MOI of 30. At indicated times post infection, trypsinized and floating cells were pooled, washed with PBS, and fixed in 70% (v/v) ethanol. For assessment of DNA contents, cells were stained with PI and monitored by a fluorescence-

activated cell sorter (FACS) (Becton Dickinson, Sunnyvale, CA). Cell cycle distribution was determined with the Modifit LT program (Verity Software House Inc.).

HGF specificity assay

U343 cells were seeded in 6-well plates to 20% confluency and were infected for 6 hours with Ad-ΔE1-shMet4, Ad-ΔE1-shMet5, and Ad-ΔE1-shMet4+5 at MOIs of 50. After 24 hr Ad infection, serum free media with or without HGF/SF (R & D Systems, Minneapolis, MN) of 25ng/ml was added to cells and the effects of c-Met inhibition were tested. After 48 hr the cells were washed three times with phosphate-buffered saline (PBS) and cells on the plate were then stained with 0.5% crystal violet in 50% methanol.

Electron microscope (EM) cytology

U343 cells were infected with Ad-ΔE1, Ad-ΔE1-Met4, Ad-ΔE1-Met5, or Ad-ΔE1-Met4+5 at a MOI of 30. Three days postinfection, cells were gently trypsinized and pelleted for 5 minutes at 3000 rpm in a microcentrifuge tube. After washing with phosphate buffered saline (PBS), pellets were fixed for 4 hours at 4℃ in 2.5% glutaraldehyde in 0.1 M sodium cacodylate buffer (pH 7.3) containing 2% sucrose and 1 mM calcium chloride. They were then postfixed with 1% OsO_4 in 0.1 M cacodylate-HCl, pH 7.4, for 1 hr. The samples were dehydrated in a gradient series of ethanol, embedded

in Epon812, and examinined using an electron microscope (EM 902A, Zeiss, Oberkochen, Germany).

Immunoblotting analysis

Cells grown in 100 mm dish were infected with Ad-ΔE1-shMet4, Ad-ΔE1-shMet5, and Ad-ΔE1-shMet4+5 at MOI of 200. Three days postinfection, cells were lysed in 50 mM Tris-HCl (pH 7.6), 1% Nonidet P-40 (NP-40), 150 mM NaCl, and 0.1 mM zinc acetate in the presence of a protease inhibitors. Protein concentration was determined using the bicinchoninic acid method (BCA assay; Pierce, Rockford, IL). Cell lysates or immunoprecipitates were fractionated by SDS-PAGE and transferred to polyvinylidene difluoride (PVDF) membranes. Blocked membranes were then incubated with antibodies against c-Met (diluted 1:50, Santa Cruz Biotechnology, Inc., San Diego, CA) or p44/42 MAP kinase (Erk), phosphor-p44/42 MAPK (Thr202/Tyr204) (phosphor-Erk), MEK1/2, phosphor-MEK1/2 (Ser217/221), Akt, phosphor-Akt (Ser473) (each diluted 1:500, Cell Signaling Technology, Beverly, MA), and the immunoreactive bands were visualized using a using enhanced chemiluminescence (ECL) (Santa Cruz Biotechnology, Inc.).

Assessment of anti-tumor effects in human xenograft model

Male athymic nu/nu mice were obtained from Charles River

(Yokohama, Japan) at 5-6 weeks of age. All mice were housed and handled in accordance with the Animal Research Committee's Guidelines at Yonsei University College of Medicine, and all facilities are approved by AAALAC (association of assessment and accreditation of laboratory animal care). Mice were implanted with 1 x 10^7 U343 human glioma, Hep3B human hepatoma, and A549 human lung cancer cells subcutaneously in the abdominal region. When tumors reached an average size of 70-100 mm^3, Ads were then administered intratumorally (1 x 10^8 PFU) on days 1, 3, and 5. First day of treatment was designated as day 1. Tumor growth was measured three times weekly by a caliper until the end of the study by measuring the length and width of the tumor. Tumor volume was calculated using the following formula: volume = $0.523LW^2$.

Evaluation of tumor xenograft by histology and immunohistochemistry

I used paraffin bloc slide to observe microvessel density (MVD) in tumor. Tumor tissue was fixed in IHC zinc fixative (formalin-free) (BD Biosciences PharMingen, San Diego, CA), embedded in paraffin, and cut into 3-μm sections (Wax-it; Vancouver, Canada). Representative sections were stained with H&E or Masson's trichrome and then examined by light microscopy. To observe microvessel density (MVD), slides were deparaffinized in xylene and then processed as described previously [46]. All

slides were counterstained with Meyer's hematoxylin. Blood vessels were counted as described previously. The most vascular area of tumors was identified on low power (×100) and vessels were counted in ten high-power fields (×200). The data are presented as mean ± SE of three tumors per group. For detecting cleaved deoxynucleotic acids in situ, the same paraffin slides were also used and performed according to the instructions in the ApoTaq peroxidase in situ apoptosis detection kit (Chemicon International, Temecula, CA) [47].

Intratumoral microvessel density assessment

Blood vessels were counted as described previously [48,49]. The most vascular area of tumors was identified on low power (x100) and vessels were counted in ten high-power fields (x200). The data are presented as mean ± SE for three tumors per group.

Statistical Analysis

The data are expressed as mean ± standard error (SE), and the significance of differences between group means was determined by the Mann-Whitney test (nonparametric rank sum test) using Stat View software (Abacus Concepts, Inc., Berkeley, CA). Differences were considered significant when $P < 0.05$.

III. RESULTS

Design of shRNAs directed to the VEGF mRNA

VEGF-A exists in seven different isoforms, VEGF-121, 145, 148, 165, 183, 189, and 206 amino acids in humans. They are generated as a result of alternative splicing from a single VEGF pre-mRNA. To generate interfering RNAs that will degrade all seven VEGF isoforms, I designed two siRNA sequences that were within the $VEGF_{121}$ mRNA (Fig. 1A). Two VEGF-specific shRNA-expressing plasmids were then constructed to express shRNAs under the control of a murine U6 promoter (RNA polymerase III-dependent promoter). The 21-nucleotide VEGF-specific targeting sequence separated by a 9-nucleotide short spacer and five thymidines (T5) as termination signal were annealed and cloned into pSilencer-2.1-hygro-U6 plasmid, generating VEGF-specific shRNA-expressing plasmids, pshVEGF-1 and pshVEGF-2 (Fig. 1B). K562 cells were then transfected with 1 μg of pshVEGF-1 or pshVEGF-2, along with psc-shRNA plasmid (pSilencer-2.1-hygro-U6 encoding scrambled sequence of RNA) as a negative control. At 48 hr post transfection, RT-PCR was performed to determine the endogenous level of VEGF mRNA expression. Relative amounts of RT-PCR products for VEGF were obtained by semi-quantitative PCR against β-actin. As shown in Fig. 1C, of the two VEGF-specific shRNA-expressing plasmids generated,

pshVEGF-2 potently suppressed the expression of VEGF mRNA (> 80%) compared with pshVEGF-1 or control plasmid, psc-shRNA. On the basis of these results, I selected shVEGF-2 as the functional shRNA sequence targeting VEGF and subsequently generated shVEGF-2 expressing Ads.

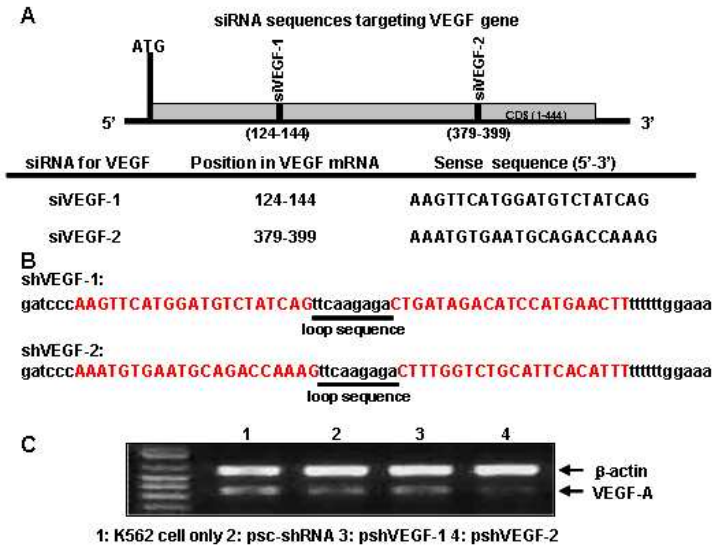

Figure 1. Design and characterization of vascular endothelial growth factor (VEGF)-specific small interfering RNAs (siRNAs). (A) Location of two VEGF-specific siRNAs examined in this study. (B) Sequences for generating two shRNA targeting VEGF, shVEGF-1 and shVEGF-2. (C) shRNA-mediated *in vitro* knockdown of VEGF gene. Cells were transfected for 48 hr with pshVEGF-1 or pshVEGF-2, and the knockdown of endogenous expression was measured by RT-PCR for VEGF. Densitometric analysis was done and the relative expression for each band was normalized with β-actin.

Construction and effects of shVEGF-expressing replication-competent Ad on the expression of VEGF

Although siRNA method is powerful genetic tool for targeting specific knock-down, direct delivery of synthetic siRNA is challenging. I therefore chose replication-competent oncolytic Ad and investigated whether shRNAs can be delivered and more importantly functionally relevant in cancer cells. Previously, we constructed cancer-specific replicating E1A-mutated (at the Rb binding sites of E1A) and E1B-deleted Ad, Ad-ΔB7 [50]. Ad-ΔB7 showed significantly improved cytopathic effect and viral replication in a cancer cell-specific manner. To induce efficient and long-term VEGF silencing, I introduced shVEGF-2 under the control of an U6 promoter at the E3 region of Ad-ΔB7, generating Ad-ΔB7-shVEGF oncolytic Ad.

To investigate whether VEGF-specific shRNA could abrogate VEGF expression, U343 glioma cells were infected with Ad-ΔB7 or Ad-ΔB7-shVEGF at an MOI of 10 and 20. Non-infected cells were used a negative control. After 24 and 48 hr, the conditioned media was harvested and VEGF ELISA was carried out. Surprisingly, the expression and secretion of VEGF was significantly reduced in cells cultured in the presence of conditioned media infected with both Ad-ΔB7 and Ad-ΔB7-shVEGF (Fig. 2A). The significant suppression of VEGF expression by Ad-ΔB7 and Ad-ΔB7-

shVEGF oncolytic Ads that was observed in the U343 cells was also true in the other cancer cell lines (U87MG, Hep3B, and Hep1). Consistent with our findings, other investigators have also reported that suppression of VEGF expression by E1A-expressing replication competent Ads [51-53]. To further demonstrate the effect of E1A-expressing replication-competent Ads in reducing VEGF expression, U343 cells were infected with replication-incompetent E1-deleted Ad (Ad-ΔE1) and replication-competent E1A-expressing Ads (YKL-1, Ad-ΔB7, Ad-ΔB7-shVEGF) at an MOI of 10 and 20. As shown in Fig. 2B, the VEGF protein level was significantly decreased in U343 cells infected with YKL-1, Ad-ΔB7, and Ad-ΔB7-shVEGF Ads in an MOI-dependent manner as compared to those in cells infected with Ad-ΔE1. Consistent with previous findings, data presented here clearly demonstrate that E1A-expressing replication-competent Ads suppress VEGF expression through a preserved E1A region.

Construction and effect of shVEGF-expressing replication-incompetent Ad on the expression of VEGF

Since E1A protein down-regulates VEGF expression, I next constructed E1-deleted replication-incompetent Ad expressing shVEGF-2, Ad-ΔE1-shVEGF, to investigate whether shRNA targeting VEGF would knock-down VEGF expression. To determine the effect of shRNA expression

on VEGF protein levels, a panel of cancer cell lines (U343, Hep3B, Hep1, C33A, U87MG, and A549) was transduced with Ad-ΔE1 or Ad-ΔE1-shVEGF at various MOIs. Four days following transduction, VEGF ELISA was carried out on cell supernatant. Uninfected cells were used as a negative control. As shown in Fig. 2C, the VEGF protein level was significantly decreased in all cancer cell lines transduced with Ad-ΔE1-shVEGF in an MOI-dependent manner. In contrast treatment of cells with Ad-ΔE1, regardless of the applied MOIs, was ineffective. More specifically, Ad-ΔE1-shVEGF almost completely knock-downed VEGF expression in the U343 cells at MOIs of ≥ 100 ($P < 0.001$ versus Ad-ΔE1) and this was also true in other cancer cell lines (Hep3B, Hep1, U87MG) at high MOIs. Despite the reduction in endogenous VEGF protein secretion by Ad-ΔE1-shVEGF-transduced cancer cells, the growth rate of these cells was not different from those cells transduced with Ad-ΔE1. Together, these data show that shVEGF-expressing replication-incompetent Ad, Ad-ΔE1-shVEGF, reduces VEGF expression with high efficiency.

***Ad-ΔE1-shVEGF inhibits angiogenesis* in vitro *and* in vivo**

To determine the functional relevance of VEGF shRNA, I first examined its effects on inhibiting capillary tube formation of HUVEC cells *in vitro*. HUVEC cells seeded onto Matrigel-coated plates were incubated in

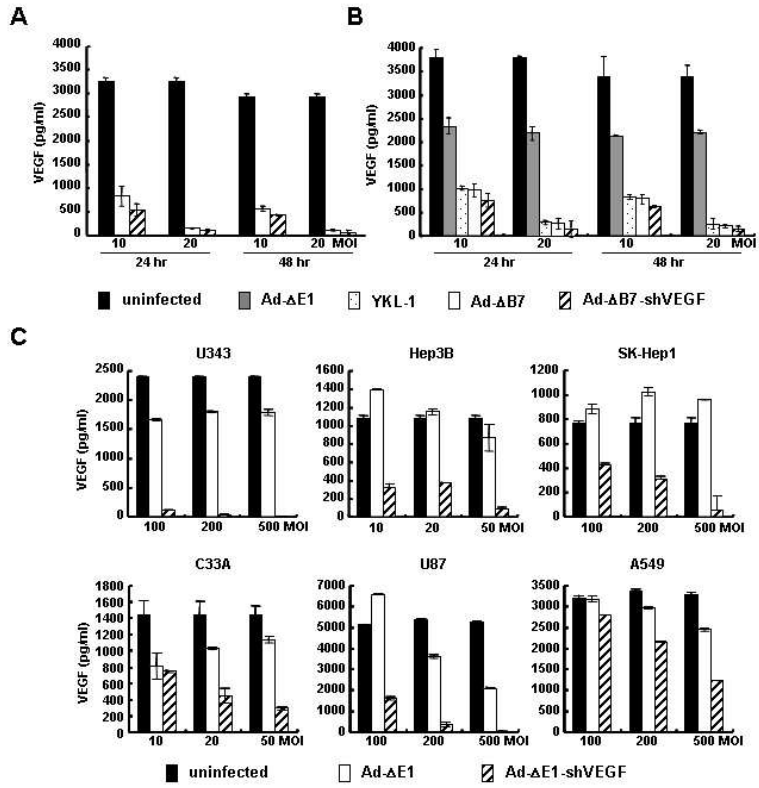

Figure 2. Quantification of VEGF. Human U343 glioma cells were infected with Ad-ΔB7 or Ad-ΔB7-shVEGF Ad (A) and Ad-ΔE1, YKL-1, Ad-ΔB7, or Ad-ΔB7-shVEGF Ad (B) at an MOI of 10 and 20. VEGF concentration was measured in the culture supernatant at 24 hr and 48 hr after infection by ELISA. (C) Various human cancer cell lines were transduced with Ad-ΔE1 or Ad-ΔE1-shVEGF replication-incompetent Ad at range of 10 ~ 500 MOIs. VEGF concentration was measured in the culture supernatant at 96 hr after transduction by ELISA. Each value represents the mean ± SE of at least three independent experiments.

the presence of medium supplemented with human recombinant $rVEGF_{165}$ protein (10 ng/ml), medium conditioned by U343 control cells, Ad-ΔE1-transduced cells, or Ad-ΔE1-shVEGF-transduced cells.

There was no effect within 12 hr of treatment with conditioned media from Ad-ΔE1-shVEGF-transduced cells, but the inhibition was evident at 16 hr and more clearly pronounced at 20 hr with minimal cytotoxicity. Treatment with human recombinant $rVEGF_{165}$ protein and the conditioned medium collected from Ad-ΔE1-transduced U343 cells led to the formation of organized elongated tube-like structures resembling capillaries with an extensive network (Fig. 3A). However, in the presence of Ad-ΔE1-shVEGF-transduced cells' conditioned medium, no such organized structures were observed and the plate was filled with incomplete network of a capillary-like structure. The conditioned medium from Ad-ΔE1-transduced cells only had a mild effect, leading to 8.6% inhibition of tube formation, whereas the conditioned medium from Ad-ΔE1-shVEGF-transduced cells reduced the relative tube length by 49.2% ($P < 0.05$ *versus* Ad-ΔE1) (Fig. 3C). These findings demonstrate that shVEGF-expressing Ad, Ad-ΔE1-shVEGF, functionally inhibits the formation of tube-like structures in the *in vitro* matrigel tube-formation assay.

Next, I tested the ability of Ad-ΔE1-shVEGF to inhibit vessel sprouting using rat aortic rings (explants) embedded in Matrigel beds. The Matrigel bed mimics physiological extracellular matrix representing its natural composition and architecture. Due to these features, Matrigel enables several cell types, including endothelial cells, to maintain in culture their *in vivo* phenotype in 3-dimensional organization. The microvessel sprouting was demonstrated by staining the aortic rings with Diff-Quick as described in the materials and methods section. When aortic rings were cultured in U343 cells' conditioned medium, rapid microvessel outgrowth was observed within 6 days (Fig. 3B). The extent of angiogenesis was comparable to that observed in the presence of human recombinant $rVEGF_{165}$ protein (20 ng/ml). In marked contrast, the aortic rings cultured in the presence of Ad-ΔE1-shVEGF-transduced cells' conditioned medium showed little or no sprouting ($P < 0.001$ *versus* Ad-ΔE1). A marked delay in outgrowth of the sprouts with smaller number of microvessels and branches was observed in the Ad-ΔE1-shVEGF-transduced cells' conditioned medium-treated aortic rings (Fig. 3D). The data further confirms the potent inhibition of angiogenesis induced by Ad-ΔE1-shVEGF.

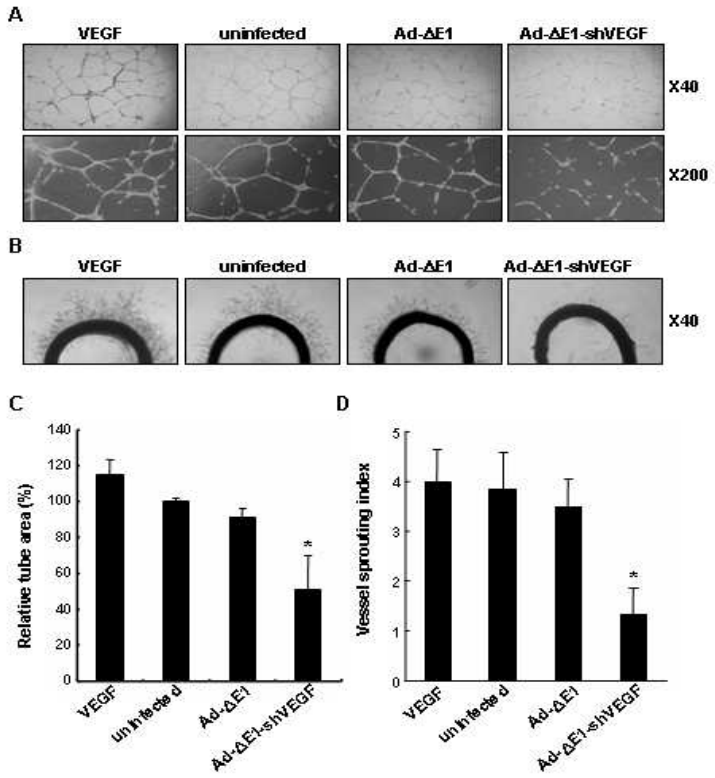

Figure 3. Characterization of replication-incompetent Ad expressing VEGF-specific shRNA. (A) Inhibition of tube formation by Ad-ΔE1-shVEGF. HUVEC cells were plated on Matrigel-coated plates and then incubated in the presence of medium supplemented with human recombinant protein $rVEGF_{165}$, medium conditioned by U343 control cells, Ad-ΔE1-transduced cells, or Ad-ΔE1-shVEGF-transduced cells. After 20 hr, changes in cell morphology were captured using an inverted microscope (×40, ×200). (B) The area covered by the tube network was quantified using Image-Pro Plus software. Experiments

were repeated three times and values are means of triplicates of representative of three independent experiment; bars, ± SE. *, $P < 0.05$ *versus* Ad-ΔE1 treatment. (C) Inhibition of vessel sprouting by Ad-ΔE1-shVEGF. Rat aortic rings in Matrigel were cultured in the presence of medium supplemented with human recombinant protein $rVEGF_{165}$, medium conditioned by U343 control cells, Ad-ΔE1-transduced cells, or Ad-ΔE1-shVEGF-transduced cells, and stained with Diff-Quick on day 6. Representative aortic rings were photographed. Original magnification: ×40. (D) Vessel sprouting index. *, $P < 0.001$ *versus* Ad-ΔE1 treatment. The assay was scored from 0 (least positive) to 5 (most positive) and the data are presented as mean (n=6). Each data point was assayed in sextuplets.

I next examined whether Ad-ΔE1-shVEGF and Ad-ΔB7-shVEGF Ads are capable of blocking angiogenesis *in vivo*. U343 cells were infected with replication-incompetent Ads (Ad-ΔE1 and Ad-ΔE1-shVEGF) at an MOI of 200 or replication-competent Ads (Ad-ΔB7 and Ad-ΔB7-shVEGF) at an MOI of 10. Infected cells were then mixed with cold Matrigel and injected into subcutaneous space above the flank region. Fourteen days later, formed Matrigel were excised and photographed. Matrigel plugs mixed with cells infected with Ad-ΔE1 or Ad-ΔB7 were abundantly filled with angiogenic

vessels (Fig. 4A). However, Matrigel plugs mixed with cells infected with VEGF-specific shRNA-expressing Ads, Ad-ΔE1-shVEGF and Ad-ΔB7-shVEGF, had markedly reduced vascularization after 14 days. The newly formed vessel contents inside the Matrigel plugs were then quantified by counting CD31-positive microvessels (Fig. 4B-C). Treatment with Ad-ΔE1-shVEGF or Ad-ΔB7-shVEGF significantly reduced the number of blood vessels by 76.5% ($P < 0.001$, versus Ad-ΔE1) and 63.2% ($P < 0.001$, versus Ad-ΔB7), respectively, as compared to their cognate control groups. These results indicate that replication-incompetent and replication-competent Ads are capable of expressing functional shVEGF, and efficiently inhibit angiogenesis *in vivo*.

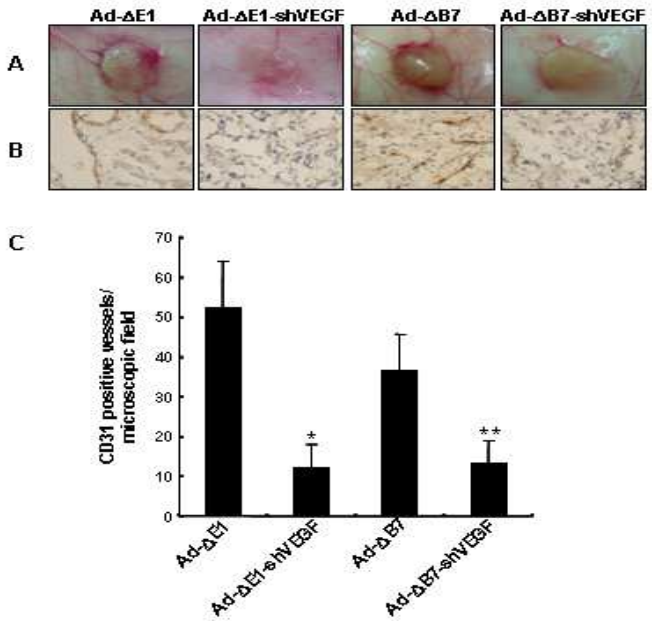

Figure 4. VEGF-specific shRNA-expressing Ads inhibit vascularization in the Matrigel plug assay. Male athymic nu/nu mice were injected s.c. at the flank region with Matrigel mixed with U343 cells infected with Ad-ΔE1, Ad-ΔE1-shVEGF, Ad-ΔB7, or Ad-ΔB7-shVEGF. Matrigel plugs were removed 14 days after implantation, photographed, and prepared for immunohistological examination. Six mice were used for each group. (A) Representative images of Matrigel plugs removed from mice showing reduction in plug vascularization by Ad-ΔE1-shVEGF- and Ad-ΔB7-shVEGF-treated cells. (B) Immunohistochemical staining of sections of Matrigel plugs with anti-CD31 antibody shows reduced numbers of endothelial cells and vessel structures in Ad-ΔE1-shVEGF- and Ad-ΔB7-shVEGF-treated plugs. Original magnification: ×400. (C) The numbers of blood vessels in ×100 were counted and averaged. Each column represents the mean ± SE of the blood vessels per group. *, **; $P < 0.001$ *versus* Ad-ΔE1 or Ad-ΔB7 treatment, respectively.

shVEGF expression does not inhibit viral replication

To determine whether virally expressed shVEGF altered viral replication, VEGF-specific shRNA-expressing replication-competent Ad, Ad-ΔB7-shVEGF, was examined for its potential to induce cytopathic effects. The assay is based on the idea that at low concentrations, viruses need to go

through multiple rounds of infection, replication, viral release, and re-infection of surrounding cells in order to completely wipe out a cell monolayer. Various cancer cells (A549, Hep1, U343, U87MG, Hep3B, C33A) were infected with Ad-ΔB7 or Ad-ΔB7-shVEGF at MOIs of 0.1-20. For a negative control, cells were infected in parallel with replication-incompetent Ad, Ad-ΔE1. As seen in Fig. 5A, virally induced cytopathic effect appeared to be same or slightly faster in Ad-ΔB7-shVEGF as compared to Ad-ΔB7. This result was consistent over several independent experiments, suggesting that shVEGF expression does not inhibit viral replication.

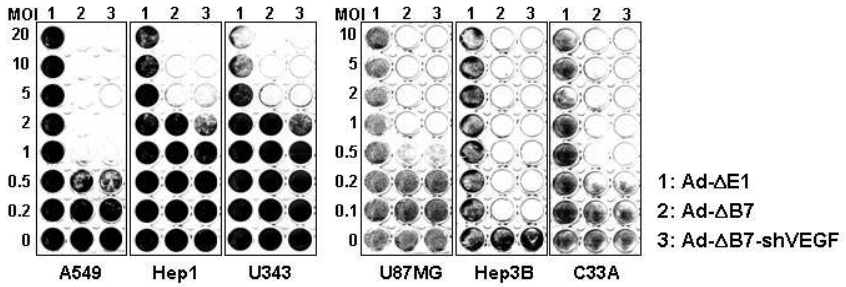

Figure 5. Cytopathic effects of shVEGF-expressing oncolytic Ad. Cells were infected with Ad-ΔE1, Ad-ΔB7, or Ad-ΔB7-shVEGF at the indicated MOIs. At 4 ~ 10 days post-infection, surviving cells were stained using crystal violet. Replication-incompetent Ad, Ad-ΔE1, served as a negative control. Each cell line was tested at least three times, and data shown are from representative experiments.

Enhanced anti-tumor effect of shVEGF-expressing oncolytic Ad

Results from the matrigel plug assay showed that Ad-ΔB7-shVEGF Ad was notably more potent in inhibiting angiogenesis than Ad-ΔE1-shVEGF Ad. Therefore, the oncolytic Ad expressing VEGF-specific shVEGF, Ad-ΔB7-shVEGF, was subsequently assessed for its ability to suppress the growth of U343 human glioma xenograft model established in nude mice and its effects were compared against that of its cognate control Ad, Ad-ΔB7. This U343 tumor model exhibits aggressive tumor growth kinetics. Tumors were generated by subcutaneous injection of cells into the mice abdominal region. When tumors reached an average size of 70-100 mm^3, tumors were injected intratumorally with PBS, Ad-ΔB7 (1 x 10^8 PFU), or Ad-ΔB7-shVEGF Ad (1 x 10^8 PFU) every 2 days for a total of three times (Q2Dx3). As seen in Fig. 6A, control tumors increased to an average size of 2770 ± 27 mm^3 by 48 days after the treatment. By day 48, all mice became moribund in the control group and thus euthanized. In marked contrast, Ad-ΔB7 or Ad-ΔB7-shVEGF Ad-treated tumors reached to an average size of 1660 ± 400 mm^3 and 504 ± 195 mm^3 by 48 days, showing a 37.6% ($P < 0.01$, versus PBS control) and 81% growth inhibition ($P < 0.001$ versus PBS and $P < 0.01$ versus Ad-ΔB7), respectively. Throughout the course of the study, no systemic toxicity, such as diarrhea, loss of weight, or cachexia was observed. Survival rate was also significantly

increased in animals treated with Ad-ΔB7-shVEGF Ad. By day 70 following treatment, 100% of the animals in the Ad-ΔB7-shVEGF Ad group were still viable as compared to 38% in the Ad-ΔB7-treated group (P <0.01). In comparison as mentioned previously all animals in the PBS-treated control group were euthanized by day 48 (Fig. 6B). These data indicate that suppression of VEGF expression by oncolytic Ad had strong inhibitory effects on tumor growth, resulting in increased survival. Moreover, no apparent toxicity was noted in animals that received this Ad during the course of these experiments.

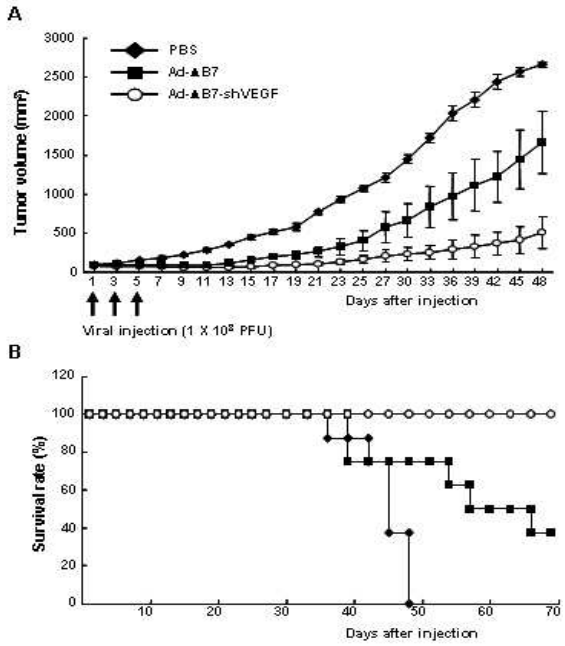

Figure 6. shVEGF-expressing oncolytic adenovirus Ad-ΔB7-shVEGF and the growth of established tumors and survival of mice. Subcutaneous implanted

tumors derived from U343 human glioma cells were treated with Ad-ΔB7 (■) or Ad-ΔB7-shVEGF (○), along with PBS (♦) as a negative control. (A) Tumor volume was monitored over time (days) after treatment with Ads. The arrow indicates when treatment was given (1 x 10^8 PFU/mouse). Values represent the means ± SE for eight animals per group. (B) Overall survival. The survival analysis of Ads treated mice were performed over a period of 70 days. By day 48, all mice in the PBS-treated groups were moribund and euthanized. In comparison, 100% of mice treated with Ad-ΔB7-shVEGF were viable after 70 days.

Antiangiogenic effects of VEGF-specific shVEGF-expressing oncolytic Ad, Ad-ΔB7-shVEGF, in U343 human glioma xenografts

To verify the proposed mechanism of action of VEGF-specific shVEGF-expressing oncolytic Ad, Ad-ΔB7-shVEGF-treated tumors were further investigated by histological examination. Tumors were harvested from each treatment group at 7 days following the three sequential treatments. As seen in Fig. 7A, a marked decrease in number of cells and large areas of necrosis was replaced by fibrous tissue was observed in Ad-ΔB7-shVEGF Ad-treated tumors. Majority of remaining tumor mass treated with Ad-ΔB7-shVEGF was necrotic, whereas necrotic lesions were barely detectable in the tumors treated with PBS or Ad-ΔB7. To determine whether the reduced size

of Ad-ΔB7-shVEGF-treated tumors coincided with reduced neovascularization, microvessel density as assessed using anti-CD31 antibody was determined. A marked decrease in number and size of CD31-positive vessels was observed in Ad-ΔB7-shVEGF Ad-treated tumors. Quantitation of microvessels showed that density was reduced by 79.8% ($P < 0.001$) and 76.7% ($P < 0.001$) in response to Ad-ΔB7-shVEGF Ad treatment as compared to PBS and Ad-ΔB7 Ad treatment groups, respectively (Fig. 7B). Apoptotic cells were also more abundantly detected in Ad-ΔB7-shVEGF-treated tumor tissue than in PBS- or Ad-ΔB7-treated tumor tissue.

Viral persistence and distribution within the tumor mass was also examined by immunohistochemistry using an antibody specific to Ad hexon protein. Ad particles were detected in wide areas of Ad-ΔB7-treated tumors, most frequently in the peripheral tumor area and in between the area of necrosis and proliferating tumor cells. In comparison few numbers of big clusters of Ad particles in patch style were detected in the peripheral tumor area of Ad-ΔB7-shVEGF-treated tumors (Fig. 7A). This staining pattern observed in the tumors treated with Ad-ΔB7-shVEGF indicates that viral replication occurred actively only in tumor areas devoid of necrosis. Moreover, a marked reduction in VEGF expression was measured by ELISA in homogenates of tumors from the Ad-ΔB7-shVEGF oncolytic Ad-treated

group (Fig. 7C). VEGF ELISA demonstrated that treatment of Ad-ΔB7-shVEGF Ad resulted in 64.9% ($P < 0.001$) and 47.4% ($P < 0.05$) reduction compared to tumors treated with PBS and Ad-ΔB7, respectively. This result closely parallels and supports the decreased neovascularization in the tumor mass and enhanced anti-tumor effect of VEGF-specific shVEGF-expressing oncolytic Ad.

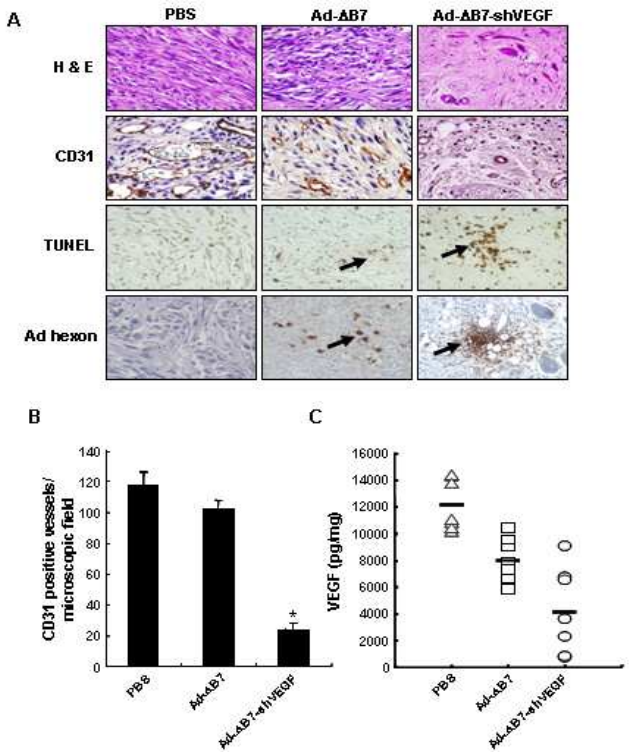

Figure 7. Antiangiogenic effects of VEGF-specific shRNA-expressing oncolytic Ad, Ad-ΔB7-shVEGF, in U343 human glioma xenografts. (A) H & E staining (H &E). Blood vessel density was assessed by

immunohistochemical staining for CD31; Hematoxylin counterstained (CD31). Brown staining indicates positive staining for endothelial cells. TUNEL staining of apoptotic cells in tumor tissue; methyl green counter stained (TUNEL). Tumors treated with Ad-ΔB7-shVEGF exhibited significant increase in apoptotic levels. Greater dark brown nuclei with double-strand DNA breaks (indicated by an arrow) can be seen in tumors treated with Ad-ΔB7-shVEGF as compared to PBS- or Ad-ΔB7-treated groups. Immunohistochemical staining of Ad hexon protein to localize Ad in tumor tissue; Hematoxylin counterstained (Ad hexon). Ad-infected cells stain brown as indicated by an arrow. Original magnification: ×400. (B) The mean microvessel density for each treatment group was determined by counting the number of CD31-positive vessels in ten high-power fields (×200) of each section in a blinded fashion. Three tumors per group were analyzed, and all data are shown as mean ± SE. *, $P < 0.001$ *versus* PBS or Ad-ΔB7 treatment. (C) VEGF contents in tumors. Treatment of Ad-ΔB7-shVEGF Ad results in significant reduction in VEGF levels as compared to treatment of PBS or Ad-ΔB7. Each data point represents mean VEGF levels for each individual tumor (7 mice per group) and the mean VEGF level for each group is represented by a line. VEGF level is expressed as picograms per milligram of total protein.

Improved efficacy of oncolytic Ad-mediated siRNA expression over replication-incompetent Ad-mediated siRNA

To better understand the time-course and magnitude of the gene silencing effect *in vitro*, I treated U343 cells with either Ad-ΔE1-shVEGF at an MOI of 100 or Ad-ΔB7-shVEGF at an MOI of 0.1, and assessed its gene silencing effect at various time points. The rationale for the difference in MOI for the two Ads is based on the fact that the oncolytic Ad is highly efficient in its cell killing effect that if the MOI is too high the interpretation of the data would be too difficult. As expected, on days 3 and 7 after Ad-ΔE1-shVEGF treatment, VEGF expression levels were 80% and 91% lower than those from untreated control, respectively, demonstrating the efficient suppression of VEGF expression of Ad-ΔE1-shVEGF up to 7 days after transduction (Fig. 8A). However on day 14, the Ad-ΔE1-shVEGF's efficacy was significantly attenuated, showing only 48% suppression compared to untreated control. In marked contrast, VEGF expression level was not visibly reduced in cells infected with Ad-ΔB7-shVEGF even until day 7. However, by day 14 VEGF expression was significantly suppressed by 98%, demonstrating that the propagation, amplification and release of viral progeny to neighboring cells takes ~two weeks to see the functional effects in this model system.

I next compared the duration and magnitude of siRNA-mediated

gene silencing elicited by Ad-ΔE1-shVEGF and Ad-ΔB7-shVEGF *in vivo*. When U343 tumors reached an average size of 70-100 mm^3, tumors were injected intratumorally with PBS, or with 3 x 10^8 PFU of either Ad-ΔE1-shVEGF or Ad-ΔB7-shVEGF Ad every 2 days for a total of three times (Q2Dx3). Tumors were then harvested at day 7 and 21 after viral injection, and VEGF expression was measured by ELISA. As shown in Fig. 8B, following 7 days of treatment, a marked suppression of VEGF expression was observed in tumor tissues treated with Ad-ΔE1-shVEGF or Ad-ΔB7-shVEGF, resulting in 58.5% and 87.3% reduction compared to PBS-treated control tumors, respectively. On day 21 however, there was almost no suppression of VEGF expression for those tumors treated with Ad-ΔE1-shVEGF. In contrast, VEGF expression was significantly suppressed by 62.5% in the tumor treated with Ad-ΔB7-shVEGF compared to PBS-treated control tumors in the same time period. These results demonstrate that *in vivo*, replication-competent Ad-mediated siRNA expression results in improved efficacy as well as sustained gene silencing effect over replication-incompetent Ad.

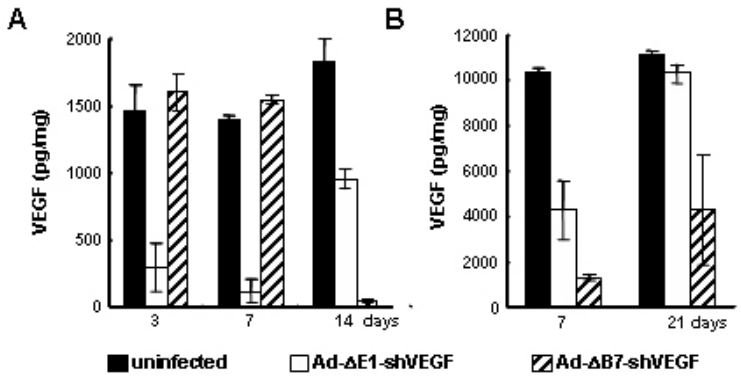

Figure 8. Time-course and magnitude of the VEGF gene silencing effect of Ad-ΔE1-shVEGF or Ad-ΔB7-shVEGF Ad. (A) Human U343 glioma cells were treated with Ad-ΔE1-shVEGF or Ad-ΔB7-shVEGF Ad at an MOI of 100 or 0.1, respectively. VEGF expression level was assessed at 3, 7, and 14 days after viral treatment. Each value represents the mean ± SE of at least three independent experiments. (B) U343 xenograft models were injected intratumorally with PBS, 3 x 10^8 PFU of either Ad-ΔE1-shVEGF or Ad-ΔB7-shVEGF Ad every 2 days for a total of three times. Tumors were then harvested on day 7 and 21 after Ad administration and subjected to VEGF ELISA. VEGF level is expressed as picograms per milligram of total protein. Results represent the mean ± SE of three animals per group.

Identification of effective siRNA sequences and generation of replication-incompetent Ads expressing shRNA specific to IL-8

To identify siRNA effective sequences against IL-8, I examined four

siRNAs targeting different regions of human IL-8 mRNA (gi:28610153) as described in Table 1. Of the various cancer cell lines assessed, Hep3B expressed the highest IL-8 levels. To evaluate possible off-target effects, Hep3B cells were also transfected with siRNA specific to lamin A/C and luciferase. Relative amounts of IL-8 were measured by semi-quantitative RT-PCR, normalized to β-actin. As shown in Fig. 9A, of the four siRNAs synthesized, IL-8 siRNA No. 2 (194-212) most potently suppressed the expression of IL-8 mRNA (> 90%). Transfection with lamin A/C- and luciferase-specific siRNA resulted in no significant alteration of IL-8 RNA expression compared to non-transfected HepB cells. On the basis of these results, IL-8 siRNA No.2 was chosen to generate shRNA specific to IL-8 for use in subsequent experiments.

Table 1. Sequences of the four IL-8-specific siRNAs examined in this study

Number	positions	sequences
#1	178 – 198	caaggagtgctaaagaactta
#2	194 – 212	gaacttagatgtcagtgcata
#3	250 – 270	aagaactgagagtgattgaga
#4	279 – 297	cacactgcgccaacacagaaa

Two IL-8-specific shRNA-expressing replication-incompetent adenoviruses, Ad-ΔE1-U6shIL8 and Ad-ΔE1-CMVshIL8 (Fig. 9B), were

constructed to express shRNAs under the control of the murine U6 promoter (RNA polymerase III-dependent promoter) and the CMV promoter (RNA polymerase II-dependent promoter), respectively. The 19-nucleotide IL-8-specific targeting sequence, separated by a 9-nucleotide short spacer and including five thymidines (T5) as a termination signal was annealed and cloned into the pdl-ΔE1 adenoviral total vector, generating Ad-ΔE1-U6shIL8 and Ad-ΔE1-CMVshIL8.

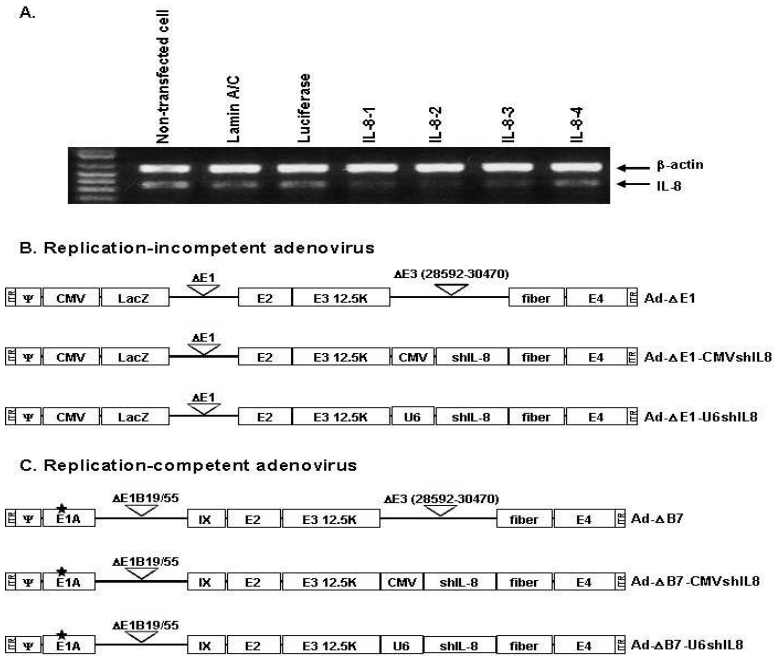

Figure 9. Characterization of IL-8-specific small interfering RNAs (siRNAs) and the structure of adenoviruses used in this study. (A) siRNA-mediated *in vitro* knockdown of IL-8 transcripts. Cells were transfected for 48 hr with four IL-8-specific siRNAs, along with siRNA specific to lamin A/C and luciferase

as controls. Knockdown of endogenous expression was measured by RT-PCR for IL-8. Densitometric analysis was performed and the relative expression of each band was normalized to β-actin. (B, C) Schematic representation of the genomic structure of adenovirus vectors used.

***Comparison of U6 and CMV promoters in IL-8 knockdown* in vitro**

To compare promoter efficiency in the knockdown of IL-8 expression, a panel of cancer cell lines (Hep3B, Huh7, Hep1, HepG2, U87, U251N, U343, and A549) was transduced with Ad-ΔE1, Ad-ΔE1-CMVshIL8, or Ad-ΔE1-U6shIL8 at various MOIs. Non-transduced cell lines were also used as negative controls. After 72 hr, conditioned media was harvested and an IL-8 ELISA was carried out. As shown in Fig. 10A, the synthesis and secretion of IL-8 was significantly reduced by Ad-ΔE1-U6shIL8. In Hep3B cells, IL-8 levels was decreased by 73.7% and 73.4% ($P < 0.05$ and $P < 0.05$) compared to non-transduced and control adenovirus (Ad-ΔE1)-transduced cells, whereas the reduction was only 8.2% and 7% with Ad-ΔE1-CMVshIL8. This efficient knockdown of IL-8 by Ad-ΔE1-U6shIL8 was also observed in each of the other cancer cell lines tested. Moreover, Ad-ΔE1-U6shIL8 strongly silenced IL-8 expression even at low MOIs, whereas a notably higher MOI of Ad-ΔE1-CMVshIL8 was needed for effective knockdown (Fig. 10B). Despite the reduction in endogenous IL-8 protein secretion by Ad-ΔE1-U6shIL8-

transduced cancer cells, the growth rate of these cells was not different from cells transduced with Ad-ΔE1. Together, these data show that IL-8-specific shRNA-expressing Ads reduce IL-8 expression, and, more importantly, that the U6 promoter is much more effective in driving IL-8-specific shRNA expression than the CMV promoter.

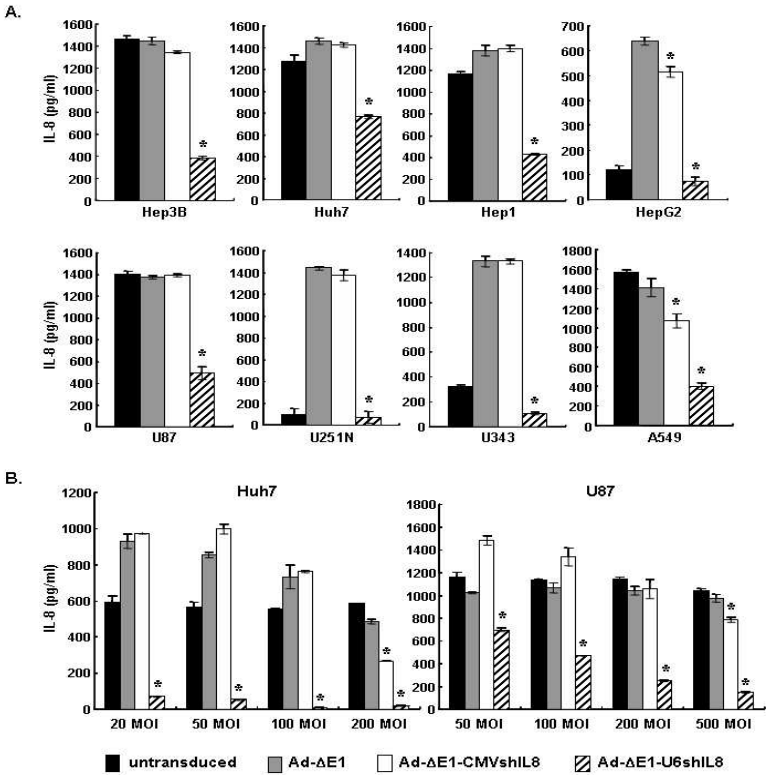

Figure 10. Quantitation of IL-8 secreted by cells transduced with replication-incompetent Ads. (A) Various human cancer cell lines were transduced with replication-incompetent Ad-ΔE1, Ad-ΔE1-CMVshIL8, or Ad-ΔE1-U6shIL8 in a range of 20 ~ 1000 MOI. IL-8 concentration was measured in culture

supernatants 72 hr after transduction by ELISA. *P<0.05 versus Ad-ΔE1 treatment. (B) Dose-dependent suppression of IL-8 expression by Ad-ΔE1-CMVshIL8 and Ad-ΔE1-U6shIL8. Each value represents the mean ± SE of at least three independent experiments. *P<0.05 versus Ad-ΔE1 treatment.

Effect of IL-8-specific shRNA expression on the function of endothelial cells in vitro

I investigated the effects of Ad-mediated IL-8-specific shRNA expression on the migration of HUVECs *in vitro*. Conditioned medium from A549 cells transduced with Ad-ΔE1-U6shIL8 reduced the migration of endothelial cells by 48.8% ($P < 0.001$ compared to Ad-ΔE1). In comparison, conditioned medium from Ad-ΔE1-CMVshIL-8-transduced cells inhibited migration only 24% ($P < 0.05$ compared to Ad-ΔE1) (Fig. 11A). Nearly identical results were observed using conditioned medium from Hep3B cell lines.

I then assessed the functional effect of Ad-mediated IL-8-specific shRNA expression on capillary tube formation *in vitro*. HUVEC cells seeded onto Matrigel-coated plates were incubated in the presence of medium supplemented with human recombinant $rVEGF_{165}$ protein (10 ng/ml) or with conditioned medium from Ad-ΔE1-, Ad-ΔE1-CMVshIL8-, or Ad-ΔE1-

U6shIL8-transduced cells. As shown in Fig. 11B, conditioned medium from Ad-ΔE1-U6shIL8-transduced cells effectively inhibited HUVEC tube formation, whereas $rVEGF_{165}$ and conditioned media collected from Ad-ΔE1- and Ad-ΔE1-CMVshIL8-transduced cells resulted in the formation of robust, elongated tube-like structures, which were organized in much larger numbers of cells. In particular, conditioned medium from Ad-ΔE1-U6shIL8-transduced cells diminished relative tube length by 65.5% ($P < 0.001$ compared to Ad-ΔE1, Fig. 11C).

Microvessel sprouting was demonstrated by staining aortic rings with Diff-Quick, as described in materials and methods. As shown in figures 11D and 11E, a marked delay in the outgrowth of sprouts from explants, with a regression in both the number of microvessels and the number of branches, was observed in aortic rings treated with conditioned medium from Ad-ΔE1-U6shIL8-transduced cells, showing a decrease in the number of microvessels of 68.2% ($P < 0.001$) and 65% ($P < 0.001$) compared to untransduced and Ad-ΔE1-transduced conditioned media, respectively. In contrast, neither Ad-ΔE1 nor Ad-ΔE1-CMVshIL8 had an inhibitory effect on microvessels sprouting from aortic rings. In fact, the extent of the capillary network was comparable to that observed in the presence of conditioned medium from untransduced

cells. These data further confirm the potent inhibition of angiogenesis induced by Ad-ΔE1-U6shIL8.

Effect of IL-8-specific shRNA expression on tumor cell migration, invasion, and MMP-2 expression

I next examined the effect of IL-8-specific shRNA expression on tumor cell invasion. Quantitative analysis showed that conditioned media collected from Ad-ΔE1-U6shIL8-transduced Hep3B and A549 cancer cells effectively blocked cellular migration and invasion after 24 hr; by 57.9% ($P < 0.05$ *versus* Ad-ΔE1) and 54% ($P < 0.05$ *versus* Ad-ΔE1) for Hep3B cells and by 61.1% ($P < 0.05$ *versus* Ad-ΔE1) and 53.3% ($P < 0.05$ *versus* Ad-ΔE1) for A549 cells (Fig. 12A, 12B). In contrast, conditioned media collected from non-transduced and Ad-ΔE1-transduced cells, failed to affect migration and basal invasion of cancer cells.

MMP expression on cancer cells as well as vascular endothelial cells has been shown to regulate neovascularization by enhancing peri-cellular fibrionolysis and cellular locomotion. Of the number of MMP family members, MMP-2 plays a critical role in the angiogenic switch during carcinogenesis. By using conventional gelatin zymography, I compared

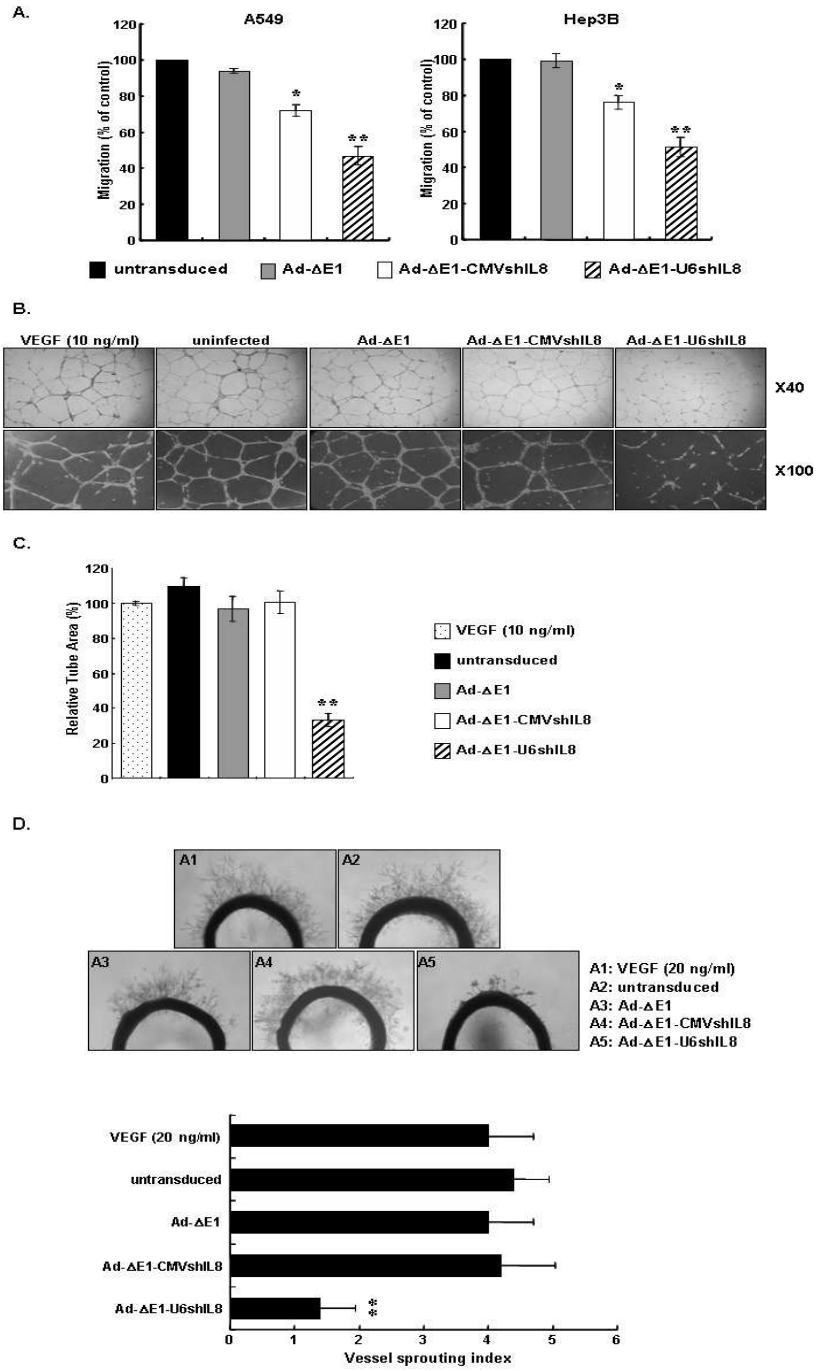
A.
A549
Hep3B
Migration (% of control)
120
100
80
60
40
20
0
*
**
untransduced
Ad-ΔE1
Ad-ΔE1-CMVshIL8
Ad-ΔE1-U6shIL8
B.
VEGF (10 ng/ml)
uninfected
Ad-ΔE1
Ad-ΔE1-CMVshIL8
Ad-ΔE1-U6shIL8
X40
X100
C.
Relative Tube Area (%)
VEGF (10 ng/ml)
untransduced
Ad-ΔE1
Ad-ΔE1-CMVshIL8
Ad-ΔE1-U6shIL8
D.
A1
A2
A3
A4
A5
A1: VEGF (20 ng/ml)
A2: untransduced
A3: Ad-ΔE1
A4: Ad-ΔE1-CMVshIL8
A5: Ad-ΔE1-U6shIL8
VEGF (20 ng/ml)
untransduced
Ad-ΔE1
Ad-ΔE1-CMVshIL8
Ad-ΔE1-U6shIL8
0
1
2
3
4
5
6
Vessel sprouting index

Figure 11. Effects of Ad-mediated IL-8-specific shRNA expression on migration, tube formation, and vessel sprouting of endothelial cells. (A) HUVEC cell migration. Migratory cells are represented as the number of migrated cells per high-power field (200x). Ten fields were counted in triplicate from each sample. bars, ± SE. *, $P < 0.05$ *versus* Ad-ΔE1 treatment; **, $P < 0.001$ *versus* Ad-ΔE1 treatment. (B, C) Tube formation assay. (B) HUVEC cells were plated on Matrigel-coated plates at a density of 2 x 10^5 cells/well and incubated in the presence of medium supplemented with human recombinant $rVEGF_{165}$ (10 ng/ml), control conditioned medium from Hep3B cells, or conditioned medium from Ad-ΔE1-, Ad-ΔE1-CMVshIL8-, or Ad-ΔE1-U6shIL8-transduced cells. After 20 hr, changes in cell morphology were captured using an inverted microscope. Original magnification: 40x and 100x. (C) The area covered by the tube network was quantified using Image-Pro Plus software. Experiments were repeated three times and values are means of triplicate measurements from one representative experiment; bars, ± SE. **, $P < 0.001$ *versus* Ad-ΔE1 treatment. (D, E) Aorta ring sprouting assay. (D) Aortic rings in Matrigel were cultured in the presence of medium supplemented with human recombinant $rVEGF_{165}$ (20 ng/ml), control conditioned medium from Hep3B cells, or conditioned medium from Ad-ΔE1-, Ad-ΔE1-CMVshIL8-, or Ad-ΔE1-U6shIL8-transduced cells for six

days, then stained with Diff-Quick. Representative aortic rings were photographed. Original magnification: 40x. (E) The assay was scored from 0 (least positive) to 5 (most positive) and data are presented as mean ± SE (n=6). **, $P < 0.001$ *versus* Ad-ΔE1 treatment.

gelatinolytic activity of MMP-2 in response to Ad-ΔE1-, Ad-ΔE1-CMVshIL8, and Ad-ΔE1-U6shIL8-transduced U343 and U251N cancer cells. As shown in Fig. 12C, MMP-2 gelatinolytic activity was reduced in Ad-ΔE1-U6shIL8-transduced cells, whereas Ad-ΔE1- or Ad-ΔE1-CMVshIL8-transduced cancer cells showed MMP-2 activity similar to the levels observed for parental cells. ELISA quantitation of MMP-2 protein in A549 cancer cells transduced with Ad-ΔE1-U6shIL8 indicated that a reduction in the MMP-2 protein level closely paralleled the observed loss of MMP-2 gelatinolytic activity (Fig. 12D). These results strongly suggest that Ad-ΔE1-U6shIL8 inhibits invasion of cancer cells, presumably through the inhibition of MMP-2 activity.

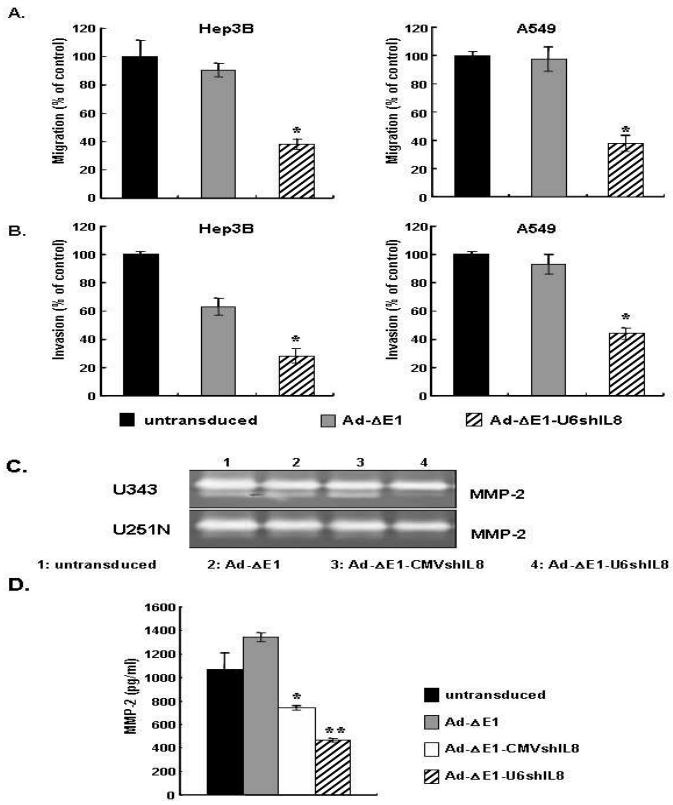

Figure 12. Inhibition of cancer cell migration, invasion, and MMP-2 expression by Ad-ΔE1-U6shIL8. (A) Quantitative evaluation of Hep3B and A549 cancer cell migration. Experiments were performed in triplicate and repeated three times, means ± SE are shown. *, $P < 0.05$ *versus* Ad-ΔE1 treatment. (B) Tumor cell invasiveness was quantified as the mean number of cells in ten fields of view per filter. Experiments were performed in triplicate and repeated three times, means ± SE are shown. *, $P < 0.05$ *versus* Ad-ΔE1 treatment. (C) Zymographic detection of secreted gelatinase activity in conditioned media from U343 and U251N cells treated with AdΔE1, AdΔE1-

CMVshIL8, or AdΔE1-U6shIL8. This is one representative result from three independent experiments. (D) Modulation of MMP-2 protein expression in A549 cells transduced with Ads. Human MMP-2 concentration in conditioned media was determined by ELISA. Each bar represents the mean ± SE (n = 3). *, $P < 0.05$ *versus* Ad-ΔE1 treatment. **, $P < 0.001$ *versus* Ad-ΔE1 treatment.

Generation and characterization of oncolytic Ad expressing shIL-8

To induce long-term IL-8 silencing, I introduced shIL-8 under the control of CMV and U6 promoters at the E3 region of Ad-ΔB7, generating Ad-ΔB7-CMVshIL8 and Ad-ΔB7-U6shIL8 oncolytic Ad, respectively (Fig. 9C). To determine whether virally expressed shIL-8 altered viral replication, the newly engineered Ads were first examined for their potential to induce cytopathic effects. Multiple cancer cells (A549, U343, Hep1, U87, and Hep3B) were infected with Ad-ΔB7, Ad-ΔB7-CMVshIL8, or Ad-ΔB7-U6shIL8 at MOIs of 0.1-20. As a negative control, cells were infected in parallel with replication-incompetent Ad, Ad-ΔE1. As seen in Fig. 13A, virally induced cytopathic effects appeared to be similar with Ad-ΔB7-CMVshIL8 and Ad-ΔB7-U6shIL8 as compared to Ad-ΔB7. This result was consistent over several independent experiments, suggesting that shIL-8 expression does not inhibit viral replication.

Next, I examined whether shIL-8-expressing oncolytic Ads can

functionally knock-down IL-8 expression. Hep3B and A549 cells were infected with Ad-ΔB7, Ad-ΔB7-CMVshIL8, or Ad-ΔB7-U6shIL8 at MOIs of 0.5 and 10, respectively. As shown in Fig. 13B, significant suppression of IL-8 expression by Ad-ΔB7-U6shIL8 oncolytic Ad was observed in both Hep3B and A549 cell lines with 62.1% ($P < 0.001$ versus Ad-ΔB7) and 53.4% ($P < 0.001$ versus Ad-ΔB7) decrease in IL-8 protein level, respectively. To demonstrate IL-8 specificity of Ad-ΔB7-U6shIL8, cells were also infected with Ad-ΔB7-U6shVEGF, an oncolytic Ad expressing VEGF-specific shRNA under the control of the U6 promoter. As predicted, no inhibition of IL-8 expression was observed in response to Ad-ΔB7-U6shVEGF treatment. IL-8 protein levels were also considerably decreased in both Hep3B and A549 cells infected with cognate control oncolytic Ad, Ad-ΔB7. This is in agreement with ours' and other investigators' previous findings that E1A expression suppresses tumor angiogenesis [47,51,53]. Together, these data demonstrate that oncolytic Ad-ΔB7-U6shIL8 reduced IL-8 expression with high degree of efficiency as well as high specificity.

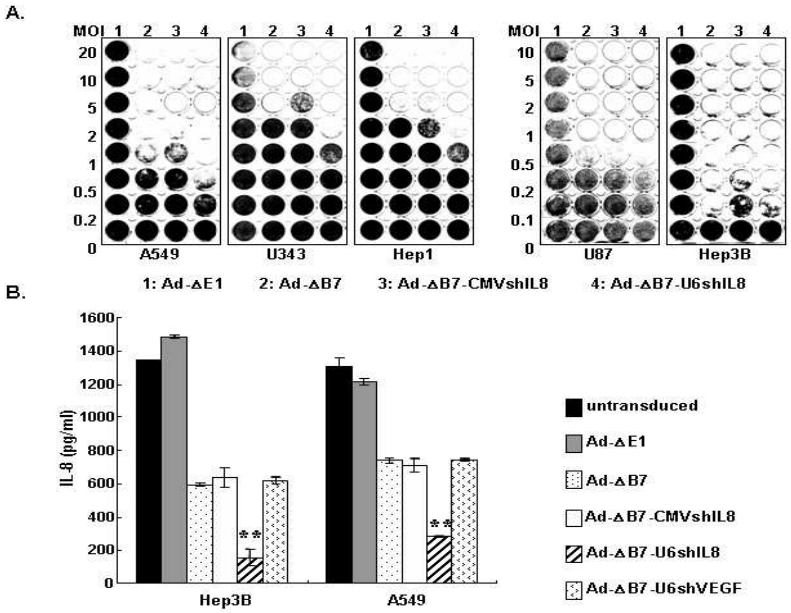

Figure 13. Characterization of IL-8-specific shRNA-expressing oncolytic Ads. (A) Semiquantitative assessment of cytotoxic potency by crystal violet cytopathic effect (CPE) assay. Cells were infected with Ad-ΔE1, Ad-ΔB7, Ad-ΔB7-CMVshIL8, or Ad-ΔB7-U6shIL8 at the indicated MOIs. At 4 ~ 10 days post-infection, surviving cells were stained using crystal violet. Replication-incompetent Ad, Ad-ΔE1, served as a negative control. Each cell line was tested at least three times, and data shown are from representative experiments. (B) Quantitation of IL-8. Hep3B and A549 cells were infected with Ad-ΔE1, Ad-ΔB7, Ad-ΔB7-CMVshIL8, or Ad-ΔB7-U6shIL8 adenovirus (MOI of 0.5 for Hep3B and 10 for A549). IL-8 was measured in culture supernatants by ELISA 24 hr after infection. Each value represents the mean

± SE of at least three independent experiments. **, $P < 0.001$ *versus* Ad-ΔE1 treatment.

Oncolytic adenovirus expressing shIL-8 inhibits tumor growth in nude mice

Since Ad-ΔB7-U6shIL8 exhibited greater IL-8 suppressive effect than Ad-ΔB7-CMVshIL8, oncolytic Ad-ΔB7-U6shIL8 was chosen to examine its effect *in vivo*. Hep3B and A549 tumor models established in nude mice showed aggressive growth kinetics. When tumors reached an average size of 100 mm^3, tumors were injected intratumorally with PBS, Ad-ΔB7, or Ad-ΔB7-U6shIL8 every 2 days for a total of three injections (Q2Dx3). As seen in Fig. 14A, tumor volume was greatly reduced in mice treated with both oncolytic Ads (Ad-ΔB7 and Ad-ΔB7-U6shIL8) compared to control mice treated with PBS. At 35 days after viral treatment, tumors of Hep3B tumor-bearing mice treated with PBS reached an average tumor volume of 3672 ± 575 mm^3 and the average tumor volumes for the Ad-ΔB7 and Ad-ΔB7-U6shIL8 groups were 942.68 ± 107 mm^3 and 335.61 ± 91 mm^3, respectively. Similarly, mice bearing A549 tumor xenograft showed tumor growth inhibition of 91.7% ($P < 0.001$) in response to Ad-ΔB7-U6shIL8 treatment. Throughout the course of the study, no systemic toxicity, such as diarrhea, loss of weight, or cachexia was observed. These data indicate that suppression of IL-8 expression by oncolytic Ad had strong inhibitory effects on the growth

of these tumor xenografts.

The histology of tumors obtained 7 days post final dose was then observed. As shown in Fig. 14B, H & E staining of A549 tumors treated with Ad-ΔB7-U6shIL8 showed dramatic effects as only number of viable tumor cells were observed. In addition apoptotic changes and cell necrosis, surrounded by stromal fibrosis was also seen. Masson's trichrome staining determined collagen type I, stained in blue, as the predominant morphological component of these fibrotic changes. Microvessel density was then examined by immunostaining with anti-PECAM (anti-CD31) antibody. A marked decrease in endothelial cells and vessel structures was observed in Ad-ΔB7-U6shIL8-treated tumors compared to PBS- or Ad-ΔB7-treated tumors. Quantitation of microvessels showed that the density was reduced by 44.7% ($P < 0.05$) and 50.6% ($P < 0.05$) in Hep3B and A549 xenograft models, respectively, compared to Ad-ΔB7 (Fig. 15A). To analyze the degree to which Ad-ΔB7-U6shIL8 induced apoptosis *in vivo*, TUNEL assay was carried out using the same tumor sections. As seen in Fig. 14B, the level of apoptosis was considerably higher in Ad-ΔB7-U6shIL8-treated tumor tissue than in PBS- or Ad-ΔB7-treated tumor tissue. This result closely parallels and supports the decreased neovascularization in the tumor mass and enhanced anti-tumor effect of IL-8-specific shRNA-expressing oncolytic Ad.

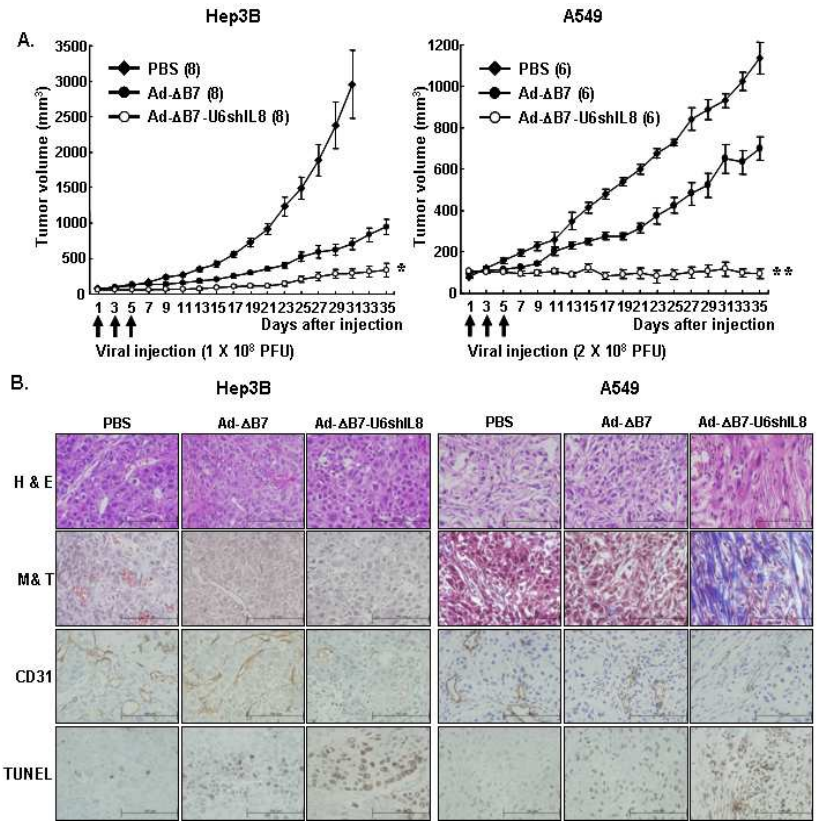

Figure 14. Effect of oncolytic adenovirus expressing IL-8-specific shRNA *in vivo*. (A) Subcutaneous implanted tumors derived from Hep3B and A549 cells were treated with Ad-ΔB7 (●) or Ad-ΔB7-U6shIL8 (○), along with PBS (♦) as a negative control. Tumor volume was monitored over time (days) after treatment with Ads. The arrow indicates when Ad was administered (1 x 10^8 PFU/mouse for Hep3B and 2 x 10^8 PFU/mouse for A549). The number of animals per group is indicated in parentheses. Values represent the mean ± SE. *, $P < 0.05$ *versus* Ad-ΔB7. **, $P < 0.001$ *versus* Ad-ΔB7. (B) Photos of

representative tumor sections from animals in each group. Hematoxylin & eosin staining (H & E). Masson's trichrome staining of extracellular matrix (blue) in the tumor tissue sections (M & T) and hematoxylin counter-stained. Microvessels were stained with anti-PECAM antibody (CD31) and hematoxylin counter-stained. Brown staining indicates positive staining for endothelial cells. TUNEL staining of apoptotic cells in tumor tissue; methyl green counter stained (TUNEL). Original magnification: 400x.

To investigate the biological significance of IL-8 down-regulation in tumor tissue, I assessed IL-8 and VEGF expression in tumor tissues. As shown in Fig. 15B, significant suppression of IL-8 expression by Ad-ΔB7-U6shIL8 oncolytic Ad was observed in both Hep3B and A549 cell lines with 31.5% ($P < 0.001$ versus Ad-ΔB7) and 71.2% ($P < 0.05$) reduction, respectively. Moreover, VEGF ELISA demonstrated that treatment with Ad-ΔB7-U6shIL8 resulted in 65% ($P < 0.05$ versus PBS) and 68.2% ($P < 0.05$) reduction in Hep3B and A549, respectively (Fig. 15C). These findings suggest that IL-8-specific shRNA down-regulated the expression of both IL-8 and VEGF, key mediators of angiogenesis.

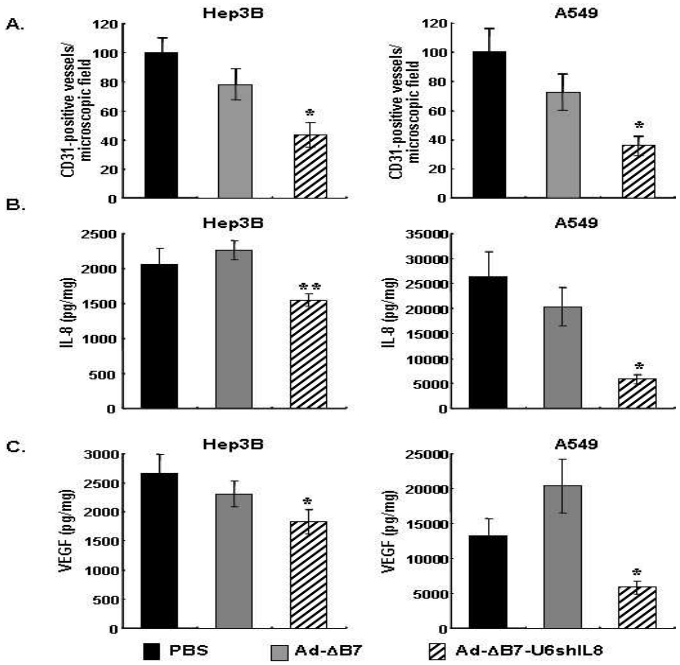

Figure 15. Effect of oncolytic adenovirus expressing IL-8-specific shRNA *in vivo*. (A) Reduction in microvessel density following treatment with Ad-ΔB7-U6shIL8. Mean microvessel density was determined by counting CD31-positive vessels in ten high-power fields (200x) of each section in a blinded fashion. Error bars represent SE. *, $P < 0.05$ compared to Ad-ΔB7 treatment. (B) IL-8 expression in tumors. (C) VEGF expression in tumors. Each data point represents mean IL-8 and VEGF levels for each individual tumor. *, $P < 0.05$ *versus* Ad-ΔB7. **, $P < 0.001$ *versus* Ad-ΔB7.

Activation of angiogenesis is also responsible for increased tumor cell entry into circulation and metastasis. Therefore, I investigated whether suppression of IL-8 expression also blocked metastasis of a malignant human

breast cancer cell line, MDA231. Administration of Ad-ΔB7-U6shIL8 resulted in a marked reduction of metastatic burden. More specifically, three of 7 mice showed no metastatic spread and the remaining two exhibited minimal tumor spread as compared to control animals treated with PBS or Ad-ΔB7. These data indicate that suppression of IL-8 expression had a strong inhibitory effect on tumor metastasis.

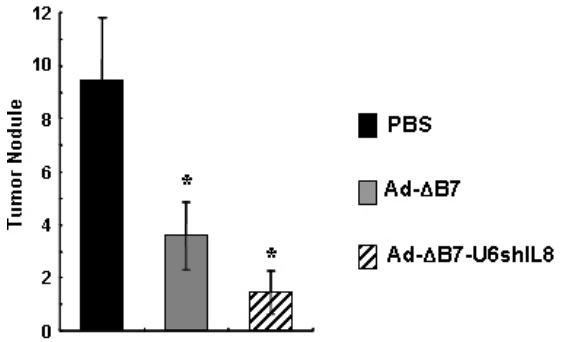

Figure 16. Ad-ΔB7-U6shIL8 treatment inhibits tumor metastasis. MD231 human breast cancer cells were injected intravenously to form pulmonary metastatic lesions. After 23 days, mice received intrapleural injections of PBS, Ad-ΔB7, or Ad-ΔB7-U6shIL8. On day 28 after viral injection, mice were sacrificed, lungs were removed and weighed, and tumor nodules were counted to evaluate therapeutic efficacy. Mean of mice treated with PBS, Ad-ΔB7, or Ad-ΔB7-U6shIL8; bars, SE (n = 11 for PBS, n = 12 for Ad-ΔB7, n = 7 for Ad-ΔB7-U6shIL8). * indicates $P < 0.05$ compared to PBS treatment.

Identification of effective siRNA sequences and generation of recombinant Ad expressing shRNA specific to c-Met

c-Met is the high-affinity receptor tyrosine kinase for hepatocyte growth factor (HGF) or scatter factor (SF) and Met/HGF signaling is involved in many cancers and regulates biological activities[35]. It has been reported that c-Met was overexpressed and mutated in a variety of malignancies. Because a number of c-Met activating mutations, many of which are located in the tyrosine kinase domain, to search effective siRNA, I examined five c-Met siRNAs except for tyrosine kinase domain. Five kinds of c-Met siRNAs to target different regions of human c-Met (gi:4557746) mRNA were described in Table 2.

Table 2. Sequences of the four c-Met-specific siRNAs examined in this study

Number	positions	sequences
#1	428 – 446	aaggttgctgagtacaagact
#2	754 – 772	aggaccggttcatcaacttct
#3	1258 – 1256	tggatcgatctgccatgtgtg
#4	1987 – 2007	aaactagagttctccttggaa
#5	3142 – 3162	aattagttcgctacgatgcaa

Of the various cancer cell lines assessed, U343 expressed the highest level of c-Met, so it was used to compare inhibition efficiency of the five

candidate siRNAs. To evaluate the possible off-target effects, I also transfected cells with siRNA specific to lamin A/C and luciferase as controls. Relative amounts of c-Met were measured by semi-quantitative RT-PCR, normalized to β-actin. As shown in Figure 17A, two of the five siRNAs synthesized, c-Met siRNA No. 4 (1987-2007) and No. 5 (3142-3162) potently suppressed the synthesis of c-Met mRNA (> 90%). Transfection with Lamin A/C- and Luciferase-specific siRNA resulted in no significant alteration of c-Met RNA expression compared to non-transfected U343 cells. On the basis of these results, I selected c-Met siRNA No.4 and No.5 as the most highly functional siRNA sequence.

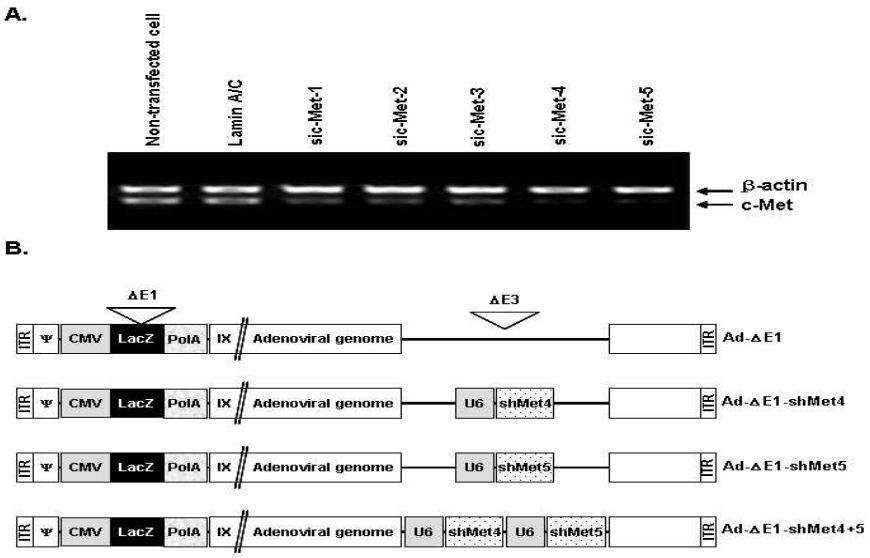

Figure 17. Characterization of c-Met-specific small interfering RNAs (siRNAs) and the structure of adenoviruses used in this study. (A) The effect

of siRNA-mediated *in vitro* knockdown of c-Met transcripts in U343 human glioma cell. Cells were transfected for 48 hr with four c-Met-specific siRNAs, along with siRNA specific to lamin A/C and luciferase as controls. Knockdown of endogenous expression was measured by RT-PCR for c-Met. Densitometric analysis was performed and the relative expression of each band was normalized to β-actin. (B) Schematic diagram of anenoviral construct used.

To inhibit c-Met expression effectively, I employed the adenovirus-delivered siRNA technique and generated recombinant adenovirus expressing c-Met shRNA No. 4 or No. 5 (shMet4 or shMet5), respectively. Also, for further effective knockdown, I generated adenovirus expressing both No.4 and No.5 in the same adenovirus, which proved to be most effective. These kinds of c-Met-specific shRNA-expressing recombinant adenoviruses, Ad-ΔE1-shMet4, Ad-ΔE1-shMet5, and Ad-ΔE1-shMet4+5 (Fig. 17B), were constructed to express shRNAs under the control of the murine U6 promoter, respectively.

Comparison of c-Met suppression by recombinant adenovirus expressing shMet4, shMet5, or shMet4+5

Next, to determine the effect of shRNA expression on c-Met protein levels and compare the knockdown efficiency of three kinds of adenoviruses

expressing shMet, Ad-ΔE1-shMet4, Ad-ΔE1-shMet5, and Ad-ΔE1-shMet4+5, various cancer cell lines (U251N, U343, U87MG, HepG2, SK-Hep1, and A549) were infected with each virus at an MOI of 100 ~ 500. Uninfected cells were used negative control. After 3 days post-infection, transduced cells were harvested and assayed to determine the amounts of c-Met protein. As shown in Fig. 18A, the synthesis and secretion of c-Met was significantly inhibited by Ad-ΔE1-shMet4, Ad-ΔE1-shMet5, and Ad-ΔE1-shMet4+5. In U343 cells with Ad-ΔE1-shMet4+5, c-Met levels were reduced by 80.4% and 79.8% ($P < 0.01$ and $P < 0.01$) compared to untransduced and control adenovirus (Ad-ΔE1)-transduced cells, whereas it was reduced to 64.5% and 63.4% with Ad-ΔE1-shMet4 and was 61.8% and 60.7% with Ad-ΔE1-shMet5. This efficient knockdown of c-Met was also observed in other cancer cell lines tested. Also, the c-Met protein level was significantly decreased with an MOI-dependent manner and Ad-ΔE1-shMet4+5 among shMet-expressing Ads inhibited c-Met expression most effectively (Fig. 18B). These results demonstrate that dual shRNA expression system is much more effective than single shRNA expression system.

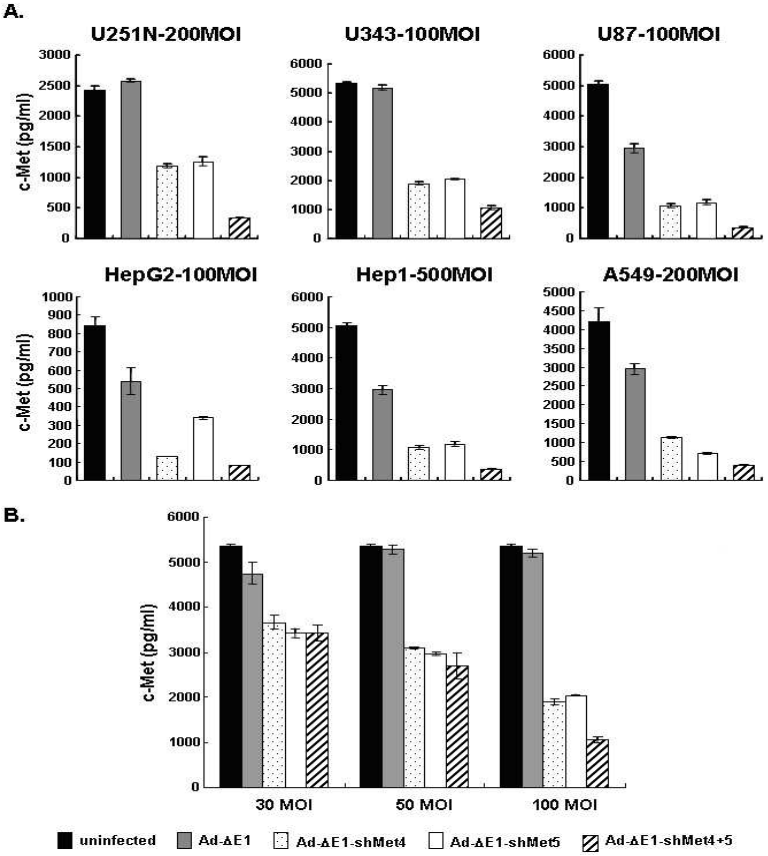

Figure 18. Quantitation of c-Met suppression in various cancer cells transduced with c-Met specific shRNA expressing Ads, Ad-ΔE1, Ad-ΔE1-shMet4, Ad-ΔE1-shMet5, or Ad-ΔE1-shMet4+5. (A) Various human cancer cell lines were transduced with Ad-ΔE1, Ad-ΔE1-shMet4, Ad-ΔE1-shMet5, or Ad-ΔE1-shMet4+5 in a range of 100 ~ 500 MOI. c-Met concentration was measured in cell lysates 72 hr after transduction by ELISA. *P<0.05 versus Ad-ΔE1 treatment. (B) Dose-dependent suppression of c-Met expression by three kinds of Ads expressing c-Met specific shRNA, Ad-ΔE1-shMet4, Ad-

ΔE1-shMet5, or Ad-ΔE1-shMet4+5. Each value represents the mean ± SE of at least three independent experiments. *P<0.05 versus Ad-ΔE1 treatment.

Reduced c-Met inhibits cell proliferation through mitotic catastrophe by senescence

I observed exciting phenotype in cancer cells infected with Ad expressing c-Met specific shRNA, Ad-ΔE1-shMet4, Ad-ΔE1-shMet5, and Ad-ΔE1-shMet4+5. After 2 days post-infection, observed with the naked eyes, cells infected with Ad-ΔE1-shMet4, Ad-ΔE1-shMet5, and Ad-ΔE1-shMet4+5 were showed definitely decreased cell confluence and after 3 days post-infection, exhibit enlargement of cell volume (lamellafodia), flattened cell morphology, and the appearance of many vacuolated cells (Figure. 19A), but did not observed characteristic of apoptotic cells. These phenomena were typical senescence like phenotype. After 5 days, most of the cells floated from the culture plate and floated cells demonstrated necrosis-like characteristics such as disruption of intact cellular boundaries, and losses of distinctive nuclear membrane structures. To further confirm, I also performed TUNEL assay. In result, I did not detect TUNEL-positive apoptotic (data not shown). For quantitative analysis of cell proliferation inhibition MTT assay was conducted. As shown in Fig. 19B, U343 cells with Ad-ΔE1-shMet4+5, c-Met levels were reduced by 78.7% and 76.6% ($P < 0.01$ and $P < 0.01$)

compared to untransduced and control adenovirus (Ad-ΔE1)-transduced cells, whereas the reduction was 73.8% and 71.2% with Ad-ΔE1-shMet4 and was 64.6% and 61.1% with Ad-ΔE1-shMet5. This efficient proliferation inhibition of reduced c-Met was also observed in each of the other cancer cell lines tested.

The morphological difference observed was further examined under the electron microscope (EM) (Fig. 19C). At three day postinfection at an MOI of 100, in majority of U343 cells infected with Ad-ΔE1-shMet4, Ad-ΔE1-shMet5, and Ad-ΔE1-shMet4+5, the nuclei became significantly larger and some cells contained several nuclei of unequal sizes and observed an increased number of micronuclei, but did not observe the condensed or fragmented nuclei characteristic of apoptotic cells. I also observed considerable increases in the numbers of vacuoles and electron-dense lysosomes, and additionally observed the convolution or collapse of some nuclear membranes.

In 1998, Gonos et al. have found eight genes that are overexpressed in senescent rat embryo fibroblasts. To confirm whether these phenomena were related with senescence; I conducted RT-PCR and determined the level of expression of a set of gene products commonly associated with cellular senescence. Used three genes were SM22, TGase II, and PAI-1 and primer

sequences used in RT-PCR were described in Table 3. As shown in Fig. 19D, after 48 hours, total RNA was extracted from cells infected with Ad-ΔE1-shMet4, Ad-ΔE1-shMet5, and Ad-ΔE1-shMet4+5. The levels of mRNA of SM22, TGase II, and PAI-1 were significantly increased (compared with Ad-ΔE1). On the basis of these results, I made certain that decrease of c-Met expression by shMet, induce senescence of cancer cell.

To analyze the mechanisms by which Ad-ΔE1-shMet4+5 inhibits cell proliferation, FACS analysis was applied to analyze the cell cycle of U343 cells after infection with adenovirus for 1 ~ 5 days. As shown in Fig. 19E, at hours 48 of adenovirus infection, the G_2/M phase cell population was dramatically increased from 16.1 ± 0.9% (Ad-ΔE1) to 42.6 ± 2.9% (Ad-ΔE1-shMet4+5), but the percentage of cells at G_0/G_1-phase-cell population was decreased from 43.1 ± 2.3% (Ad-ΔE1) to 22.3 ± 3.5% (Ad-ΔE1-shMet4+5) and S-phase cell population was also slightly reduced by 5.6% compared to control adenovirus (Ad-ΔE1)-transduced cells. No apoptosis peak was detected in sub G_1 population. Taken together, these results showed that apoptosis might not be the major mode of the cell death by knockdown of c-Met, but arrest cells at G_2-M phase. Taken together, these results suggest that reduced c-Met using Ad expressing c-Met specific shRNA inhibit cancer cell proliferation through mitotic catastrophe by senescence.

Table 3. Primer used for the analysis of the gene expression related to cellular senescence

Gene	primer sequence	product (bp)
Osteonectin	Forward:5'-CTGTGGGAGCTAATCCTG-3'	602
	Reverse:5'-GGGTGCTGGTCCAGCTGG-3'	
SM22	Forward:5'-TGGCGTGATTCTGAGCAA-3'	534
	Reverse:5'-CTGCCAAGCTGCCCAAGG-3'	
TGaseII	Forward:5'-CTCGTGGAGCCAGTTATCAACAGCTAC-3'	310
	Reverse:5'-TCTCGAAGTTCACCACCAGCTTGTG-3'	
PAI-1	Forward:5'-GTGTTTCAGCAGGTGGCGC-3'	300
	Reverse:5'-CCGGAACAGCCTGAAGAAGTG-3'	
β-actin	Forward: 5'-CGTCTTCACCATGGAGA-3'	310
	Reverse: 5'-CGGCCATCACGCCCACAGTTT-3'	

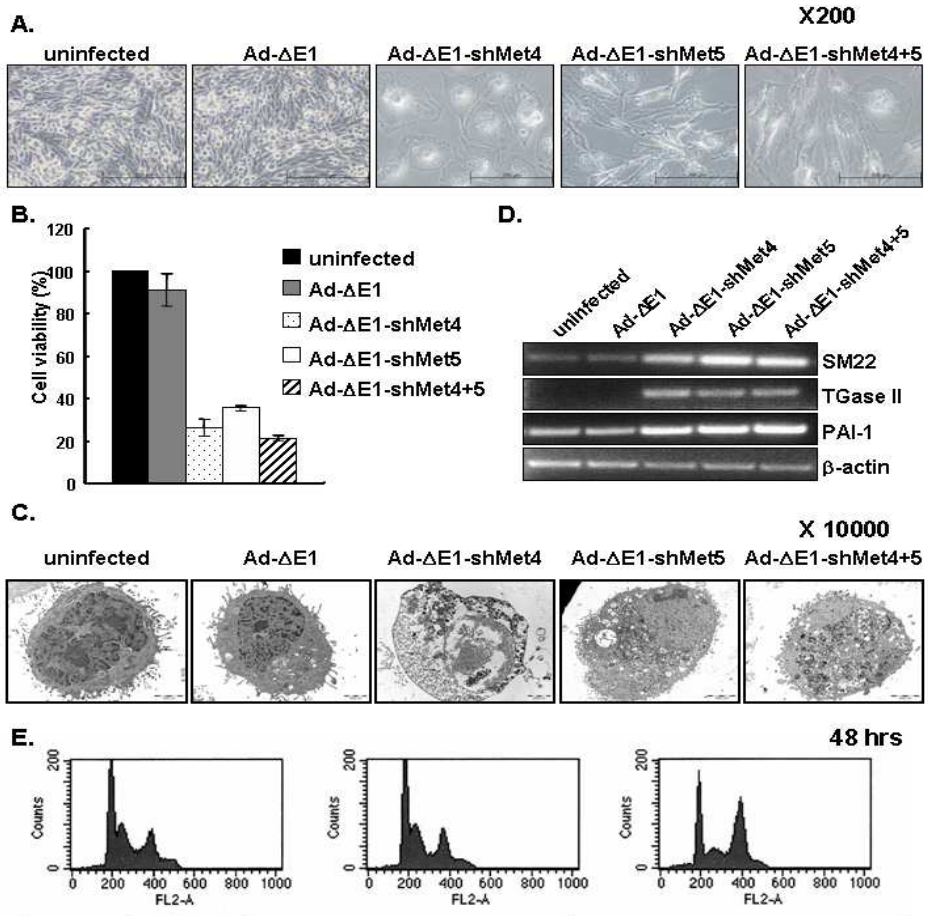

	0일	1일			2일		
	uninfected	uninfected	Ad-ΔE1	Ad-ΔE1-MetC	uninfected	Ad-ΔE1	Ad-ΔE1-MetC
sub G1							
G0/G1	41.5 ± 8.7	49.3 ± 3.0	48.7 ± 1.0	41.8 ± 3.8	39.9 ± 3.4	43.1 ± 2.3	22.3 ± 3.5
S	46.9 ± 9.4	46.5 ± 2.7	41.4 ± 2.8	47.2 ± 2.3	45.9 ± 3.8	40.8 ± 3.1	35.2 ± 6.4
G2/M	11.6 ± 1.9	4.2 ± 0.6	9.9 ± 2.2	11.0 ± 3.1	14.2 ± 1.3	16.1 ± 0.9	42.6 ± 2.9

Figure 19. Changes in the cellular morphologies of U343 cells transduced with Ads expressing c-Met specific shRNA, Ad-ΔE1-shMet4, Ad-ΔE1-shMet5, or Ad-ΔE1-shMet4+5. (A) After 48 hr of infection with Ad-ΔE1, Ad-ΔE1-shMet4, Ad-ΔE1-shMet5, or Ad-ΔE1-shMet4+5 of 50 MOI, cell morphology was monitored under the microscope. (B) The reduced cell

proliferation by the Ads expressing c-Met specific shRNA was measured by MTT assay. Viability of control cells was set at 100% and viability relative to the control is presented. *P<0.05 versus Ad-ΔE1 treatment. (C) The morphologies of dying cells were monitored using an electron microscope. U343 cells grown in six-well culture plated were infected with MOI of 50. After 72 hr of infection, cells were treated as described in Materials and Methods, and cell morphology was observed under the electron microscope. Representative high power (X 50,000) images are shown. (D) Analysis of gene expression associated with cellular senescence using RT-PCR. Total mRNAs were isolated, and semiquantitative RT-PCR was performed using specific primers for genes (human SM22, TGaseII, and PAI-1) over-expressed in senescent cells. β-actin was served as an internal control. (E) DNA content analysis. At 48 hr after transduced with Ad-ΔE1 or Ad-ΔE1-shMet4+5, cells were fixed with ethanol, treated with RNAase and stained with propidium iodide (PI). The stained cells were then analyzed by flow cytometry. Data shown are representative fluorescence histograms of at least three independent experiments. Percentages of G0/G1-, S-, G2/M-, and sub-G1-phase cells were calculated by Modfit program (Verity Software House, Topsham, ME).

Reduced c-Met inhibits VEGF expression and accordingly the function of endothelial cells

c-Met also was reported to induce angiogenesis in various cancer by inducing of vascular endothelial growth factor [38,39] and by simulataneously downregulating the antiangiogenesis factor thrombospodin-1 [40]. Based on these report, I made certain VEGF expression level by c-Met inhibition using VEGF ELISA. Various cancer cell lines (U251N, U343, U87MG, HepG2, SK-Hep1, and A549) were infected with Ad-ΔE1, Ad-ΔE1-shMet4, Ad-ΔE1-shMet5, and Ad-ΔE1-shMet4+5 at a MOI of 30 ~ 500. Uninfected cells were used negative control. After 72 hr, conditioned media was harvested and VEGF ELISA was carried out. As shown in Fig. 20A, in accordance with c-Met ELISA result, the synthesis and secretion of VEGF was significantly inhibited by Ad-ΔE1-shMet4, Ad-ΔE1-shMet5, and Ad-ΔE1-shMet4+5. In U343 cells transduced with Ad-ΔE1-shMet4+5, c-Met levels were reduced by 71.4%% and 80% ($P < 0.05$ and $P < 0.05$) compared to untransduced and control adenovirus (Ad-ΔE1)-transduced cells, whereas the reduction was 53% and 67% with Ad-ΔE1-shMet4 and was 44.4% and 61% with Ad-ΔE1-shMet5. This efficient inhibition of VEGF by knockdown of c-Met was also observed in each of the other cancer cell lines tested. Also, Ad-ΔE1-shMet4+5 of these shMet-expressing Ads inhibited VEGF expression very efficiently.

On the basis of these results, I made certain that decrease of c-Met expression by shMet, inhibit expression of VEGF.

I also investigated the effects of Ad-ΔE1-shMet4+5 on the migration of HUVECs *in vitro*. When conditioned medium from U343 cells transduced with Ad-ΔE1-shMet4+5 was placed in the lower chamber of a Transwell plate, migration of endothelial cells was reduced by 48.8% ($P < 0.001$ compared to Ad-ΔE1) whereas conditioned medium from Ad-ΔE1-shMet4+5-transduced cells inhibited migration only 24% ($P < 0.05$ compared to Ad-ΔE1) (Fig. 20B).

I next examined whether decreased c-Met by infection of Ad-ΔE1-shMet4+5 would have an inhibitory effect on morphological differentiation of endothelial cells, I conducted in vitro tube formation experiments using two-dimensional Matrigel in HUVECs (Figure 20C). To do this, I used U343 conditioned media and HUVECs were infected with conditioned media, and then plated on growth factor-reduced Matrigel. There was no effect within 12 hr of conditioned media treatment, but the inhibition was shown at 19 hr and more clearly at 24 hr with little cytotoxicity. Positive control (10 ng/ml) and conditioned media collected from Ad-ΔE1-infected U343 cells led to the formation of elongated and robust tube-like structures, which were organized by much larger number of cells. In contrast, conditioned media collected from

Ad-ΔE1-shMet4+5-infected U343 cells markedly inhibited the width and the length of endothelial and after 24 hours, tubes were broken, shortened, and much thinner at many sites. In particular, conditioned medium from Ad-ΔE1-shMet4+5-transduced cells diminished relative tube length by 44.1% ($P < 0.001$ compared to Ad-ΔE1, Fig. 20D). These findings demonstrate that a c-Met-specific shRNA-expressing Ad, Ad-ΔE1-shMet4+5, functionally inhibits the formation of tube-like structures in the in vitro Matrigel tube-formation assay.

As angiogenesis involves multiple steps, I assessed inhibition of vessel sprouting using rat aortic rings (explants) embedded in Matrigel beds. The Matrigel bed mimics a physiological extracellular matrix, representing its natural composition and architecture. Due to these features, Matrigel enables several cell types, including endothelial cells, to maintain their 3-dimensional, *in vivo* phenotype in culture. Microvessel sprouting was demonstrated by staining aortic rings with Diff-Quick, as described in materials and methods. As shown in figures 20E and 20F, a marked delay in the outgrowth of sprouts from the explants, with a regression in both the number of microvessels and the number of branches, was observed in aortic rings treated with conditioned medium from Ad-ΔE1-shMet4+5-transduced cells, showing a decrease in the

number of microvessels of 90.5% ($P < 0.001$) and 85.7% ($P < 0.001$) compared to untransduced and Ad-ΔE1-transduced conditioned media, respectively. In contrast, neither Ad-ΔE1 had an inhibitory effect on microvessels sprouting from aortic rings. In fact, the extent of the capillary network was comparable to that observed in the presence of conditioned medium from untransduced cells. These data further confirm the potent inhibition of angiogenesis induced by Ad-ΔE1-shMet4+5.

The process of the formation of new blood vessels, angiogenesis, is complex and involves several discrete steps, including extracellular matrix degradation, proliferation, and migration of endothelial cells and morphological differentiation of endothelial cells to form tubes [54]. I have first examined the effect of reduced c-Met by infection of Ad-ΔE1-shMet4+5 on HUVEC. HUVECs were infected with Ad-ΔE1 and Ad-ΔE1-shMet4+5 at a MOI of 100. After 48 hrs post-infection, cells infected with Ad-ΔE1-shMet4+5 were showed definitely decreased cell confluence and exhibit lengthen cell morphology (Figure. 20G), and eventually the lengthened cells floated from the plate. MTT assay showed that cell viability was inhibited (Fig. 20H). These results indicate that Ad-ΔE1-shMet4+5 inhibits not only proliferation of cancer cell but also of endothelial cell.

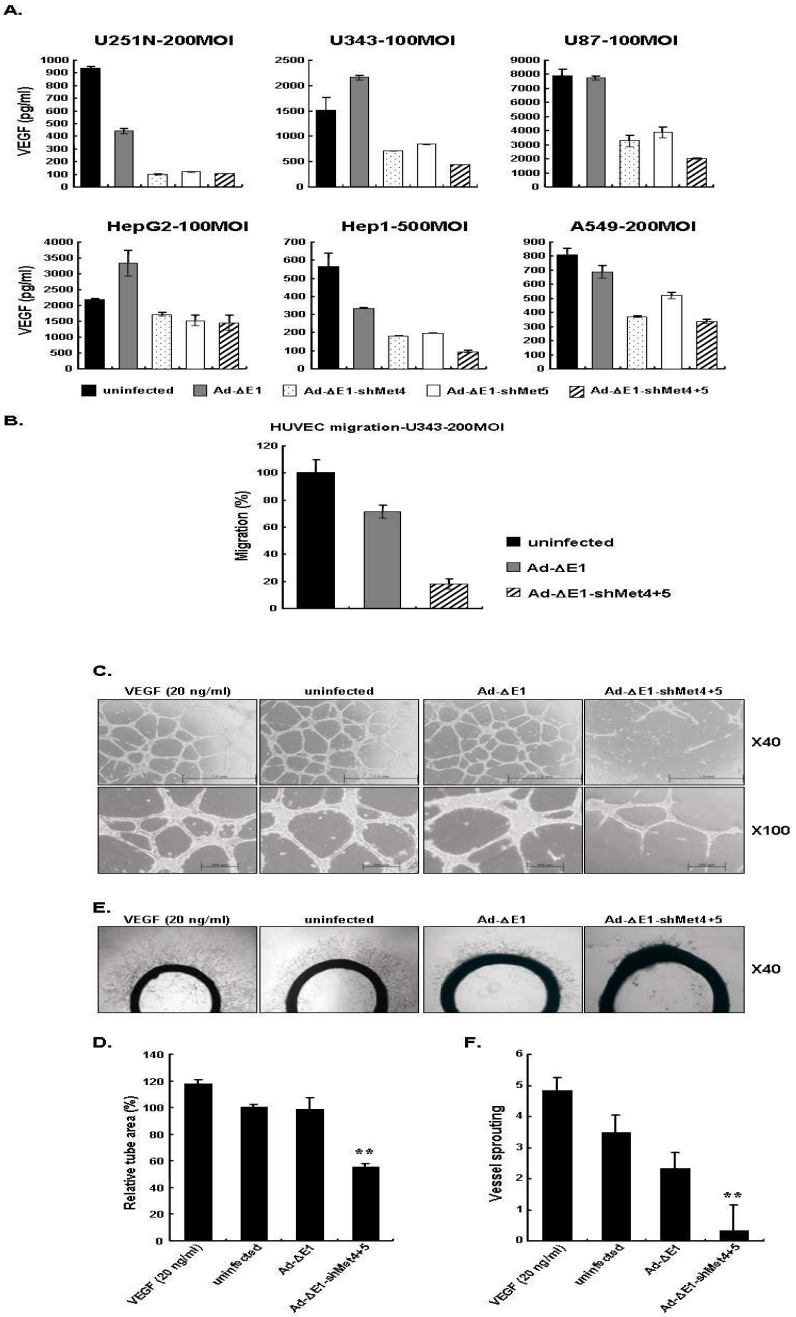
A.
U251N-200MOI
U343-100MOI
U87-100MOI
HepG2-100MOI
Hep1-500MOI
A549-200MOI
VEGF (pg/ml)
uninfected
Ad-ΔE1
Ad-ΔE1-shMet4
Ad-ΔE1-shMet5
Ad-ΔE1-shMet4+5
B.
HUVEC migration-U343-200MOI
Migration (%)
uninfected
Ad-ΔE1
Ad-ΔE1-shMet4+5
C.
VEGF (20 ng/ml)
uninfected
Ad-ΔE1
Ad-ΔE1-shMet4+5
X40
X100
E.
VEGF (20 ng/ml)
uninfected
Ad-ΔE1
Ad-ΔE1-shMet4+5
X40
D.
Relative tube area (%)
**
VEGF (20 ng/ml)
uninfected
Ad-ΔE1
Ad-ΔE1-shMet4+5
F.
Vessel sprouting
**
VEGF (20 ng/ml)
uninfected
Ad-ΔE1
Ad-ΔE1-shMet4+5

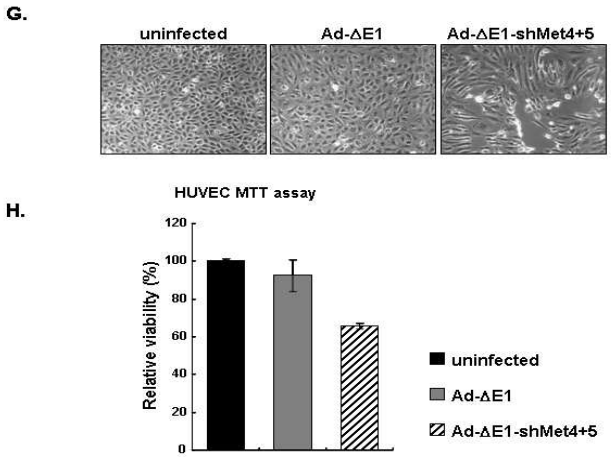

Figure 20. Effects of Ads expressing c-Met-specific shRNA in endothelial cell functions. (A) Reduced c-Met expression down regulates VEGF expression. Various human cancer cell lines were transduced with Ad-ΔE1, Ad-ΔE1-shMet4, Ad-ΔE1-shMet5, or Ad-ΔE1-shMet4+5 with 100~500 MOI. VEGF concentration was measured in the culture supernatant at 72 hr after infection by ELISA. Each value represents the mean ± SE of at least three independent experiments. (B) Inhibition of HUVEC cell migration by Ad-ΔE1-shMet4+5. Migratory cells are represented as the number of migrated cells per high-power field (200x). Ten fields were counted in triplicate from each sample. bars, ± SE. *, $P < 0.05$ *versus* Ad-ΔE1 treatment; **, $P < 0.001$ *versus* Ad-ΔE1 treatment. (C) Inhibition of tube formation by Ad-ΔE1-shMet4+5. HUVEC cells were plated on Matrigel-coated plates at a density of 2 x 10^5 cells/well and incubated in the presence of medium supplemented with human

recombinant $rVEGF_{165}$ (10 ng/ml), control conditioned medium from U343 cells, or conditioned medium from Ad-ΔE1- or Ad-ΔE1-shMet4+5-transduced cells. After 20 hr, changes in cell morphology were captured using an inverted microscope. Original magnification: 40x and 100x. (D) The area covered by the tube network was quantified using Image-Pro Plus software. Experiments were repeated three times and values are means of triplicate measurements from one representative experiment; bars, ± SE. **, $P < 0.001$ *versus* Ad-ΔE1 treatment. (E) Inhibition of vessel sprouting by Ad-ΔE1-shMet4+5. Representative aortic rings were photographed. (F) Vessel sprouting index. The assay was scored from 0 (least positive) to 5 (most positive) and data are presented as mean ± SE (n=6). **, $P < 0.001$ *versus* Ad-ΔE1 treatment. Original magnification: 40x (G) Changes in the cellular morphologies of HUVEC cells transduced with Ad-ΔE1-shMet4+5 of 50 MOI. Cell morphology was monitored under the microscope. (H) The reduced cell proliferation by the Ad-ΔE1-shMet4+5 was measured by MTT assay. Viability of control cells was set at 100% and viability relative to the control is presented. *P<0.05 versus Ad-ΔE1 treatment.

Effect of Ad-ΔE1-shMet4+5 on tumor cell migration, invasion, and MMP-2 expression

I next examined whether the expression of c-Met-specific shRNA

could affect the cellular locomotion/invasion activity of cancer cell lines using a migration/invasion assay. Quantitative analysis showed that conditioned media collected from Ad-ΔE1-shMet4+5-transduced U343 cancer cells effectively blocked cellular migration and invasion after 24 hr: by 65.6% ($P < 0.05$ *versus* Ad-ΔE1) and 69% ($P < 0.05$ *versus* Ad-ΔE1) for U343 cells (Fig. 21A, 21B). In contrast, conditioned media collected from untransduced and Ad-ΔE1-transduced cells, did not significantly affect migration and basal invasion of cancer cells in this assay.

Expression of MMPs in cancer cells (as well as vascular endothelial cells) has been shown to regulate neovascularization by enhancing peri-cellular fibrionolysis and cellular locomotion. Of the many MMPs, MMP-2 plays a critical role in the angiogenic switch during carcinogenesis. By using conventional gelatin zymography, I compared gelatinolytic activity of MMP-2 in Ad-ΔE1-, and Ad-ΔE1-shMet4+5-transduced U343 cancer cells. As shown in Fig. 21C, MMP-2 gelatinolytic activity was reduced in Ad-ΔE1-shMet4+5-transduced U343 cancer cells, whereas Ad-ΔE1-transduced cancer cells showed MMP-2 activity similar to parental cells. ELISA quantitation of MMP-2 protein in U343 cancer cells transduced with Ad-ΔE1-shMet4+5 indicated that a reduction in the MMP-2 protein level closely paralleled the observed loss of MMP-2 gelatinolytic activity (Fig. 21D). These results

indicate that Ad-ΔE1-shMet4+5 inhibits invasion of cancer cells, presumably by the inhibition of MMP activity.

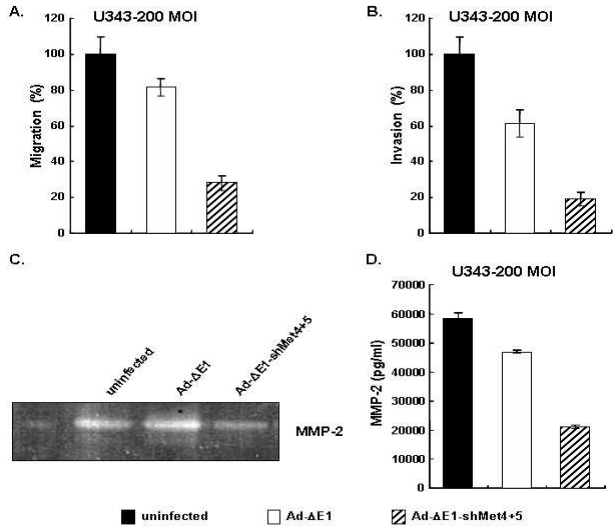

Figure 21. Inhibition of cancer cell migration, invasion, and MMP-2 expression by A Ad-ΔE1-shMet4+5. (A) Inhibition of tumor cellular migration by Ad-ΔE1-shMet4+5. U343 (1 X 10^6 cells/ml) cells were added to transwell chamber and treated with conditioned medium from Ad-ΔE1- or Ad-ΔE1-shMet4+5-transduced cells. After 6 hr incubation, migrated cells were quantified by counting the cells that migrated to the lower side of the filter with optical microscopy at 200x magnification. Results are expressed as percentage of control conditioned medium from U343 cells. Experiments were performed in triplicate and repeated three times, means ± SE are shown. *, $P < 0.05$ *versus* Ad-ΔE1 treatment. (B) Inhibition of tumor cellular invasion by Ad-ΔE1-shMet4+5. U343 (1 X 10^6 cells/ml) cells were added to transwell

chamber coated with Matrigel and treated with conditioned medium from Ad-ΔE1- or Ad-ΔE1-shMet4+5-transduced cells. After 18 hr incubation, the number of invaded cells was quantified by counting as the mean number of cells that invaded to the lower side of the filter with optical microscopy at 200x magnification. Experiments were performed in triplicate and repeated three times, means ± SE are shown. *, $P < 0.05$ *versus* Ad-ΔE1 treatment. (C) Zymographic detection of secreted gelatinase activity in conditioned media from U343 cells treated with AdΔE1 or Ad-ΔE1-shMet4+5. This is one representative result from three independent experiments. (D) Modulation of MMP-2 protein expression in U343 cells transduced with Ads. Human MMP-2 concentration in conditioned media was determined by ELISA. Each bar represents the mean ± SE (n = 3). *, $P < 0.05$ *versus* Ad-ΔE1 treatment.

Ad-ΔE1-shMet4+5 Suppresses Met signaling

On signaling by HGF/SF, c-Met is activated via phosphorylation of the cytoplasmic domain and further activates downstream pathways such as the mitogen-activated protein kinase (MAPK), PI3K, and STAT or Erk signaling pathways. These pathways are essential for mediating biological activities such as cell migration, proliferation, morphogenesis, and survival. To evaluate the effect of c-Met inhibition-induced c-Met phosphorylation and downstream pathway, ERK1/2 and Akt phosphorylation were analyzed. As

shown in Fig. 22, cells treated with Ads expressing c-Met specific shRNA, Ad-ΔE1-shMet4, Ad-ΔE1-shMet5, and Ad-ΔE1-shMet4+5, the basal as well as the inducible activation of AKT and ERK1/2 were significantly inhibited.

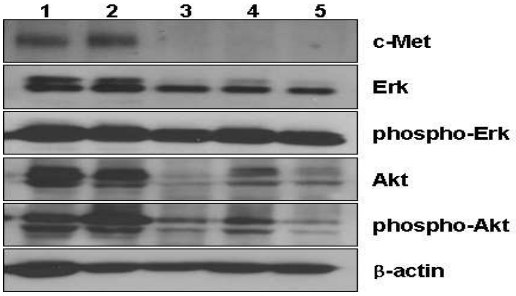

Figure 22. Inhibition of down signal pathway by c-Met inhibition. U343 cells were infected at an MOI of 100 with Ad-ΔE1, Ad-ΔE1-shMet4, Ad-ΔE1-shMet5, or Ad-ΔE1-shMet4+5. After 48 hr, cell lysates were prepared and subjected to SDS-PAGE. Western blot was probed with anti-c-Met, anti-Erk, anti-phspho-Erk, anti-Akt, and anti-phspho-Akt antibodies and reprobed with an anti-actin antibody to verify equal loading of protein.

Inhibition of HGF-dependent or -independent cell proliferation by shMet-expressing recombinant Ad

Hepatocyte growth factor/scatter factor (HGF/SF) is a specific ligand for c-Met and has a markedly stimulatory activity on mortality of cancer cells but not on their growth [55]. To determine whether c-Met specific shRNA inhibits the proliferation and scattering by HGF, I investigated the role of

HGF in U343 cell proliferation. After 24 hours Ad infection, serum free media with or without HGF/SF of 25ng/ml was added to cells and the effects of c-Met inhibition were tested. Increased cell scattering effect was observed in the untransduced and Ad-ΔE1-transduced cells, whereas no scattering effect was observed in the Ad-ΔE1-shMet4+5 transduced cells (Fig. 23A). Next, using MTT assay I investigated the role of HGF in cancer cell proliferation. As shown in Fig. 23B, HGF doesn't inhibit showing that reduction of Met expression can affect Met-dependent cell scattering without affecting cell viability or proliferation.

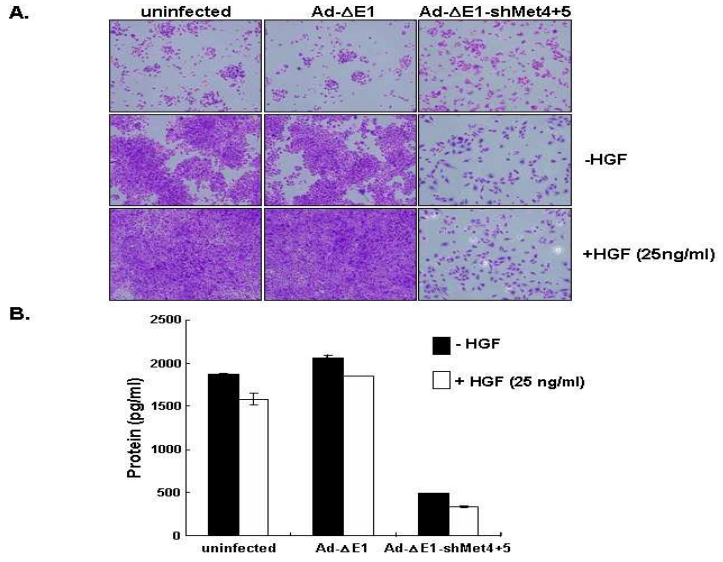

Figure 23. Inhibition of HGF-dependent or HGF-independent cell motility by Ad-ΔE1-shMet4+5. (A) U343 cells were plated in six-well plates to 20% confluency and were infected with Ad-ΔE1-shMet4+5 at an MOI of 50. After

24 hr adenoviral infection, serums free media with or without 25 ng/ml of HGF were added to the cells and following 48 hours, viable cells were stained with crystal violet. (B) The reduced cell proliferation by the Ad-ΔE1-shMet4+5 was measured by MTT assay. Viability of control cells was set at 100% and viability relative to the control is presented. Infected cells with Ad-ΔE1-shMet4+5 reduced cell viability or proliferation with or without HGF. *P<0.05 versus Ad-ΔE1 treatment. Cell scattering activity was suppressed in a Met-dependent manner (100x magnification).

Enhanced anti-tumor effect of shMet-expressing recombinant Ad

Recombinant Ad expressing c-Met-specific shRNA, Ad-ΔE1-shMet4, Ad-ΔE1-shMet5, and Ad-ΔE1-shMet4+5 were subsequently assessed for its ability to suppress the growth of U343 human glioma xenograft model established in nude mice. Tumors were generated by subcutaneous injection of cells into the mice abdominal region. When tumors reached an average size of 70 mm^3, tumors were injected intratumorally with PBS, Ad-ΔE1, Ad-ΔE1-shMet4, Ad-ΔE1-shMet5, and Ad-ΔE1-shMet4+5 (1×10^8 PFU) every 2 days for a total of three times (Q2Dx3). As seen in Fig. 24, the growth of all tumors treated with Ad expressing c-Met-specific shRNA was substantially delayed compared with that of tumors treated with PBS or with Ad-ΔE1, which does not express c-Met-specific shRNA. By 45 days after treatment, tumors treated

with PBS reached an average tumor volume of 2771.6 ± 467.6 mm^3 and those treated with Ad-ΔE1 reached 1468.1 ± 268.8 mm^3. In marked contrast, the tumor growth was severely suppressed in mice injected with Ad-ΔE1-shMet4 ($P < 0.05$, versus PBS or Ad-ΔE1 group), Ad-ΔE1-shMet5 ($P < 0.05$, versus PBS or Ad-ΔE1 group), or Ad-ΔE1-shMet4+5 ($P < 0.01$, versus PBS or Ad-ΔE1 group). More specifically, in the same time period those treated with Ad-ΔE1-shMet4 reached 841.4 ± 244.2 mm^3, those treated with Ad-ΔE1-shMet5 reached 785.1 ± 201.6 mm^3, and those treated with Ad-ΔE1-shMet4+5 reached 433.3 ± 108.7 mm^3. Throughout the course of the study, no systemic toxicity, such as diarrhea, loss of weight, or cachexia was observed. The survival advantage conferred by Ad-ΔE1-shMet4+5 was statistically significant when compared with either of the Ad-ΔE1 group ($P < 0.01$, versus Ad-ΔE1 group).

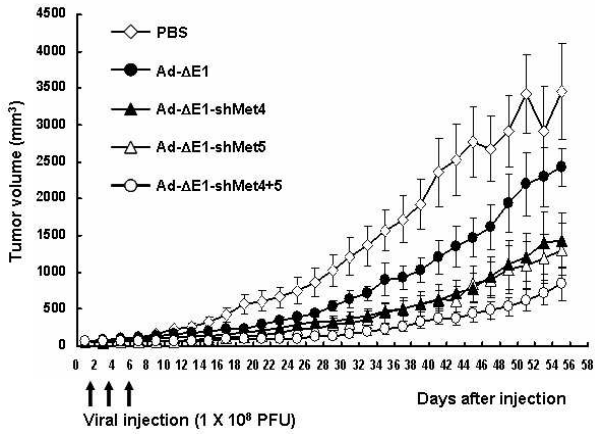

Figure 24. *In vivo* antitumor effect of Ads expressing the c-Met specific shRNA. Subcutaneous implanted tumors derived from U343 cells were injected with Ad-ΔE1 (●), Ad-ΔE1-shMet4 (▲), Ad-ΔE1-shMet5 (△), or Ad-ΔE1-shMet4+5 (○), along with PBS (◊) as a negative control. Tumor growth was monitored at 2 day intervals after each injection. Arrows indicate when treatment was given 1 X 10^{10} viral particles per 50 $\mu\ell$. Data points represent the mean (± SE) tumor size (in cubic millimeters) for each group at the indicated times. Values represent the mean ± SE. *, $P < 0.05$ *versus* Ad-ΔE1. **, $P < 0.001$ *versus* Ad-ΔE1.

In Vivo histologic and immunohistochemical characterization

Since Ad-ΔE1-shMet4+5 is far superior to Ad-ΔE1-shMet4 and Ad-ΔE1-shMet5 in suppression of c-Met expression, Ad-ΔE1-shMet4+5 was chosen for the subsequent assessment in nude mice. To verify the proposed mechanism of action of c-Met-specific shMet-expressing Ad, Ad-ΔE1-shMet4+5-treated tumors were further investigated by histological examination. Tumors were harvested from each treatment group at 7 days following the three sequential treatments. As seen in Figure 25A, most of the tumor mass remaining after treatment with the Ad-ΔE1-shMet4+5 was necrotic as shown by hematoxylin-eosin staining, whereas necrotic lesions were barely detectable in the tumors treated with PBS or Ad-ΔE1. In addition

apoptotic changes and cell necrosis, surrounded by stromal fibrosis was also seen. Masson's trichrome staining determined collagen type I, stained in blue, as the predominant morphological component of these fibrotic changes. To determine whether the reduced size of Ad-ΔE1-shMet4+5-treated tumors coincided with reduced neovascularization, microvessel density as assessed using anti-CD31 antibody was determined. A marked decrease in number and size of CD31-positive vessels was observed in Ad-ΔE1-shMet4+5 Ad-treated tumors. Quantitation of microvessels showed that density was reduced by 79.8% ($P < 0.001$) and 76.7% ($P < 0.001$) in response to Ad-ΔE1-shMet4+5 Ad treatment as compared to PBS and Ad-ΔE1 Ad treatment groups, respectively (Fig. 25B). To analyze the degree to which Ad-ΔE1-shMet4+5 induced apoptosis *in vivo*, TUNEL assay was carried out using the same tumor sections. As seen in Fig. 25A, apoptotic cells were also more abundantly detected in Ad-ΔE1-shMet4+5-treated tumor tissue than in PBS- or Ad-ΔE1-treated tumor tissue.

Next I investigate the biological significance of c-Met down-regulation in tumor tissue. When U343 tumors reached an average size of 70 mm^3, tumors were injected intratumorally with PBS, or with 1 x 10^8 PFU of either Ad-ΔE1 or Ad-ΔE1-shMet4+5 Ad every 2 days for a total of three times (Q2Dx3). Tumors were then harvested at day 10 and 20 after viral injection,

and c-MET, VEGF, IL-8, and MMP-2 expression were measured by ELISA. As shown in Fig. 25B, following 10 and 20 days of treatment, a marked suppression of c-Met expression was observed in tumor tissues treated with Ad-ΔE1-shMet4+5, resulting in 56.4% and 20.9% reduction compared to Ad-ΔE1-treated control tumors, respectively. Moreover, ELISA results demonstrated that treatment with Ad-ΔE1-shMet4+5 resulted in 32.8% and 49.4% ($P < 0.05$ versus Ad-ΔE1) reduction in VEGF and 76.7% and 76.7% ($P < 0.05$ versus Ad-ΔE1) reduction in IL-8, at day 10 and 20 after viral injection. Also, MMP-2 expression reduced in tumors treated with Ad-ΔE1-shMet4+5.

These findings suggest that c-Met-specific shRNA down-regulates the expression of both IL-8 and VEGF, key mediators of angiogenesis and also, MMP-2 expression, appeared to play a crucial role in many stages of tumor progression, including angiogenesis and the invasion and metastasis of tumor cells. Therefore, the antimigratory and antiangiogenic activities of c-Met-specific shRNA expression may inhibit tumor growth and metastasis in animals by suppressing tumor angiogenesis, suggesting a crucial role for c-Met in angiogenesis and tumor growth and metastasis *in vivo*.

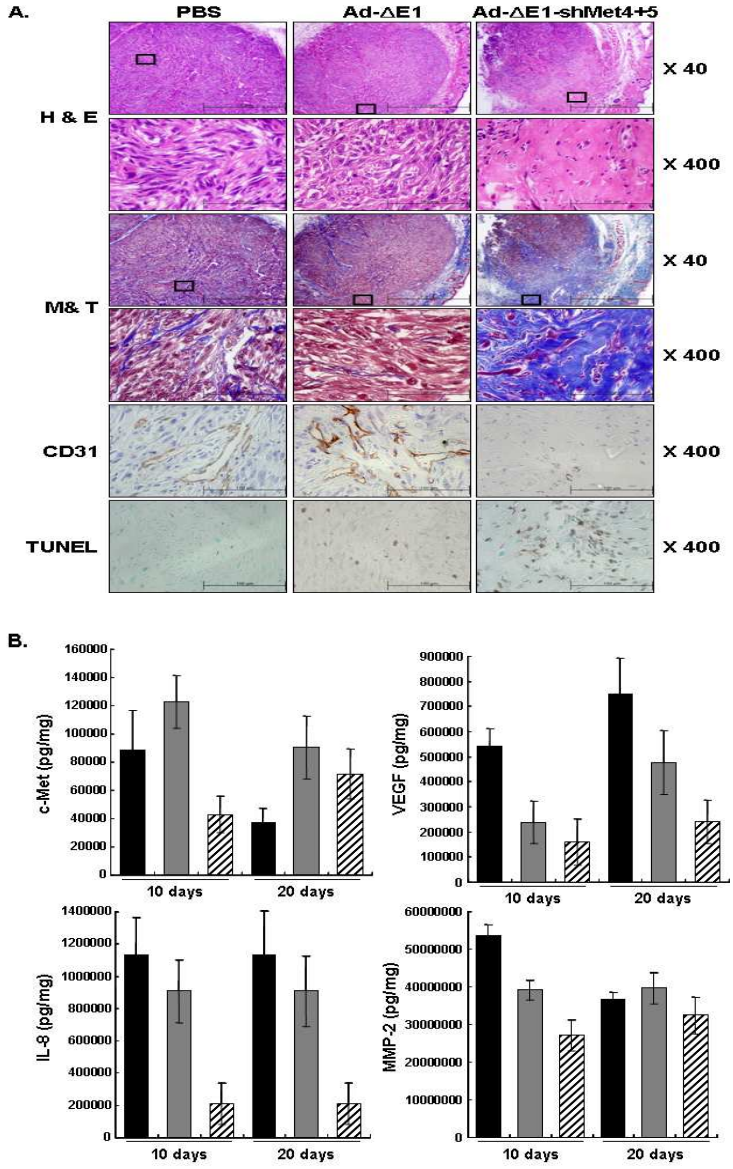

Figure 25. Histological characterization of tumor tissues in U343 human glioma xenografts. (A) Hematoxylin & Eosin staining (H & E). Masson's trichrome staining of extracellular matrix (blue) in the tumor tissue sections

(M & T) and hematoxylin counter-stained. Blood vessel density was assessed by immunohistochemical staining for CD31; Hematoxylin counterstained (CD31). Brown staining indicates positive staining for endothelial cells. TUNEL staining of apoptotic cells in tumor tissue; methyl green counter stained (TUNEL). Tumors treated with Ad-ΔE1-shMet4+5 exhibited significant increase in apoptotic levels. Greater dark brown nuclei with double-strand DNA breaks (indicated by an arrow) can be seen in tumors treated with Ad-ΔE1-shMet4+5 as compared to PBS- or Ad-ΔE1-treated groups. Original magnification: 40× and 400×. (B) c-Met down-regulation in tumor tissue. Tumor tissues were collected 28 days after final virus injection, and ELISA was done to determine the levels of c-Met, VEGF, IL-8, and MMP-2. Treatment of Ad-ΔE1-shMet4+5 Ad results in significant reduction in c-Met levels as well as VEGF, IL-8, and MMP-2 as compared to treatment of PBS or Ad-ΔE1. Each data point represents mean c-Met, VEGF, IL-8 and MMP-2 levels for each individual tumor (8 mice per group). Each protein levels are expressed as picograms per milligram of total protein. *, $P < 0.05$ *versus* Ad-ΔE1. **, $P < 0.001$ *versus* Ad-ΔE1.

Inhibition of tumor metastasis by shMet-expressing recombinant Ad

Activation of angiogenesis is also responsible for increased tumor cell metastasis. Therefore, I investigated whether suppression of c-Met

expression also blocks metastasis of a malignant human breast cancer cell line, MDA231. As illustrated in Fig. 26A, lung tissues from PBS- and Ad-ΔE1-treated mice possessed approximately 7.6 ± 2.7 and 2.1 ± 0.7 tumor nodules caused by MDA231 metastasis. However, the number of tumor nodules was decreased to 0.4 ± 0.2 after administration of Ad-ΔE1-shMet4+5. In fact, nine of thirteen mice in the Ad-ΔE1-shMet4+5-treated group showed no metastatic spread. Hematoxylin and eosin staining revealed that the PBS- and Ad-ΔE1-treated mice lung had a relatively large number of sizable tumor masses due to the metastasis of the MDA231 (Fig. 26B) and Masson's trichrome staining revealed that most tumor tissues treated with Ad-ΔE1-shMet4+5 were surrounded by stromal fibrosis. Also, microvessel density as assessed using anti-CD31 antibody was determined. A marked decrease in number and size of CD31-positive vessels was observed in Ad-ΔE1-shMet4+5-treated tumors. Quantitation of microvessels showed that density was reduced by 79.8% ($P < 0.001$) and 76.7% ($P < 0.001$) in response to Ad-ΔE1-shMet4+5 Ad treatment as compared to PBS and Ad-ΔE1 Ad treatment groups, respectively (Fig. 26C). These results indicate that c-Met specific shRNA-expressing Ad, Ad-ΔE1-shMet4+5, had a strong inhibitory effect on tumor metastasis.

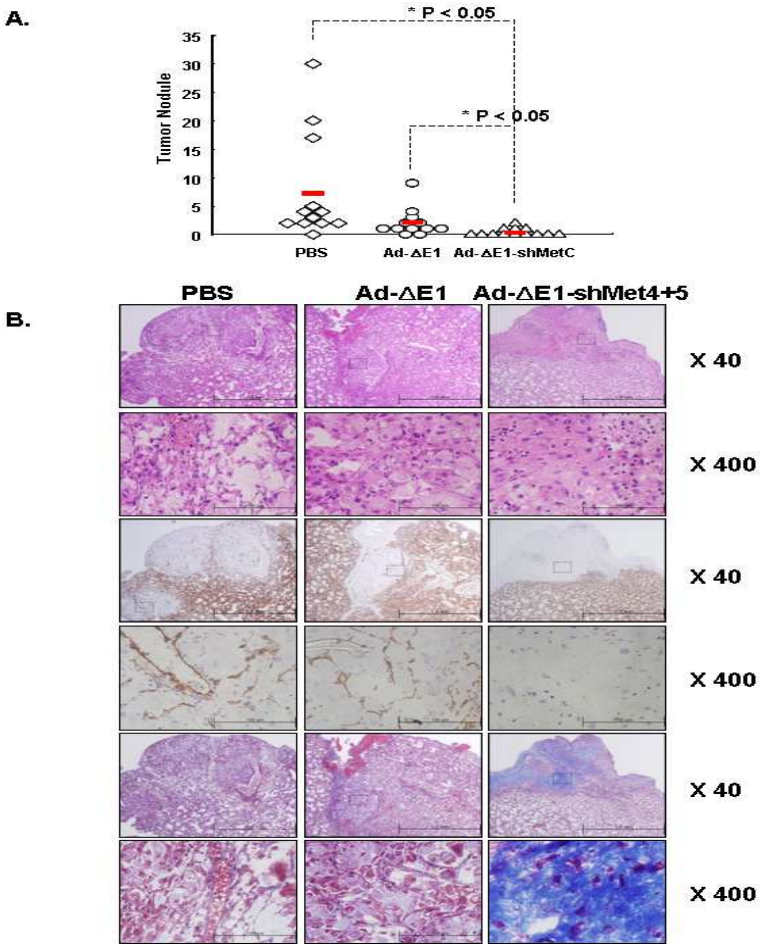

Figure 26. Therapeutic efficacy of Ad-ΔE1-shMet4+5 on MDA-MB-231 lung metasis tumor model. (A) MDA-MB-231 human breast cancer cells were injected intravenously to form pulmonary metastatic lesions. At 28 days following cell injection, MDA-MB-231 tumor-bearing mice received intrapleural injections of PBS, Ad-ΔE1, or Ad-ΔE1-shMet4+5. On day 28 after viral injection, mice were sacrificed, lungs were removed and tumor nodules were counted to evaluate therapeutic efficacy. Mean of mice treated

with PBS, Ad-ΔE1, or Ad-ΔE1-shMet4+5; bars, SE (n = 12 for PBS, n = 12 for Ad-ΔE1, n = 13 for Ad-ΔE1-shMet4+5). * indicates $P < 0.05$ compared to PBS treatment. (B) Histologic analysis of lung tissue from mice treated with adenovirus Ad-ΔE1, or Ad-ΔE1-shMet4+5. After tumor nodule counting, lungs were fixed with zinc fixative, stained with H & E, M & T, and anti-CD31. Original magnificataion:40x and 200x).

IV. DISCUSSION

RNAi has emerged as an important tool in downregulating sequence-specific gene expression at both the transcriptional and post-transcriptional levels. In mammalian systems, sequence-specific RNAi effect can easily be achieved by introducing synthetic siRNAs via transfection [56,57]. However, their use in a therapeutic setting has been limited, mainly due to high costs in synthesis and short-lived half-life. To overcome this limitation, significant efforts have also been made to construct siRNA-delivery vectors based on naked DNA, Ad, adeno-associated virus, retrovirus, or lentivirus [3,58-61]. Colby et al. reported that the MMP-1-specific siRNA-expressing plasmid selectively blocked MMP-1 expression in MDA-231 breast cancer cells that have constitutively high levels of MMP-1 [62]. In 2004, Yang et al. demonstrated that the expression of Her-2/neu can be silenced through retrovirus-mediated transfer of a Her-2/neu-specific siRNA [63]. Ads-mediated siRNA specific to Hec1 has also been shown to inhibit tumor growth *in vivo* [64]. These studies clearly demonstrated that siRNA-mediated “reverse genetics” can open the new avenue as a novel therapeutic strategy in combating human cancer.

In this study, oncolytic Ad-mediated infection with siRNA against VEGF successfully inhibited the secretion and expression of VEGF in various cancer cell lines. In addition, it suppressed the growth of U343 xenograft

tumors, demonstrating the oncolytic Ad-mediated siRNA silencing is a powerful approach for treating human cancer. VEGF has at least seven subtypes due to the alternative splicing of a single gene [65-67]. Although the $VEGF_{165}$ isoform plays a central role in vascular development, recent studies have demonstrated that each VEGF isoform plays a distinct role in vascular patterning and arterial development. Among the seven isoforms of VEGF, $VEGF_{121}$ sequence is shared by all seven VEGF isotypes. Accordingly, I designed two siRNAs targeting $VEGF_{121}$ mRNA, with hopes of degrading all seven isoforms of VEGF. Of the two generated plasmids expressing VEGF-specific shRNA targeting $VEGF_{121}$ mRNA, pshVEGF-2 elicited potent suppression of VEGF expression (Fig. 1C).

I next determined whether VEGF-specific shRNA could functionally reduce endogenous VEGF expression in cancer cells. Previous studies have shown that replication-competent Ad suppresses tumor angiogenesis through preserved E1A region [53]. Zhou et al. demonstrated that transfection of the Ad type 5 E1A gene into TC71 cells downregulated VEGF expression *in vitro*. Moreover, they demonstrated that intratumoral injection of E1A-expressing Ad vector decreased VEGF expression, inhibited tumor growth, and increased the survival rates. Recently, Saito *et al.* also demonstrated that E1A suppressed the production of VEGF and inhibited tumor angiogenesis by

binding to p300, resulting in the inhibition of the HIF-1α-mediated transcription of genes through binding to hypoxia responsive element (HRE) [51]. In agreement with these previous results, I observed that oncolytic Ads without expressing VEGF-specific shRNA (YKL-1, Ad-ΔB7) substantially suppressed VEGF expression as potently as oncolytic Ad expressing VEGF-specific shRNA (Ad-ΔB7-shVEGF) (Fig. 2A-B).

To address this point of concern, I constructed E1-deleted replication-incompetent Ad expressing shVEGF-2, Ad-ΔE1-shVEGF, and evaluated the functional effect of Ad expressing VEGF-specific shRNA. Ad-ΔE1-shVEGF was highly effective in reducing VEGF expression and the level of suppression of VEGF expression correlated with viral loading (Fig. 2C). Moreover, Ad-ΔE1-shVEGF effectively inhibited tube formation of primary cultured human endothelial cells *in vitro* and microvessel sprouting from rat aorta ring *ex vivo* (Fig. 3). The effects of VEGF-specific shRNA-expressing Ad on angiogenesis-associated endothelial cell function observed *in vitro* and *ex vivo* were then confirmed in an *in vivo* Matrigel angiogenesis assay (Fig. 4). Interestingly, oncolytic Ad-mediated expression of VEGF-specific shRNA was much more potent in inhibiting angiogenesis as compared to those by replication-incompetent Ad. Ad-ΔB7-shVEGF at the $1/20^{th}$ of the viral dose elicited almost equivalent anti-angiogenesis driven by

Ad-ΔE1-shVEGF Ad *in vivo*.

Along the same line in *in vivo* xenograft studies, Ad-ΔB7-shVEGF demonstrated enhanced antitumor effect and a higher incidence of complete tumor regression compared to its cognate control oncolytic Ad, Ad-ΔB7 (Fig. 5B-C). Survival rate was also significantly prolonged in the Ad-ΔB7-shVEGF-treated mice. In addition, U343 human glioma xenograft tumors analyzed at 7 days after treatment with Ad-ΔB7-shVEGF Ad demonstrated extensive areas of necrosis replaced by fibrous tissue, whereas necrotic lesions were barely detectable in the tumors treated with PBS or Ad-ΔB7. Consistent with the results reported here, Thorne et al. recently demonstrated that co-administration of oncolytic adenovirus and replication-incompetent adenovirus expressing soluble VEGF receptor elicits significantly greater anti-tumor effect than its respective monotherapies [68]. Furthermore, in accord with *in vitro*, *ex vivo*, and *in vivo* experiments, infection with oncolytic Ad expressing a VEGF-directed siRNA significantly reduced the extent of angiogenesis in the U343 xenograft model. Microvessel density in tumor tissue assessed by immunostaining with anti-CD31 antibody was reduced by more than 75% in tumors treated with Ad-ΔB7-shVEGF Ad as compared to PBS- or Ad-ΔB7-treated groups. Based on these results, I conclude that

inhibition of tumor growth is caused, in part, by the reduction in number of tumor vessels in Ad-ΔB7-shVEGF Ad-treated mice.

Many angiogenic functions are attributed to VEGF, including the stimulation of endothelial cell invasion, migration, and proliferation [69]. Equally important is the tight balance between proangiogenic and antiangiogenic factors in the tumor microenvironment that governs the response of endothelial cells in angiogenesis [70]. Therefore, down-regulating the synthesis of one of the most potent proangiogenic factors, VEGF, can critically shift this balance to interrupt in formation of new vessels. As demonstrated in Fig. 6C, VEGF level expressed in the tumor mass was substantially decreased when tumors were treated with Ad-ΔB7-shVEGF Ad compared to tumors treated with PBS or Ad-ΔB7 Ad. This reduction in VEGF levels may in turn further decrease angiogenesis through an antiangiogenic "switch", in which the collective action of proangiogenic factors are decreased and the collective action of angiogenic inhibitors augment. Further investigation for balance between proangiogenic and antiangiogenic factors in tumor tissues before and after treatment with Ad-ΔB7-shVEGF Ad is now under way in our laboratory to understand this observation more rigorously.

The duration of gene suppression is largely dependent on the rate of cell growth and turnover of the targeted protein in actively dividing cell in

culture. Since cancer cells are actively dividing, the duration of siRNA-mediated gene silencing *in vivo* might be governed by the efficiency of the siRNA-expressing vector and the stability of the functional siRNA. Oncolytic Ad-mediated siRNA expression may lead to improved efficacy over nonreplicating vectors because of the self-perpetuating nature of viral multiplication and secondary infections of adjacent cells, which will ultimately allow the delivery of therapeutic siRNA molecules that are replenished over time. In general, ~10,000 viral progenies are generated in a single cell after viral infection [71]. Therefore, I could also expect to have gene amplification of therapeutic siRNA in a cancer cell-specific manner, as oncolytic Ad would be able to infect and deliver to neighboring cancer cells. As demonstrated in Fig. 7, the duration and magnitude of the gene silencing effect following infection with Ad-ΔB7-shVEGF was longer and more effective as compared to the non-replicating Ad. Its worth noting that the initial viral load was 1000-fold less for Ad-ΔB7-shVEGF than Ad-ΔB7, but the overall effect of this VEGF-silencing oncolytic Ads was much greater. The initial lack of downregulation of VEGF was most likely due to the low number of initial viral load. However, by day 14 the Ad was able to propagate and amplify the shRNA against VEGF to see the functional effect of downregulation of VEGF levels. In accord with this *in vitro* result, Ad-

ΔB7-shVEGF was able to continuously suppress VEGF production *in vivo*, supporting the idea of long-lasting therapeutic effect.

VEGF has shown to inhibit immune cell function, impairing both effector function and early stages of hematopoiesis [72]. *In vivo* data suggested that blockade of VEGF receptors on hematopoietic progenitors may improve the function of DCs in tumor-bearing hosts [73]. Therefore, lowering VEGF expression by Ad-ΔB7-shVEGF Ad would also lead to increase the anti-tumoral immune response. I are currently investigating this phenomenon in more detail to determine whether siRNA specific to VEGF has a positive effect on immune response in tumor-bearing hosts. Additionally, combination therapy using Ad-ΔB7-shVEGF and immunotherapy may not only be effective in blocking tumor angiogenesis mediated by VEGF but also can improve of immune cell function in tumor-bearing hosts and the effectiveness of specific immunotherapy. Moreover, the therapeutic strategy of combining oncolytic Ad with VEGF-specific siRNA could decrease vascular dissemination from infected tumor site, resulting in Ad sequestration within the tumor and increase of local siRNA expression level, which ultimately could lead to a decrease in systemic toxicity [68].

Taken collectively, the findings of this study demonstrate the effectiveness of augmenting the antitumor effect with oncolytic Ad expressing

shRNA against VEGF. Ad-ΔB7-shVEGF oncolytic Ad elicited potent anti-tumor effect through shRNA-mediated inhibition of VEGF, in addition to cancer cell-specific lysis by active viral replication in comparison to its cognate control oncolytic virus, Ad-ΔB7. Moreover, the therapeutic advantage of Ad-ΔB7-shVEGF oncolytic Ad would be enhanced in human system because VEGF produced by tumor stromal cells would also be inhibited by this shRNA for human VEGF. Therefore, it provides further support in considering this oncolytic Ad expressing shRNA directed against VEGF as a novel therapeutic approach in the treatment of cancer.

Most shRNA-expressing vectors have used RNA polymerase III promoters (U6, H1, or 7SK). Polymerase III promoters have the advantage of directing the synthesis of small, noncoding transcripts whose 3' ends are defined by termination within a stretch of 4-5 thymidines (Ts) [74,75]. Synthesis of shRNAs from a single DNA template driven by polymerase III promoters has made it possible to develop plasmids and virus-derived vectors as RNAi-delivery vehicles. In addition to mRNA, polymerase II promoters synthesize many noncoding RNAs, including small nuclear and nucleolar RNAs. Although the polymerase II promoter-based shRNA system has also been reported to be effective [15,76-79], no information is yet available on whether polymerase III promoters are superior to polymerase II promoters in their

ability to express shRNA. To explore the utility of RNA polymerase II promoters for expression of shRNAs, I initially constructed two replication-incompetent adenoviruses, Ad-ΔE1-U6shIL8 and Ad-ΔE1-CMVshIL8, which express IL-8-specific shRNA under the control of the U6 and CMV promoters, respectively. As demonstrated in Fig. 10, Ad-ΔE1-U6shIL8 was highly effective in reducing IL-8 expression, whereas no significant gene silencing was achieved with the CMV promoter-driven Ad in various cancer cell lines. Moreover, a 10-fold greater Ad-ΔE1-CMVshIL8 viral dose is needed to suppress IL-8 expression to the extent elicited by Ad-ΔE1-U6shIL8 transduction (Fig. 10B). This finding concurs with recent reports that an unmodified CMV promoter is inefficient at gene silencing through shRNA expression [80,81]. Xia *et al.* have demonstrated that the placement of the hairpin immediately adjacent to the transcription start site and use of a minimal polyadenylation cassette is highly critical in driving shRNA expression [79,81,82]. RNA polymerase II promoters, are very valuable in both biomedical research and clinical applications, such as gene therapy, because they allow inducible, tissue-specific or cell-type-specific RNA expression [83,84]. Therefore, design and optimization of polymerase II promoters that effectively drive shRNA expression would be very beneficial.

Endothelial cell migration, tube formation, and vessel sprouting are

required for the angiogenic process, and acquisition of an angiogenic phenotype is crucial for tumor progression. Therefore, I investigated whether IL-8-specific shRNA expressed from an adenovirus could inhibit migration and differentiation of HUVEC into the capillary-like structures of precursory vessels. Addition of conditioned media from Ad-ΔE1-U6shIL8-transduced cells in transwell migration assays suppressed migration of endothelial cells by more than 48 % relative to conditioned media from Ad-ΔE1-transduced cells (Fig. 11). The ability of endothelial cells to form tubes on a matrix and of microvessels to sprout from rat aorta rings was also effectively inhibited by Ad-ΔE1-U6shIL8. These results demonstrate that Ad-mediated expression of IL-8-specific shRNA is functionally active and acts on endothelial cells to block several critical steps in angiogenesis. In addition to inhibition of endothelial cells function, Ad-ΔE1-U6shIL8 effectively suppressed migration and invasion of cancer cells (Fig. 12). Moreover in gelatin zymography and ELISA assays, expression of IL-8-specific shRNA reduced both the expression and activity of MMP-2. MMPs appear to play a crucial role in many stages of tumor progression, including angiogenesis and the invasion and metastasis of tumor cells. Studies by Bergers et al. and Blavier et al. have also reported that MMP-2 is upregulated in angiogenic lesions and plays an active role during carcinogenesis of Wnt1-induced mammary tumors in

transgenic mice [85,86]. Downregulation of MMP-2 may thus be directly responsible for inhibition of cellular locomotion and invasive ability *in vitro* and may play a role in angiogenesis inhibition *in vivo*.

I next determined whether oncolytic Ad expressing IL-8-specific shRNA could functionally reduce endogenous IL-8 expression in cancer cells. I and others have previously shown that replication-competent Ad suppresses tumor angiogenesis through the preserved E1A region[47,51,53]. In agreement with these previous results, I observed that control oncolytic Ad that does not express IL-8-specific shRNA (Ad-ΔB7) substantially suppressed IL-8 expression compared to E1A-deleted replication-incompetent Ad (Ad-ΔE1). Interestingly, Ad-ΔB7-U6shIL8 further enhanced suppression of IL-8 expression in cancer cells relative to Ad-ΔB7, demonstrating that replication-competent adenovirus expressing IL-8-specific shRNA reduces IL-8 expression with high efficiency.

Moreover, treatment with Ad-ΔB7-U6shIL8 markedly inhibited the growth of established Hep3B and A549 xenograft tumors in nude mice and significantly delayed morbidity related to large tumor size. To better understand the mechanism of action of Ad-ΔB7-U6shIL8, microvessel density was assessed using an anti-CD31 antibody. Tumor angiogenesis was found to be significantly suppressed in Ad-ΔB7-U6shIL8-treated mice versus control

mice or mice treated with Ad-ΔB7-treated mice in both xenograft models. Based on these data, I conclude that inhibition of tumor growth is caused, in part, by the reduced number of tumor vessels in Ad-ΔB7-U6shIL8-treated mice. The antitumor efficacy of Ad-ΔB7-U6shIL8 was not limited to s.c. tumor xenograft models but was also evident in a metastatic tumor model where intrapleural injection of Ad-ΔB7-U6shIL8 inhibited the growth of disseminated MDA231 breast cancer metastases. These findings suggest that in addition to affecting the growth of a localized primary tumor, Ad-ΔB7-U6shIL8 is also able to inhibit the dissemination and/or growth of distant metastases.

Recently, inhibition of IL-8 activity using anti-IL-8 neutralizing antibody or IL-8 antisense oligodeoxynucleotides or by disabling the function of its receptors has been shown to inhibit both tumor growth and metastasis in a variety of animal tumor models [25-27]. Moreover, Dinney et al. have demonstrated that Ad IL-8-AS therapy decreased the *in vivo* expression of IL-8 and matrix metalloproteinase type 9 (MMP-9), reduced microvessel density, and enhanced endothelial cell apoptosis [87]. Therefore, the therapeutic effects in terms of inhibiting tumor growth and metastasis by inhibiting IL-8 activity or disabling the function of its receptors appears to be a promising therapeutic

target for cancer. As demonstrated in Fig. 16, suppression of IL-8 by Ad-ΔB7-U6shIL8 may provide the initial trigger for an antiangiogenic amplification loop, with subsequent reduction of VEGF, one of the main angiogenic switch inducers. Further experiments are planned to address this observation more rigorously and to investigate the underlying mechanisms.

Overall, this study indicates that the use of cancer cell-specific, replicating oncolytic adenovirus to deliver IL-8-specific shRNA offers the potential benefits of restricted and renewable siRNA expression within the tumor microenvironment, an additive anti-tumor outcome through viral oncolysis, and siRNA-mediated IL-8 silencing. In addition, our data provide the first evidence that siRNA directed against IL-8, delivered by oncolytic Ad directly into the tumor, has the ability to down-regulate the target gene and can suppress the progression of human cancer xenografts in mice.

The c-Met receptor tyrosine kinase and its ligand, hepatocyte growth factor (HGF), are dysregulated in many human cancers and this change contributes to oncogenesis and tumor progression in several human cancers and promotes aggressive cellular invasiveness that is strongly linked to tumor metastasis. It implies that c-Met receptor tyrosine kinase and HGF can be attractive therapeutic targets in cancer treatments. For the c-Met/HGF

targeting treatment applications, various approaches have been attempted: a) An inhibition of the HGF-mediated biological function by blocking c-Met/HGF interaction using HGF-specific monoclonal antibodies[88]; b) An inhibition of c-Met/HGF coupling by a ligand displacement using a competitive antagonist for HGF, such as NK4[37]; c) An inhibition of a c-Met receptor tyrosine kinase activity by small molecule inhibitors[32]; d) An inhibition of HGF-mediated c-Met receptor tyrosine kinase activation using decoy soluble Met receptors[36]; e) An inhibition of HGF/Met RNA and/or protein expression by a ribozyme or siRNA technology[29].

Recently, multiple shRNAs-combined vector systems have been developed to improve the silencing efficiency. Ter Brake et al. showed that the multiple effective shRNAs inhibit HIV-1 production much more strongly compared to a single shRNA, implying that such RNAi-based combinational approaches against HIV-1might result in an increase in the magnitude of inhibition along with decreased possibilities of escape from the inhibition [89]. In 2006, it has been shown by Henry et al. that the triple shRNA expression simultaneously downregulates multiple independent targets involving in viral replication and viral attachment, suggesting that the multiple shRNAs can be more efficient than the single shRNA expression system in treatments of many multifactorial diseases including diabetes or cancers[90].

In this report, I employed an adenoviral vector-mediated RNA interference technology to efficiently induce knock down of c-Met expression in cancer cells, then investigated the effects of c-Met inhibition in both tumor growth and angiogenesis. To enhance the c-Met knockdown efficiency, I constructed adenoviruses expressing two kinds of c-Met-specific shRNAs from a single adenoviral vector. c-Met ELISA results showed that all our constructed c-Met specific shRNA-expressing Ads, such as Ad-ΔE1-shMet4, Ad-ΔE1-shMet5, and Ad-ΔE1-shMet4+5, successfully inhibited the expression of c-Met in various cancer cell lines tested and especially, Ad-ΔE1-shMet4+5 among these shMet-expressing Ads inhibited c-Met expression very efficiently (Fig. 18). Adenoviral vectors expressing c-Met-specific shRNA have been described recently and have been reported therapeutic efficiency. However, in contrast to previously described viral vector, I showed that expressing two different shRNA. This is the first time observation that two different shRNAs can be expressed from the novel single adenoviral vector system, which is strongly indication that the inhibition of c-Met expression by dual c-Met specific shRNA expression system will be a promising strategy in cancer therapies.

HGF/c-Met signaling is involved in number of signal pathways [91] such as the Ras mitogen-activated protein kinase (MAPK) pathways through

Grb2-SOS complex formation, MEK1/2, and ERK1/2 activation that is responsible for cell growth, differentiation, and development and inhibition of apoptotic cell death by activation of phosphatidylinositol 3'-kinase activation through Akt phosphorylation[92,93]. I observed that the Ads including Ad-ΔE1-shMet4, Ad-ΔE1-shMet5, or Ad-ΔE1-shMet4+5 gave rise to multiple effects to the infected cancer cells: a) decrease of cell confluence; b) enlargement of cell volume (lamellafodia); c) flattenning of cell morphology, and d) appearance of many vacuolated cells, such as typical senescence-like phenotype (Fig. 19A). RT-PCR analysis for gene products including osteonectin, SM22, TGaseII, and PAI-1, which are commonly associated with cellular senescence, showed that the mRNA levels of the genes are significantly increased in the cells, especially infected with Ad-ΔE1-shMet4+5 (Fig. 19D). Also, FACS analysis clearly showed that the infected cells are arrested at G2/M phase, which implies that the reduction of the c-Met expression might inhibit the proliferation of the infected cells (Fig. 19E). The data were also confirmed by TUNEL assay, in which no TUNEL-positive apoptosis was observed, and by western blot analysis (Fig. 22). These results strongly imply that Ad-ΔE1-shMet4+5 inhibits not only c-Met protein expression but also the ERK1/2 and Akt expression, or phosphorylation, the signaling event in the down-stream pathway of c-Met activation, supporting

the speculation that the reduction of c-Met expression level by the c-Met specific shRNA-expressing Ad efficiently inhibits the downstream signal of the HGF/c-Met. Most of all, the reduced expression level of the c-Met by the Ad-ΔE1-shMet4+5 inhibits cancer cell proliferation by senescence mechanism in *in vitro* tested tumor cells, and the same result might be expected in *in vivo*. It has not been reported that the reduction of the c-Met expression inhibits tumor cell proliferation and growth by the senescence mechanism.

I observed that all viruses expressing c-Met specific shRNA substantially suppressed VEGF expression compared to control Ad (Ad-ΔE1) (Fig. 20A), which agreed to the previous report that the activation of c-Met protein involves in the induction of VEGF[38,39]. In general, stimulation of endothelial cells by growth factors leads to morphological differentiation and formation of tube-like structures. On Matrigel substratum, the endothelial cells form aggregates, then start to sprout and fuse to form tube-like structures. Ad-ΔE1-shMet4+5 was highly effective in preventing the tube formation of HUVECs in *in vitro*, and the relative tube length in the infected cells was inhibited to 44.1% of that in the Ad-ΔE1-infected U343 cell controls (Fig. 20C, 20D). Also, Ad-ΔE1-shMet4+5 inhibited microvessel sprouting from rat

aorta ring in *ex vivo* with a decrease in the number of microvessels to 85.7% ($p<0.05$) compared to that in the Ad-ΔE1 control (Fig. 20E, 20F). In addition to the inhibition of endothelial cells function, Ad-ΔE1-shMet4+5 effectively suppressed proliferation of HUVEC (Fig. 20G, 20H). Based on these results, it is obvious that the Ad-ΔE1-shMet4+5 inhibits the c-met expression in the endothelial cells as efficiently as the expression of intratumorous c-met and acts on endothelial cells to block certain critical steps in angiogenesis so that Ad-ΔE1-shMet4+5 can be exerted its more efficient anti-tumoral therapeutic effect in *in vivo.*

In addition, recently it has been shown that HGF/c-Met signaling can up-regulate the production of matrix metalloproteinases (MMPs) that induce the degradation of extracellular matrices and basement membrane, and enhance tumor invasion and metastasis via enhanced motility[94,95]. In migration and invasion assay using transwell performed to sustain the reduced c-Met expression level and to inhibit migration and invasion of cancer cells by reducing the expression of matrix metalloproteinases, migration and invasion in Ad-ΔE1-shMet4+5-transduced cells were remarkably decreased compared to that in the Ad-ΔE1-transduced control cells (Fig 21A, Fig 21B). In addition, in gelatin zymogram and ELISA assays, the expression of c-Met-specific

shRNA decreased the expression of MMP-2, a key mediator in metastasis, and its activity. Previous studies reported by Bergers et al. and Blavier et al. have shown that the MMP-2 is up-regulated in angiogenic lesions and plays an active role during carcinogenesis of Wnt1-induced mammarain tumors in transgenic mice[85,86], from which together with our data it can be deduced that a down-regulation of the MMP-2 might be directly responsible for the inhibition of cellular locomotion and invasive ability in *in vitro*, and play a critical role in angiogenesis inhibition in *in vivo*. Moreover, as a result of reduction of the c-Met expression by the Ad-ΔE1-shMet4+5, the cancer cell migration and the invasion is inhibited, which suggests that the c-Met might plays essential roles in growth, migration, and progression of cancer cells.

The strong effects of dual c-Met specific shRNA-expressing Ad on anti-proliferation and anti-angiogenesis were also demonstrated in *in vivo* U343 xenograft model (Fig. 24). Concerning that the U343 is derived from highly growing and vascularizing glioma, it can be postulated that the Ad-ΔE1-shMet4+5-treated group showed the most remarkable decrease of tumor growth compared to group treated with Ad-ΔE1. The mechanism of Ad-ΔE1-shMet4+5 can be understood from the result of microvessel density assay using an anti-CD31 antibody, in which the tumor angiogenesis was

significantly suppressed in the Ad-ΔE1-shMet4+5-treated mice compared to either control mice or Ad-ΔE1-treated mice. Based on these data, I conclude that the inhibition of tumor growth is caused in part by the decreased number of tumor vessels in Ad-ΔE1-shMet4+5-treated mice. The antitumor efficacy of the Ad-ΔE1-shMet4+5 was not limited to s.c. tumor xenograft models, while it was also evident in a metastatic tumor model. Intrapleural injection of the Ad-ΔE1-shMet4+5 inhibited the growth of disseminated MDA231 breast cancer metastases. These findings suggest that Ad-ΔE1-shMet4+5 is also able to inhibit the dissemination and/or the growth of distant metastases, and to diminish the primary tumor. In conclusion, it can be proposed that Ad-ΔE1-shMet4+5 can elicit a potent anti-tumor efficacy by local injection and systemic delivery as well against solid tumors and metastatic tumor lesions.

In *in vitro*, Ad-ΔE1-shMet4+5 showed the inhibition of endothelial cell function such as tube formation, vessel sprouting, and migration. In addition to these direct roles in regulating endothelial cell function, our investigation on the biological significance of c-Met down-regulation in the tumor tissue implies the regulation of secretion of angiogenic factors by epithelial and tumor cells. In tumor cell lysate ELISA, Ad-ΔE1-shMet4+5 modulated the expression of both IL-8 and VEGF, which are key mediators of

angiogenesis and MMP-2 expression playing central roles in many stages of tumor progression, including angiogenesis, invasion and metastasis of tumor cells. Taken together, the antimigratory and antiangiogenic activities of c-Met-specific shRNA expression may inhibit tumor growth and metastasis in animals by suppressing tumor angiogenesis, suggesting a crucial role for c-Met in angiogenesis and tumor growth and metastasis *in vivo.* Also, since VEGF and IL-8 play involve in tumor survival, especially in endothelial cells, the treatment of c-Met-specific shRNA-expressing Ad in combination with radiation or chemotherapeutic agents can block the protective effect of VEGF and IL-8.

Studies on the resistance mechanism to overcome the resistance for chemo drugs are urgent, since resistance against radiation and anticancer reagents hinder complete recovery from cancer therapies. HGF/Met signaling has shown to induce chemo- and radio-resistance of tumors[96]. Aebersold and his colleagues have recently provided clinical evidence that c-Met expression involves in resistance of otopharyngeal cancer to radiation[97]. Qian et al has also reported that c-Met up-regulation might contribute to an intrinsic resistance of certain tumor cells to radiation[98]. Paul Timpson et al. have reported that head and neck squamous cell carcinoma cells (HNSCC)

overcome resistance to the epidermal growth factor receptor inhibitor gefitinib by an aberrant expression of cortactin, which stabilizes the c-Met receptor tyrosine kinase and enhances hepatocte growth factor-induced mitogenesis and cell scattering. Recently, Jeffrey A. Engelman et al. have reported mechanisms of acquired resistances to treatment with kinase inhibitors, such as anti-tumor drug gefitinib (ZD1839 or Irressa) or erlotinib (Tarceva), in that MET amplification promotes gefitinib resistance by driving ERBB3 (HER3)-dependent activation of PI3K in 4 of 18 (22%) lung cancer specimens[99]. In this report, they also demonstrated that the treatment of gefitinib or PHA-665752 (a MET tyrosine kinase inhibitor) alone has no effect on gefitinib-resistant cells, while combination treatment with both agents results in substantial growth inhibition and induces apoptosis. Notably, EGFR TKI-naïve patients of a small percentage of NSCLCs have been reported to contain both an EGFR-activating mutation and MET amplification[100,101]. For theses reasons, the combination of Ad-ΔE1-shMet4+5 with other anticancer agents (for examples, gefitinib or erlotinib) or radiation might be beneficial to overcome not only *de novo* resistance, but also acquired resistance to chemotherapeutic agents or radiation therapy.

In summary, I generated recombinant adenoviruses against different regions of c-Met gene by single adenoviral vector to express two kinds of c-Met-specific shRNA and successfully showed that down-regulation of c-Met protein expression caused significant inhibition on proliferation, migration, invasion, and angiogenesis of cancer cells. Our findings presented here indicate that the expression of two kinds of c-Met specific shRNA by adenovirus-delivered siRNA may be a useful strategy potential therapeutic strategy in the treatment of cancer.

V. CONCLUSION

In this study, it was suggested that the use of cancer cell-specific, replicating oncolytic adenovirus to deliver shRNA offers the potential benefits of restricted and renewable siRNA expression within the tumor microenvironment, an additive anti-tumor outcome through viral oncolysis, and siRNA-mediated gene silencing. I also confirmed that U6 promoter is superior to CMV in its ability to efficiently express shRNA and multiple shRNAs expression against different regions of a gene is more effective than single shRNA expression. Therefore, these results are going to provide a new strategy to improve the silencing efficiency.

VI. REFERENCES

1. Lou TF, Gray CW, Gray DM. The reduction of Raf-1 protein by phosphorothioate ODNs and siRNAs targeted to the same two mRNA sequences. Oligonucleotides 2003;13:313-24.
2. Wacheck V, Losert D, Gunsberg P, Vornlocher HP, Hadwiger P, Geick A, et al. Small interfering RNA targeting bcl-2 sensitizes malignant melanoma. Oligonucleotides 2003;13:393-400.
3. Wannenes F, Ciafre SA, Niola F, Frajese G, Farace MG. Vector-based RNA interference against vascular endothelial growth factor-A significantly limits vascularization and growth of prostate cancer in vivo. Cancer Gene Ther 2005;12:926-34.
4. Azkur AK, Kim B, Suvas S, Lee Y, Kumaraguru U, Rouse BT. Blocking mouse MMP-9 production in tumor cells and mouse cornea by short hairpin (sh) RNA encoding plasmids. Oligonucleotides 2005;15:72-84.
5. Spankuch B, Matthess Y, Knecht R, Zimmer B, Kaufmann M, Strebhardt K. Cancer inhibition in nude mice after systemic application of U6 promoter-driven short hairpin RNAs against PLK1. J Natl Cancer Inst 2004;96:862-72.
6. Brummelkamp TR, Bernards R, Agami R. A system for stable expression of short interfering RNAs in mammalian cells. Science 2002;296:550-3.
7. Jolly D. Viral vector systems for gene therapy. Cancer Gene Ther 1994;1:51-64.
8. Ganly I, Kirn D, Eckhardt G, Rodriguez GI, Soutar DS, Otto R, et al. A phase I study of Onyx-015, an E1B attenuated adenovirus, administered intratumorally to patients with recurrent head and neck cancer. Clin Cancer Res 2000;6:798-806.
9. Heise C, Ganly I, Kim YT, Sampson-Johannes A, Brown R, Kirn D.

Efficacy of a replication-selective adenovirus against ovarian carcinomatosis is dependent on tumor burden, viral replication and p53 status. Gene Ther 2000;7:1925-9.

10. Khuri FR, Nemunaitis J, Ganly I, Arseneau J, Tannock IF, Romel L, et al. a controlled trial of intratumoral ONYX-015, a selectively-replicating adenovirus, in combination with cisplatin and 5-fluorouracil in patients with recurrent head and neck cancer. Nat Med 2000;6:879-85.
11. Kirn D. Clinical research results with dl1520 (Onyx-015), a replication-selective adenovirus for the treatment of cancer: what have we learned? Gene Ther 2001;8:89-98.
12. Kirn D. Oncolytic virotherapy for cancer with the adenovirus dl1520 (Onyx-015): results of phase I and II trials. Expert Opin Biol Ther 2001;1:525-38.
13. Hermiston TW, Kuhn I. Armed therapeutic viruses: strategies and challenges to arming oncolytic viruses with therapeutic genes. Cancer Gene Ther 2002;9:1022-35.
14. Hanahan D, Weinberg RA. The hallmarks of cancer. Cell 2000;100:57-70.
15. Kim KJ, Li B, Winer J, Armanini M, Gillett N, Phillips HS, et al. Inhibition of vascular endothelial growth factor-induced angiogenesis suppresses tumour growth in vivo. Nature 1993;362:841-4.
16. Yancopoulos GD, Davis S, Gale NW, Rudge JS, Wiegand SJ, Holash J. Vascular-specific growth factors and blood vessel formation. Nature 2000;407:242-8.
17. Wang Y, Fei D, Vanderlaan M, Song A. Biological activity of bevacizumab, a humanized anti-VEGF antibody in vitro. Angiogenesis 2004;7:335-45.
18. Ellis LM. Bevacizumab. Nat Rev Drug Discov 2005;Suppl:S8-9.
19. Zakarija A, Soff G. Update on angiogenesis inhibitors. Curr Opin

Oncol 2005;17:578-83.

20. Arora A, Scholar EM. Role of tyrosine kinase inhibitors in cancer therapy. J Pharmacol Exp Ther 2005;315:971-9.
21. Koch AE, Polverini PJ, Kunkel SL, Harlow LA, DiPietro LA, Elner VM, et al. Interleukin-8 as a macrophage-derived mediator of angiogenesis. Science 1992;258:1798-801.
22. Hu DE, Hori Y, Fan TP. Interleukin-8 stimulates angiogenesis in rats. Inflammation 1993;17:135-43.
23. Shi Q, Abbruzzese JL, Huang S, Fidler IJ, Xiong Q, Xie K. Constitutive and inducible interleukin 8 expression by hypoxia and acidosis renders human pancreatic cancer cells more tumorigenic and metastatic. Clin Cancer Res 1999;5:3711-21.
24. Xie K. Interleukin-8 and human cancer biology. Cytokine Growth Factor Rev 2001;12:375-91.
25. Arenberg DA, Kunkel SL, Polverini PJ, Glass M, Burdick MD, Strieter RM. Inhibition of interleukin-8 reduces tumorigenesis of human non-small cell lung cancer in SCID mice. J Clin Invest 1996;97:2792-802.
26. Arici A, Seli E, Zeyneloglu HB, Senturk LM, Oral E, Olive DL. Interleukin-8 induces proliferation of endometrial stromal cells: a potential autocrine growth factor. J Clin Endocrinol Metab 1998;83:1201-5.
27. Mian BM, Dinney CP, Bermejo CE, Sweeney P, Tellez C, Yang XD, et al. Fully human anti-interleukin 8 antibody inhibits tumor growth in orthotopic bladder cancer xenografts via down-regulation of matrix metalloproteases and nuclear factor-kappaB. Clin Cancer Res 2003;9:3167-75.
28. Laird AD, Cherrington JM. Small molecule tyrosine kinase inhibitors: clinical development of anticancer agents. Expert Opin Investig Drugs 2003;12:51-64.

29. Jiang WG, Grimshaw D, Lane J, Martin TA, Abounader R, Laterra J, et al. A hammerhead ribozyme suppresses expression of hepatocyte growth factor/scatter factor receptor c-MET and reduces migration and invasiveness of breast cancer cells. Clin Cancer Res 2001;7:2555-62.
30. Abounader R, Lal B, Luddy C, Koe G, Davidson B, Rosen EM, et al. In vivo targeting of SF/HGF and c-met expression via U1snRNA/ribozymes inhibits glioma growth and angiogenesis and promotes apoptosis. Faseb J 2002;16:108-10.
31. Herynk MH, Stoeltzing O, Reinmuth N, Parikh NU, Abounader R, Laterra J, et al. Down-regulation of c-Met inhibits growth in the liver of human colorectal carcinoma cells. Cancer Res 2003;63:2990-6.
32. Sattler M, Pride YB, Ma P, Gramlich JL, Chu SC, Quinnan LA, et al. A novel small molecule met inhibitor induces apoptosis in cells transformed by the oncogenic TPR-MET tyrosine kinase. Cancer Res 2003;63:5462-9.
33. Christensen JG, Schreck R, Burrows J, Kuruganti P, Chan E, Le P, et al. A selective small molecule inhibitor of c-Met kinase inhibits c-Met-dependent phenotypes in vitro and exhibits cytoreductive antitumor activity in vivo. Cancer Res 2003;63:7345-55.
34. Firon M, Shaharabany M, Altstock RT, Horev J, Abramovici A, Resau JH, et al. Dominant negative Met reduces tumorigenicity-metastasis and increases tubule formation in mammary cells. Oncogene 2000;19:2386-97.
35. Furge KA, Zhang YW, Vande Woude GF. Met receptor tyrosine kinase: enhanced signaling through adapter proteins. Oncogene 2000;19:5582-9.
36. Michieli P, Mazzone M, Basilico C, Cavassa S, Sottile A, Naldini L, et al. Targeting the tumor and its microenvironment by a dual-function decoy Met receptor. Cancer Cell 2004;6:61-73.

37. Matsumoto K, Nakamura T. NK4 (HGF-antagonist/angiogenesis inhibitor) in cancer biology and therapeutics. Cancer Sci 2003;94:321-7.
38. Tomita N, Morishita R, Taniyama Y, Koike H, Aoki M, Shimizu H, et al. Angiogenic property of hepatocyte growth factor is dependent on upregulation of essential transcription factor for angiogenesis, ets-1. Circulation 2003;107:1411-7.
39. Rosen EM, Lamszus K, Laterra J, Polverini PJ, Rubin JS, Goldberg ID. HGF/SF in angiogenesis. Ciba Found Symp 1997;212:215-26; discussion 27-9.
40. Zhang YW, Su Y, Volpert OV, Vande Woude GF. Hepatocyte growth factor/scatter factor mediates angiogenesis through positive VEGF and negative thrombospondin 1 regulation. Proc Natl Acad Sci U S A 2003;100:12718-23.
41. Puri N, Khramtsov A, Ahmed S, Nallasura V, Hetzel JT, Jagadeeswaran R, et al. A selective small molecule inhibitor of c-Met, PHA665752, inhibits tumorigenicity and angiogenesis in mouse lung cancer xenografts. Cancer Res 2007;67:3529-34.
42. Zou HY, Li Q, Lee JH, Arango ME, McDonnell SR, Yamazaki S, et al. An orally available small-molecule inhibitor of c-Met, PF-2341066, exhibits cytoreductive antitumor efficacy through antiproliferative and antiangiogenic mechanisms. Cancer Res 2007;67:4408-17.
43. Jaffe EA, Nachman RL, Becker CG, Minick CR. Culture of human endothelial cells derived from umbilical veins. Identification by morphologic and immunologic criteria. J Clin Invest 1973;52:2745-56.
44. Yun CO, Kim E, Koo T, Kim H, Lee YS, Kim JH. ADP-overexpressing adenovirus elicits enhanced cytopathic effect by induction of apoptosis. Cancer Gene Ther 2005;12:61-71.
45. Nicosia RF, Ottinetti A. Modulation of microvascular growth and morphogenesis by reconstituted basement membrane gel in three-

dimensional cultures of rat aorta: a comparative study of angiogenesis in matrigel, collagen, fibrin, and plasma clot. In Vitro Cell Dev Biol 1990;26:119-28.

46. Yoo J, Kim, Joo-Hang, Kim, Jaesung , Kang, Yoon-A, and Yun, Chae-Ok. Short hairpin RNA-expressing oncolytic adenovirus-mediated inhibition of IL-8: Effects on anti-angiogenesis and tumor growth inhibition. Gene Therapy 2007;In trvision.
47. Yoo JY, Kim JH, Kwon YG, Kim EC, Kim NK, Choi HJ, et al. VEGF-specific short hairpin RNA-expressing oncolytic adenovirus elicits potent inhibition of angiogenesis and tumor growth. Mol Ther 2007;15:295-302.
48. de Jong JS, van Diest PJ, Baak JP. Heterogeneity and reproducibility of microvessel counts in breast cancer. Lab Invest 1995;73:922-6.
49. Marson LP, Kurian KM, Miller WR, Dixon JM. Reproducibility of microvessel counts in breast cancer specimens. Br J Cancer 1999;81:1088-93.
50. Kim J, Kim JH, Choi KJ, Kim PH, Yun CO. E1A- and E1B-Double mutant replicating adenovirus elicits enhanced oncolytic and antitumor effects. Hum Gene Ther 2007;18:773-86.
51. Saito Y, Sunamura M, Motoi F, Abe H, Egawa S, Duda DG, et al. Oncolytic replication-competent adenovirus suppresses tumor angiogenesis through preserved E1A region. Cancer Gene Ther 2006;13:242-52.
52. Shao R, Xia W, Hung MC. Inhibition of angiogenesis and induction of apoptosis are involved in E1A-mediated bystander effect and tumor suppression. Cancer Res 2000;60:3123-6.
53. Zhou Z, Zhou RR, Guan H, Bucana CD, Kleinerman ES. E1A gene therapy inhibits angiogenesis in a Ewing's sarcoma animal model. Mol Cancer Ther 2003;2:1313-9.
54. Bussolino F, Mantovani A, Persico G. Molecular mechanisms of

blood vessel formation. Trends Biochem Sci 1997;22:251-6.

55. Lai JF, Kao SC, Jiang ST, Tang MJ, Chan PC, Chen HC. Involvement of focal adhesion kinase in hepatocyte growth factor-induced scatter of Madin-Darby canine kidney cells. J Biol Chem 2000;275:7474-80.

56. Matsui Y, Kobayashi N, Nishikawa M, Takakura Y. Sequence-specific suppression of mdr1a/1b expression in mice via RNA interference. Pharm Res 2005;22:2091-8.

57. Tran N, Cairns MJ, Dawes IW, Arndt GM. Expressing functional siRNAs in mammalian cells using convergent transcription. BMC Biotechnol 2003;3:21.

58. Shen C, Buck AK, Liu X, Winkler M, Reske SN. Gene silencing by adenovirus-delivered siRNA. FEBS Lett 2003;539:111-4.

59. Tomar RS, Matta H, Chaudhary PM. Use of adeno-associated viral vector for delivery of small interfering RNA. Oncogene 2003;22:5712-5.

60. Li MJ, Rossi JJ. Lentiviral vector delivery of recombinant small interfering RNA expression cassettes. Methods Enzymol 2005;392:218-26.

61. Davidson BL, Harper SQ. Viral delivery of recombinant short hairpin RNAs. Methods Enzymol 2005;392:145-73.

62. Wyatt CA, Geoghegan JC, Brinckerhoff CE. Short hairpin RNA-mediated inhibition of matrix metalloproteinase-1 in MDA-231 cells: effects on matrix destruction and tumor growth. Cancer Res 2005;65:11101-8.

63. Yang G, Cai KQ, Thompson-Lanza JA, Bast RC, Jr., Liu J. Inhibition of breast and ovarian tumor growth through multiple signaling pathways by using retrovirus-mediated small interfering RNA against Her-2/neu gene expression. J Biol Chem 2004;279:4339-45.

64. Gurzov EN, Izquierdo M. RNA interference against Hec1 inhibits tumor growth in vivo. Gene Ther 2006;13:1-7.

65. Hoeben A, Landuyt B, Highley MS, Wildiers H, Van Oosterom AT, De Bruijn EA. Vascular endothelial growth factor and angiogenesis. Pharmacol Rev 2004;56:549-80.
66. Takei Y, Kadomatsu K, Yuzawa Y, Matsuo S, Muramatsu T. A small interfering RNA targeting vascular endothelial growth factor as cancer therapeutics. Cancer Res 2004;64:3365-70.
67. Byrne AM, Bouchier-Hayes DJ, Harmey JH. Angiogenic and cell survival functions of vascular endothelial growth factor (VEGF). J Cell Mol Med 2005;9:777-94.
68. Thorne SH, Tam BY, Kirn DH, Contag CH, Kuo CJ. Selective intratumoral amplification of an antiangiogenic vector by an oncolytic virus produces enhanced antivascular and anti-tumor efficacy. Mol Ther 2006;13:938-46.
69. Folkman J, Shing Y. Angiogenesis. J Biol Chem 1992;267:10931-4.
70. Bergers G, Benjamin LE. Tumorigenesis and the angiogenic switch. Nat Rev Cancer 2003;3:401-10.
71. Green M, Daesch GE. Biochemical studies on adenovirus multiplication. II. Kinetics of nucleic acid and protein synthesis in suspension cultures. Virology 1961;13:169-76.
72. Ohm JE, Carbone DP. VEGF as a mediator of tumor-associated immunodeficiency. Immunol Res 2001;23:263-72.
73. Gabrilovich D, Ishida T, Oyama T, Ran S, Kravtsov V, Nadaf S, et al. Vascular endothelial growth factor inhibits the development of dendritic cells and dramatically affects the differentiation of multiple hematopoietic lineages in vivo. Blood 1998;92:4150-66.
74. Makinen PI, Koponen JK, Karkkainen AM, Malm TM, Pulkkinen KH, Koistinaho J, et al. Stable RNA interference: comparison of U6 and H1 promoters in endothelial cells and in mouse brain. J Gene Med 2006;8:433-41.
75. Robb GB, Brown KM, Khurana J, Rana TM. Specific and potent

RNAi in the nucleus of human cells. Nat Struct Mol Biol 2005;12:133-7.

76. Banan M, Puri N. The ins and outs of RNAi in mammalian cells. Curr Pharm Biotechnol 2004;5:441-50.

77. Unwalla HJ, Li MJ, Kim JD, Li HT, Ehsani A, Alluin J, et al. Negative feedback inhibition of HIV-1 by TAT-inducible expression of siRNA. Nat Biotechnol 2004;22:1573-8.

78. Tiscornia G, Singer O, Ikawa M, Verma IM. A general method for gene knockdown in mice by using lentiviral vectors expressing small interfering RNA. Proc Natl Acad Sci U S A 2003;100:1844-8.

79. Xia H, Mao Q, Eliason SL, Harper SQ, Martins IH, Orr HT, et al. RNAi suppresses polyglutamine-induced neurodegeneration in a model of spinocerebellar ataxia. Nat Med 2004;10:816-20.

80. Song J, Pang S, Lu Y, Chiu R. Poly(U) and polyadenylation termination signals are interchangeable for terminating the expression of shRNA from a pol II promoter. Biochem Biophys Res Commun 2004;323:573-8.

81. Xia H, Mao Q, Paulson HL, Davidson BL. siRNA-mediated gene silencing in vitro and in vivo. Nat Biotechnol 2002;20:1006-10.

82. Zhou H, Xia XG, Xu Z. An RNA polymerase II construct synthesizes short-hairpin RNA with a quantitative indicator and mediates highly efficient RNAi. Nucleic Acids Res 2005;33:e62.

83. Snove O, Jr., Rossi JJ. Expressing short hairpin RNAs in vivo. Nat Methods 2006;3:689-95.

84. Huynh T, Walchli S, Sioud M. Transcriptional targeting of small interfering RNAs into cancer cells. Biochem Biophys Res Commun 2006;350:854-9.

85. Bergers G, Brekken R, McMahon G, Vu TH, Itoh T, Tamaki K, et al. Matrix metalloproteinase-9 triggers the angiogenic switch during carcinogenesis. Nat Cell Biol 2000;2:737-44.

86. Blavier L, Lazaryev A, Dorey F, Shackleford GM, DeClerck YA. Matrix metalloproteinases play an active role in Wnt1-induced mammary tumorigenesis. Cancer Res 2006;66:2691-9.
87. Inoue K, Slaton JW, Kim SJ, Perrotte P, Eve BY, Bar-Eli M, et al. Interleukin 8 expression regulates tumorigenicity and metastasis in human bladder cancer. Cancer Res 2000;60:2290-9.
88. Cao B, Su Y, Oskarsson M, Zhao P, Kort EJ, Fisher RJ, et al. Neutralizing monoclonal antibodies to hepatocyte growth factor/scatter factor (HGF/SF) display antitumor activity in animal models. Proc Natl Acad Sci U S A 2001;98:7443-8.
89. ter Brake O, Konstantinova P, Ceylan M, Berkhout B. Silencing of HIV-1 with RNA interference: a multiple shRNA approach. Mol Ther 2006;14:883-92.
90. Henry SD, van der Wegen P, Metselaar HJ, Tilanus HW, Scholte BJ, van der Laan LJ. Simultaneous targeting of HCV replication and viral binding with a single lentiviral vector containing multiple RNA interference expression cassettes. Mol Ther 2006;14:485-93.
91. Birchmeier C, Birchmeier W, Gherardi E, Vande Woude GF. Met, metastasis, motility and more. Nat Rev Mol Cell Biol 2003;4:915-25.
92. Shinomiya N, Gao CF, Xie Q, Gustafson M, Waters DJ, Zhang YW, et al. RNA interference reveals that ligand-independent met activity is required for tumor cell signaling and survival. Cancer Res 2004;64:7962-70.
93. Xiao GH, Jeffers M, Bellacosa A, Mitsuuchi Y, Vande Woude GF, Testa JR. Anti-apoptotic signaling by hepatocyte growth factor/Met via the phosphatidylinositol 3-kinase/Akt and mitogen-activated protein kinase pathways. Proc Natl Acad Sci U S A 2001;98:247-52.
94. Harvey P, Clark IM, Jaurand MC, Warn RM, Edwards DR. Hepatocyte growth factor/scatter factor enhances the invasion of mesothelioma cell lines and the expression of matrix

metalloproteinases. Br J Cancer 2000;83:1147-53.

95. Kermorgant S, Aparicio T, Dessirier V, Lewin MJ, Lehy T. Hepatocyte growth factor induces colonic cancer cell invasiveness via enhanced motility and protease overproduction. Evidence for PI3 kinase and PKC involvement. Carcinogenesis 2001;22:1035-42.

96. Fan S, Wang JA, Yuan RQ, Rockwell S, Andres J, Zlatapolskiy A, et al. Scatter factor protects epithelial and carcinoma cells against apoptosis induced by DNA-damaging agents. Oncogene 1998;17:131-41.

97. Aebersold DM, Kollar A, Beer KT, Laissue J, Greiner RH, Djonov V. Involvement of the hepatocyte growth factor/scatter factor receptor c-met and of Bcl-xL in the resistance of oropharyngeal cancer to ionizing radiation. Int J Cancer 2001;96:41-54.

98. Qian LW, Mizumoto K, Inadome N, Nagai E, Sato N, Matsumoto K, et al. Radiation stimulates HGF receptor/c-Met expression that leads to amplifying cellular response to HGF stimulation via upregulated receptor tyrosine phosphorylation and MAP kinase activity in pancreatic cancer cells. Int J Cancer 2003;104:542-9.

99. Engelman JA, Zejnullahu K, Mitsudomi T, Song Y, Hyland C, Park JO, et al. MET amplification leads to gefitinib resistance in lung cancer by activating ERBB3 signaling. Science 2007;316:1039-43.

100. Kosaka T, Yatabe Y, Endoh H, Kuwano H, Takahashi T, Mitsudomi T. Mutations of the epidermal growth factor receptor gene in lung cancer: biological and clinical implications. Cancer Res 2004;64:8919-23.

101. Shibata T, Uryu S, Kokubu A, Hosoda F, Ohki M, Sakiyama T, et al. Genetic classification of lung adenocarcinoma based on array-based comparative genomic hybridization analysis: its association with clinicopathologic features. Clin Cancer Res 2005;11:6177-85.

Abstract (in Korean)

신생 혈관 형성 유도인자(VEGF-A, IL-8, and c-MET) 특이적 shRNA 를 발현하는 종양 선택적 살상 아데노바이러스의 항종양 상승효과 검증

<지도교수 윤채옥>

연세대학교 대학원 의과학과

유지영

기존의 혈관으로부터 새로운 혈관이 형성되는 신생 혈관 형성은 종양이 성장하고 전이되는데 있어 매우 중요한 역할을 한다. 신생혈관 형성이 일어나기 위해서는 여러 종류의 성장인자들이 필요한데, 현재 acidic fibroblast growth factor (aFGF), basic fibroblast growth factor (bFGF), transforming growth factor alpha and beta (TGF-α and β), interleukin-8 (IL-8), c-MET 등 여러 물질들이 보고되어 있다. 따라서 이들의 발현을 억제한다면, 불필요한 신생혈관형성에 기인하는 종양의 성장을 억제할 수 있다. siRNA 는 21-25 nucleotide

(nt)의 RNA 로서 상보적인 염기서열을 갖는 유전자의 mRNA 에 결합해서 분해를 유도한다. siRNA 는 기존의 antisense 나 ribozyme 을 이용한 방법보다 훨씬 빠르고 효율적으로 gene 의 knockdown 을 일으킬 수 있기 때문에 그 이용 범위가 확대되고 있으며, 바이러스의 증식억제나 발암억제 등을 통해 각종 질병을 치료할 수 있는 새로운 형태의 치료물질로 주목 받고 있다. 현재 동물세포내로 siRNA 를 도입하는 여러 가지 방법들이 보고되고 있으나, 대부분의 경우 transfection 효율이 낮고, 대상 세포에서 발현기간이 낮기 때문에, 장기간 효과적으로 siRNA 를 발현시키기 위해서는 더 나은 벡터 시스템의 개발이 요구된다. 이러한 배경 하에 본 연구에서는, 신생 혈관형성 유도 인자들인 VEGF-A 와 IL-8 그리고 c-Met 유전자를 이용하여 이들 유전자의 발현을 선택적으로 저해할 수 있는 shRNA 를 종양 세포에 대한 살상능과 특이성이 보다 개선된 Ad-ΔB7 아데노바이러스에 도입함으로써, 암세포에 대한 살상효과의 개선 여부를 검증하고자 하였다.

먼저, 가장 강력한 혈관형성 유도인자인 VEGF-A 특이적 shRNA 를 p53 이 불활성화된 종양세포들에서만 선택적으로 복제가 가능하여 암세포 특이적 세포 살상 및 세포고사를 함께 유발할 수 있는 종양선택적 복제가능 아데노바이러스인 Ad-ΔB7 에 탑재한 Ad-ΔB7-shVEGF 를 제작하고, ELISA 를 통하여 복제가능

아데노바이러스에 의해 shRNA 가 효과적으로 전사되어 VEGF 의 발현을 억제하는지 확인하였다. 그 결과, shVEGF 를 발현하는 종양선택적 복제가능 아데노바이러스가 대조군 복제불능 바이러스에 비해 50 배 낮은 역가에서도 바이러스 감염 24 시간 후에 VEGF 의 발현이 효과적으로 억제됨을 확인할 수 있었으며, 이와 더불어 종양 선택적 복제가능 아데노바이러스의 E1A 단백질이 VEGF 의 발현을 억제함을 확인함으로써 보다 나은 VEGF 발현 억제능을 관찰하였다. *in vitro* 와 *in vivo* 에서 시간별 VEGF 발현 억제능을 비교한 결과, 종양선택적 복제가능 아데노바이러스가 암세포 특이적 바이러스의 복제에 따라 shVEGF 가 암세 포에서 장기간 효과적으로 전사되어 VEGF 의 발현을 억제함을 확인하였고, U343 인체 뇌암 세포주의 xenograft 모델을 이용한 항종양 실험에서도 우수한 항종양 효과를 확인하였다. 또한, 조직 면역염색을 통하여. 이러한 개선된 항종양 효과가 실제로 종양 선택적 살상 아데노바이러스의 효과적인 shVEGF 발현에 의한 혈관 형성 억제에 의한 결과임을 확인하였다.

또한, IL-8 유전자를 이용하여 shRNA 발현에 효과적인 프로모터를 선정하였다. IL-8 의 발현을 선택적으로 억제하는 shRNA 를 CMV 또는 human U6 프로모터에 의해 그 발현이 조절될 수 있는 두 종류의 아데노바이러스를 각각 제작하여 shRNA 발현에

유용한 프로모터를 검증한 결과, U6 프로모터가 shRNA 발현에 보다 효과적인 프로모터임을 확인하였다. 다양한 기능적 분석을 통해서 IL-8 발현 억제로 인한 혈관 내피세포의 기능 저하로 항종양 효과가 크게 증가되었음을 확인할 수 있었고, 또한 IL-8 의 발현 감소로 인하여 강력한 전이인자인 MMP-2 발현이 억제됨으로써 전이암의 치료에에도 효과적으로 이용될 수 있음을 확인하였다.

상기에서 선정된 U6 프로모터를 이용하여 하나의 유전자를 발현시키는 것보다 두 개의 유전자를 발현시킬 경우 항종양 효과가 증가되는지를 c-Met 유전자를 이용하여 검증하였다. c-Met 은 간세포 성장인자 (HGF/SF) 특이적 리셉터로써 대부분의 암세포에서 과발현되거나 돌연변이 되어 암의 성장과 전이를 유도하는 인자로 알려져 있다. 두 종류의 효과적인 c-Met 특이적인 shRNA 를 각각 발현하는 바이러스와 두 종류의 shRNA 를 하나의 바이러스 벡터에서 동시에 발현하는 바이러스 등 모두 세 종류의 바이러스를 제작하여 c-Met 발현 억제능을 검증하였다. ELISA 를 수행한 결과, 각각의 shRNA 를 발현하는 바이러스에 비하여 두 종류의 shRNA 를 동시에 발현하는 바이러스가 보다 효과적으로 c-Met 의 발현을 억제함을 확인하였으며, 이 바이러스에 의한 효과적인 c-Met 발현 감소로 VEGF 의 발현이 억제되어 혈관내피세포의 기능이

저하되었으며, 세포 노화기전에 의해 세포증식 또한 억제됨을 검증하였다.

결론적으로, 본 연구를 통해 종양 선택적 증식 및 살상이 가능한 Ad-ΔB7 는 다양한 인체 종양 세포주에서 적은 역가의 바이러스의 감염으로 *in vitro* 에서 뿐만 아니라 *in vivo* 에서 shRNA 를 효과적으로 전달할 수 있음을 증명하였으며, CMV 프로모터와 U6 프로모터의 비교를 통하여 U6 프로모터가 shRNA 발현에 효과적임을 확인하였고, 또한, 하나의 유전자에 대해 다른 염기서열을 가지는 shRNA 를 동시에 발현시킴으로써 대상 유전자의 발현 억제능을 보다 증진시킬 수 있음을 확인하였다. 즉, 본 연구에서 제작한 신생혈관형성 유도인자 특이적 shRNA 를 발현하는 아데노바이러스는 암세포 특이적 복제 및 살상을 유도할 수 있을 뿐 아니라 이들 유전자 특이적 shRNA 를 암세포에서만 전사시킴으로써 종양 내 신생혈관 형성을 선택적으로 억제할 수 있으며 아데노바이러스의 복제에 따른 지속적이고 증폭된 shRNA 의 전사로 신생혈관 형성 억제능이 증가되고, 이에 따라 항종양 효과가 현저하게 증진될 수 있을 것으로 기대된다. 또한, 아데노바이러스의 E1 단백질이 신생혈관형성을 유도하는 인자인 VEGF 와 IL-8 을 효과적으로 억제함으로써 상승효과를 가질 것이다. 종합적으로 결론을 내리면, 바이러스의 선택적 복제에 따른 체내에서의

안전성과 신생혈관 형성억제에 따른 증대된 바이러스의 암세포 살상능에 따른 상승효과로 더욱 개선된 항종양 효과를 유도할 수 있어 바이러스를 이용한 암의 치료연구에 효과적으로 이용될 수 있을 것으로 사료된다.

핵심되는 말: 아데노바이러스, shRNA, VEGF-A, IL-8, c-Met, Ad-ΔB7

PUBLICATION LIST

1. Short hairpin RNA-expressing oncolytic adenovirus-mediated inhibition of IL-8: Effects on anti-angiogenesis and tumor growth inhibition, Ji Young Yoo, Joo-Hang Kim, Jaesung Kim, Jing-Hua Huang, Song Nam Zhang, Yoon-A Kang, Hoguen Kim, and Chae-Ok Yun, Gene Therapy, accepted, 2007.

2. VEGF-specific short hairpin RNA-expressing oncolytic adenovirus elicits potent inhibition of angiogenesis and tumor growth, Ji Young Yoo, Joo-Hang Kim, Young-Guen Kwon, Eok-Cheon Kim, Nam Kyu Kim, Hye Jin Choi, and Chae-Ok Yun, Molecular Therapy, 15(2):295-302, Feb, 2007.

3. Suicide cancer gene therapy using pore forming toxin, streptolysin O, WS Yang, SO Park, AR Yoon, JY Yoo, MK Kim, CO Yun, CW Kim, Molecular Cancer Therapeutics, 5 (6), p1610-1619, June, 2006.

4. Markedly enhanced cytolysis by E1B 19kD-deleted oncolytic adenovirus in combination with cisplatin, A-Rum Yoon, Joo-Hang Kim, Young-Sook Lee, Hoguen Kim, Ji Young Yoo, Joo-Hyuk Sohn, and Chae-Ok Yun, Human Gene Therapy, 17 (4), p379-390, April. 2006.

5. CAR-binding ablation reduces adenovirus liver tropism and toxicity, Chae-Ok Yun, A-Rum Yoon, Ji young Yoo, Hoguen Kim, Minjung Kim, Taeyong Ha, and Joo-Hang Kim, Human Gene Therapy, 16 (2) p248-261, Feb. 2005.